HUNGARIAN JOURNAL OF INDUSTRY AND CHEMISTRY (HJIC)
formerly (until 2012) Hungarian Journal of Industrial Chemistry

The HJIC is an international periodicals that focuses on results of fundamental and applied research in the field of

- Biotechnology
- Chemical Engineering Science
- Chemical Processes
- Energetics
- Environmental Chemistry
- Environmental Engineering & Technology
- Industrial Management
- Material Science
- Mechanical Engineering
- Mechatronics
- Process & System Engineering
- Recycling

in the form of original papers, reviews, short communications, and conference proceedings written in English.

EDITORIAL BOARD

EDITORIAL OFFICE: UNIVERSITY OF PANNONIA, P.O. BOX 158, VESZPRÉM H-8201 (HUNGARY)
Tel.: +36 (88) 624-746, E-mail: hjic@almos.uni-pannon.hu; web: hjic.mk.uni-pannon.hu
Felelős szerkesztő: Szilágyi Róbert Károly PhD
Kiadja: Pannon Egyetem, 8200 Veszprém, Egyetem u. 10.
Levélcím: H-8201 Veszprém, Postafiók 158, Tel.: (88) 624-000
Felelős kiadó: a Pannon Egyetem, Mérnöki Kar dékánja

EDITORIAL PREFACE

The Editorial Board of HJIC dedicates this Issue to the National Scientific Students' Associations (Tudományos Diákkör, in Hungarian, abbreviated as TDK) that is a real Hungaricum with a 62 years old tradition. This Association includes all the Universities and Colleges of Hungary, where scientific research of any kind is being conducted. The members of the Association are the faculty members, scientific advisors, and their B.Sc. or M.Sc. students.

Participation in the work of TDK is completely voluntary. Students spend some of their free time with a faculty mentor, choose a research topic, learn the basics of the field, do the measurements or the calculations under the supervision of the chosen teacher/researcher in addition to their regular academic duties. At the end, they write a dissertation based on their results. These dissertations are peer reviewed and then presented at yearly institutional TDK-Conferences, where the students receive suggestions from a panel of scientists and professors, receive a score for their written documents and oral presentations. Based on these scores, they may win legitimacy to present their results at the National TDK-Conference. TDK is a remarkable organization in Hungary that was kept alive by people who do their work from pure enthusiasm for the love of their profession. It is not an exaggeration to say that the TDK-students form the elite of all the University students. They are the ones who proceed to M.Sc. level, become PhD students, and, at the end, ideally become colleagues of their former faculty advisors.

During their work as part of TDK, students learn systematic problem-solving, formulating good questions, critical thinking, composing their thoughts into concise, well-formulated sentences, preparing meaningful figures, elaborating the literature of the field, and presenting their result in front of a scientific panel and an audience. Even those students who do not continue their life in the academia tend to remember their time spend on TDK activities as useful and memorable. Often, the skills acquired while being involved in a TDK project are not part of the regular education at a given University. TDK gives them something extra.

This issue contains selected articles from students and their supervisors about their results presented at the TDK conferences during 2013-2014. With this issue, the Editorial Board wishes to honour the effort of all TDK students and their advisors for keeping this unique tradition alive with their devoted work.

DEZSŐ BODA AND TIBOR DULAI
University of Pannonia, Veszprém, HUNGARY
Guest Editors

Hung. J. Ind. & Chem. *2014*, Vol. 42(1), pp. 1-56

Table of Contents

HUNGARIAN JOURNAL
OF INDUSTRY AND CHEMISTRY
VESZPRÉM
Vol. 42(1) pp. 1–5 (2014)

COMPARATIVE ASSESSMENT OF THE MUSSEL MICRONUCLEUS TEST VERSUS BACTERIAL BIOASSAYS FOR GENOTOXICITY TESTING OF BENZO[A]PYRENE

BETTINA ECK-VARANKA,[1]✉ ESZTER HORVÁTH,[1] ÁRPÁD FERINCZ,[1] GÁBOR PAULOVITS,[2] AND NÓRA KOVÁTS[1]

[1] Department of Limnology, University of Pannonia, Egyetem str. 10, Veszprém, H-8200, HUNGARY
[2]Centre for Ecological Research, Hungarian Academy of Sciences, Balaton Limnological Institute, Klebelsberg K. str. 3., Tihany, H-8237, HUNGARY
✉E-mail: kovats@almos.vein.hu

Polycyclic aromatic hydrocarbons are hazardous compounds to the environment and human health, thus their detection is an important task. In this study the genotoxic effect of benzo[a]pyrene (B[a]P) was examined on a freshwater mussel *Unio pictorum* and results were compared to bacterial tests, such as the Ames test and SOS chromotest. The aim of the study was to calibrate the sensitivity of the mussel micronucleus test to that of the two bacterial tests using B[a]P as a reference chemical. The Ames and the micronucleus tests gave similar response both in sensitivity and in concentration-response pattern. These two tests are proposed to be applied in a battery for genotoxicity testing.

Keywords: micronucleus test, Ames fluctuation test, SOS chromotest, PAH

Introduction

Polycyclic aromatic hydrocarbons (PAHs) are ubiquitous widespread contaminants. The US Environmental Protection Agency (EPA) created a list of priority pollutants that have the greatest concern due to potential exposure and adverse health effects on humans. There are 16 PAHs on this list, of which the most hazardous are acenaphthene, fluoranthene, naphthalene, benzo[a]anthracene and benzo[a]pyrene [1]. These compounds have proven to have carcinogenic and mutagenic effects on animals and humans, hence their regulation is very important [2].

Major sources of PAHs are internal combustion engines, residential heating, incineration, and coke production. There are also natural sources, such as forest fires or volcanoes. PAHs are present in the atmosphere as gas and/or particulate phases and might be transported to other environmental compartments such as soil, sediment, and water *via* dry or wet deposition. Heavier PAHs, such as benzo[a]pyrene (B[a]P), are almost totally adsorbed onto particles. Their further environmental fate in solid compartments is mostly influenced by their low water solubility. However, once taken up by the organism, the detoxification mechanism converts these compounds into more soluble molecules. It was shown that the seawater bivalve, *Mytilus sp*. can activate B[a]P to mutagenic compounds and produce reactive oxygen species (ROS) [3]. For assessing environmental exposure, benzo[a]pyrene seems to be a good indicator, due to the strong correlation between B[a]P and other PAHs [4]. In IARC Monograph Volume 3 it was concluded that benzo[a]pyrene produced tumours in a wide range of animals tested, following exposure by many different routes (oral, dermal, inhalation, intratracheal, intrabronchial, subcutaneous, intraperitoneal, intravenous). It had both a local and a systemic carcinogenic effect [5].

There are various reasons why the genotoxicity of PAHs as well as of other mutagenic compounds is tested on mussels. First of all, bivalves are sedentary creatures, being exposed to both water and sediment contamination. Secondly, their ability to bioaccumulate contaminants is well known and widely used in biomonitoring studies. Actually, the fact that they can not only bioaccumulate waterborne mutagens, but also metabolise them into active forms, on one hand increase their usefulness in these studies but on the other hand may enhance the potential risk to consumers [6].

Of genotoxicity markers, the micronucleus test (MN) is the most widely established, relatively easy-to-perform test. Micronuclei formation indicates chromosomal DNA damage occurring as a result of either chromosome breakage or chromosome mis-segregation during mitosis [7].

BANNI *et al*. used digestive gland cells of the marine mussel *Mytilus galloprovincialis* in an acute test. In this assay, mussels were exposed to 75 nM B[a]P for different exposure time. Micronucleus frequency started to show significant response after 24 hours exposure, reaching the maximum after 72 hours [8]. WOZNICKI *et al.* also tested B[a]P genotoxicity using the MN test, but

on another species, the freshwater *Sinanodonta woodiana* (referred to *Anodonta woodiana* in the original article) [9] in which the time-dependency of ecological effect was demonstrated. Maximum micronucleus formation was experienced after 4 days of exposure, but after it started to decrease, most possibly due to adaptive mechanisms.

The mussel micronucleus (MN) test has also been used in real-world environments, especially for detecting contamination from oil spills. BOLOGNESI *et al.* demonstrated that even 10 years after the wreck of the tanker Haven at the Ligurian coast of Italy, micronucleus frequency in caged oysters was a reliable way to detect the release of genotoxic compounds [10]. MARTINS *et al.* assessed genotoxicity of sediment containing PAHs and metals after dredging operations. The sediment previously was classified as 'trace contaminated', but dredging modified the mobility of pollutants, which was clearly visible in the mussel MN test [11]. In addition to the MN test for eukaryotic organisms, which results in chromosomal damage, several bacterial tests are also available for screening purposes due to their rapid response and short exposure time.

The SOS chromotest is a short-term, enzymatic colorimetric assay for the detection of the presence of genotoxic compounds using *Escherichia coli* PQ 37 strain as described by QUILLARDET *et al.* [12]. The SOS system is a complex, DNA-damage activated response under the regulation of the SOS promoter. In *E. coli* PQ 37 the only functioning β-galactosidase gene *(lacZ)* is fused to the bacterial *sfiA* SOS operon. Thus, SOS response initiates *lacZ* transcription, and β-galactosidase activity is detected spectrophotometrically by the addition of X-gal (5-bromo-4-chloro-3-indolyl-β-D-galactopyranoside) [13, 14].

The Ames bacterial reverse mutation assay applies genetically engineered strains of *Salmonella typhimurium*. The method is based on the chemical triggered reversion of histidine producing ability of the strains, enabling them to grow on histidine free medium. Several different methods have been developed, including the plate incorporation assay, the pre-incubation method, and the fluctuation test [15–17].

The Ames fluctuation test is a microplate adapted version of the Salmonella reverse mutation assay with a pH change indicated colorimetric endpoint. This method is suitable for the screening of large numbers of samples, and because of its sensitivity it is ideal for water sample testing [18].

The ability of both the SOS chromotest and the Ames test to detect genotoxicity of B[a]P has been long established [19, 20]. B[a]P was also used as a reference chemical for calibrating the newt micronucleus test or Jaylet test [21].

The correlation between the genotoxic substances and the number of micronuclei in an organism has been used in water toxicological tests since the 1980's [22]. The micronuclei are small bodies containing DNA parts that appear near the nucleus as a result of chromosome breakage or mitotic spindle dysfunction. This process can occur without external factors as well, but the effect of genotoxic substances made a far greater number of micronuclei than normal. Therefore the micronuclei frequency may characterise the extent of genetic damage that accumulate over the life of the individual [23]. The MN test, performed on freshwater mussel species, is widely distributed for assessing genotoxic effects triggered by environmental pollutants [24, 25].

Still, the micronucleus test has gained relatively low attention in Hungary, therefore a native freshwater mussel, *Unio pictorum* was introduced as test organism. Main aim of the study was to calibrate this test also using B[a]P as reference chemical, by comparing its sensitivity to that of the bacterial assays.

Materials and Methods

Test organisms

Unio pictorum specimens were collected from Lake Balaton and were kept in a flow-through aquarium. Water source was Lake Balaton water, therefore not only proper oxygenation was ensured, but a constant food supply as well. Animals were acclimatized for 4 weeks prior to testing.

Test conditions and treatment

The assay was performed based on the protocol described by WOZNICZKI *et al.* with some modifications. A B[a]P stock solution was prepared in acetonitrile in 1 mg cm^{-3} concentration for the following series: 70 µg dm^{-3}, 175 µg dm^{-3}, 350 µg dm^{-3} and 700 µg dm^{-3}. For solvent control 0.07% acetonitrile was used, and solvent quantity was adjusted to 0.07% in each treatment. *U. pictorum* specimens with length of 5–8 cm were used. Treatments were performed in triplicates. For each concentration and for the controls, the volumes of the aquaria were 3 l. They were aerated during the experiment and temperature was set at 22 ^{o}C. Exposure time was 4 days.

Micronucleus test

After 4 days, haemolymph was taken from the posterior adductor using the non-lethal technique described by GUSTAFSON *et al.* [26]. A 1 ml aliquot of haemolymph was mixed with 0.3 ml, 10% acetic acid in methanol as a fixative and centrifuged at 1000 rpm for 5 minutes. The supernatant was discarded and the rest was fixed in 1 ml 80 % ethanol. In this way the sample can be kept refrigerated for several weeks. For processing the samples, refrigerated samples were centrifuged again at 1000 rpm for 5 minutes. The supernatant was discarded and the pellet containing the cells was smeared onto a microscope slide and allowed to dry. After that the slides were fixed in 80 % methanol, dried and stained with 5 % Giemsa in distilled water for 20 minutes.

Photos were taken by a Zeiss AxioScope A1 microscope with an AxioCam ICC1 camera and Zen 2011 program at 400x magnification. Micronuclei were

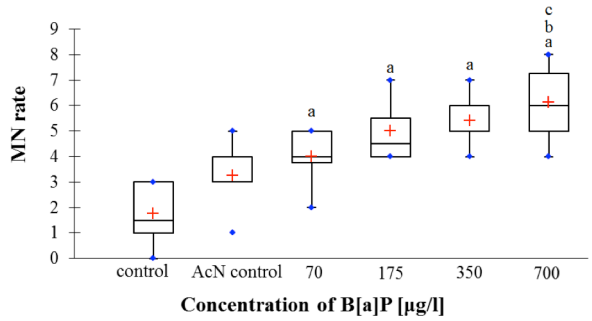

Figure 1: Result of the MN test with B[a]P showing significant difference compared to control (a), to AcN control (b) and to 70 µg dm^{-3} B[a]P (c)

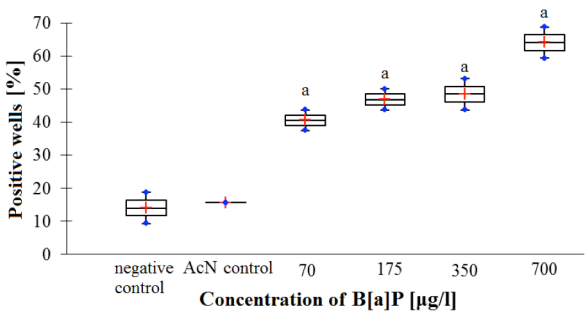

Figure 2: Result of the S9 supplemented fluctuation Ames test with B[a]P (significant difference compared to control (a))

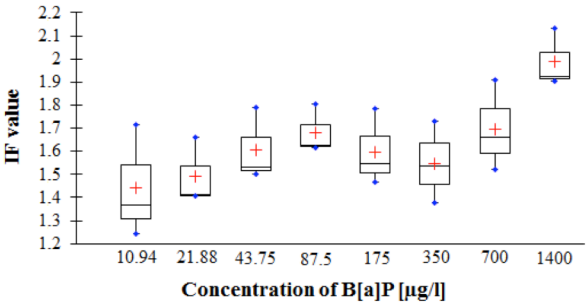

Figure 3: Result of the S9 supplemented SOS chromotest with B[a]P

identified according to FENECH [27]. For each animal 250 cells were counted. One-way ANOVA with Tukey post hoc test was used to compare the mean MN numbers between the treatments.

For SOS chromotest the SOS chromotest TM kit (EBPI – Environmental Bio-detection Products Inc.) was used according to the manufacturer's instructions, and in compliance with the OECD guidelines No 471:1977 [28]. B[a]P concentrations were 1400 µg dm^{-3}, 700 µg dm^{-3}, 350 µg dm^{-3}, 175 µg dm^{-3}, 87.5 µg dm^{-3}, 43.75 µg dm^{-3}, 21.88 µg dm^{-3}, 10.9 µg dm^{-3}, 0 µg dm^{-3}. Acetonitrile concentration was adjusted to 0.07% in each sample, and an additional DMSO solvent control was also used. The absorbance of samples was detected on 615 and 405 nm with DiareaderELx800 ELISA device. The SOS repair system induction was measured by the calculation of induction factor (IF) and induction potential (SOSIP) according to KRIFATON [29]. Samples with 1.5 or higher IF were considered genotoxic.

Ames test

The fluctuation Ames test was performed according to HUBBARD with slight modification. In short, *Salmonella typhimurium* TA100 cells were pre-cultured overnight in nutrient broth (Oxoid) on 37 ºC. Cells were washed twice in Davis minimal medium (67.4 mM PO_4^{3-}, 8.38 mM SO_4^{2-}, 15.1 mM NH_4^+, 5.1 mM Na^+, 98.1 mM K^+, 0.83 mM Mg^{2+}, 1.7 mM citrate, 139 µM glucose 10 µg cm^{-3} histidine, 0.1 mg cm^{-3} D-biotin) and cell number was adjusted to 10^6 cells cm^{-3}. B[a]P was added to the samples in 700 µg dm^{-3}, 350 µg dm^{-3}, 175 µg dm^{-3}, 70 µg dm^{-3} and 0 µg dm^{-3} and acetonitrile concentration was adjusted to 0.07%. Samples were distributed in 200 µl volumes to 96 well microplates. Cell free control, a solvent free negative control, and a positive control with 0.5 µg cm^{-3} concentration NaN_3 were also applied. Plates were incubated in humid chamber for 72 hours in 37 ºC. On the day of evaluation 20 µl of 2 mg cm^{-3} aqueous solution of bromcresolpurple was added to each sample. Purple colour signified negative, yellow positive (cell growth) result. Intermediate shades were regarded positive. The experiment was also performed with S9 activation, in which case 10 ml suspension contained 2.5 ml S9 mix (EBPI) assembled according to the producer's guide (S9 activation simulates metabolic processes in the liver of higher organisms). For positive control 2-amino-antracene was used in 100 µg cm^{-3} concentration. For the evaluation of mutagenic effect the χ^2-test was applied with 95% confidence level [30].

Results and Discussions

Genotoxic response is expressed as number of micronuclei/250 cells in case of the mussel micronucleus test, percentage of positive wells in case of the Ames test and IF value in case of the SOS chromotest. Significant difference between the control and all treatments was observed in case of micronucleus numbers (ANOVA: $F = 12.015$; $df = 5$; $P < 0.00001$, Tukey post hoc: $P < 0.002$); however, only the highest concentration treatment differed from the AcN-control (Tukey post hoc $P = 0.02$). The difference between the lowest (70 µg dm^{-3}) and highest (700 µg dm^{-3}) concentrations was also indicated *(Fig.1)*.

χ^2-square tests indicated significant differences between the control and all treatments in case of ratios of Ames fluctuations test ($P < 0.0017$) *(Fig.2)*. The results of SOS chromotest are shown in *Fig.3*.

To date no assessment has been published for comparing the sensitivity of the mussel micronucleus test and bacterial genotoxicity assays. There are a few comparative works; however, those are based on amphibian micronucleus tests. One protocol uses *Xenopus laevis* embryos and the end-point of the test is number of micronucleated erythrocytes per thousand. The test is standardised, international and some national

test protocols apply, e.g. the AFNOR NFT 90-325 procedure [31]. MOUCHET *et al.* tested genotoxicity of PAH-contaminated soil leachates on the amphibian MN test and two bacterial tests (Ames and Mutatox) [30]. The latter test developed by the Microbics Company (now Azur Environmental) uses dark mutants of the luminescent bacterium *Vibrio fischeri*. In the presence of mutagenic compounds, these mutants can revert and recover their luminescence, which is easily measurable by a luminometer. It was found that the MN test was able to detect genotoxicity, while the Ames test was not. Sensitivity of the Mutatox test was intermediate. It should be noted that chemical analysis of both soil and leachate samples revealed much lower individual PAH concentration in leachates than in the soil samples.

LE CURIEUX *et al.* used the SOS chromotest, the Ames fluctuation test and another amphibian, the newt *Pleurodeles waltl* for a comparative assessment of 7 chemicals, including B[a]P. In their study, the newt micronucleus test was the most sensitive, the fluctuation test and the SOS chromotest gave practically similar but lower response [33].

In our study all three tests gave positive response, but analysis of the concentration-response graphs shows somewhat different patterns. Bacterial tests gave positive response only with S9 activation. Ideal concentration-response graphs were found for the MN test and the S9 supplemented Ames test. Ideal concentration-response curve is observed when the response steadily increases for each higher effluent concentration [34]. Main difference is the response given in the AcN control, which elucidated micronucleus formation but the Ames test gave practically the same response for both controls. Notably, WOZNICZKI *et al.* did not find concentration-response relationship when tested B[a]P on *Sinanodonta woodiana*.

In the SOS chromotest after S9 activation, positive response was given for the lowest concentration, but no clear concentration-response relationship could be established. In general, sensitivity of the SOS chromotest is considered lower than that of the Ames test. For example, there are mutagenic compounds that do not induce the SOS response, such as benzidine, cyclophosphamide, acridines, and ethidiumbromide [13].

Conclusions

The very similar response of the Ames test and the micronucleus test (considering both sensitivity and concentration-response pattern) indicate that B[a]P elucidates both chromosomal aberrations and point mutation, and is genotoxic for prokaryotes and eukaryotes as well; however, this is not necessarily the case for all potentially genotoxic chemicals. As such, for testing genotoxicity of either individual compounds or environmental samples, application of both tests can be advised, defining the minimum necessary battery as the MN and Ames tests.

Acknowledgements

This work was supported by the TÁMOP-4.2.2.A-11/1/KONV-2012-0064 research program. This project is supported by the European Union and co-financed by the European Social Fund.

REFERENCES

[1] USEPA: Priority Pollutants List (Appendix A to 40 CFR Part 423). U.S. Environmental Protection Agency, Office of Water, *2000*

[2] GASPARI L., CHANG S.S., SANTELLA R.M., GARTE S., PEDOTTI P., TAIOLI E.: Polycyclic aromatic hydrocarbon-DNA adducts in human sperm as marker of DNA damage and infertility, Mutation Res., *2003*, 535, 155–160

[3] LIVINGSTONE D.R., GARCIA MARTINEZ P., MICHEL X., NARBONNE J.F., O'HARA S., RIBERA D., WINSTONE G.W.: Oxyradical generation as a pollution-mediated mechanism of toxicity in the common mussels, *Mytilus edulis L.*, and other mollusks, Func. Ecol., *1990*, 4, 415–424

[4] RUBAILO I., OBERENKO A.V.: Polycyclic Aromatic Hydrocarbons as Priority Pollutants, J. Siberian Fed. Uni. – Chem. *2008*, 4(1), 344–354

[5] IARC: Certain polycyclic aromatic hydrocarbons and heterocyclic compounds. IARC Monographs of the Evaluation of the Carcinogenic Risk of Chemicals to Humans, *1973*, 3, 1–271

[6] FERGUSON L.R., GREGORY T.J., PEARSON A.E., HAY J.E., LEWIS G.D.: Mutagenicity tests as a monitoring tool for potential mutagens and carcinogens in shellfish gathering areas of New Zealand, New Zealand J. Marine Freshwater Res., *1996*, 30(4), 413–421

[7] BOLOGNESI C., FENECH M.: Mussel micronucleus cytome assay, Nature Protocols, *2012*, 7(6), 1125–1137

[8] BANNI M., NEGRI A., DAGNINO A., JEBALI J., AMEUR S., BOUSSETTA H.: Acute effects of benzo[a]pyrene on digestive gland enzymatic biomarkers and DNA damage on mussel *Mytilus galloprovincialis*, Ecotoxicology Environ. Safety, *2010*, 73, 842–848

[9] WOZNICZKI P., LEWANDOWSKA R., BRZUZAN P., ZIOMEK E., BARDEGA R.: The level of DNA damage and the frequency of micronuclei in haemolymph of freshwater mussels *Anodonta woodiana* exposed to benzo[a]pyrene, Acta Toxicologia, *2004*, 12(1), 41–45

[10] BOLOGNESI C., PERRONE E., ROGGIERI P., SCIUTTO A.: Bioindicators in monitoring long term genotoxic impact of oil spill: Haven case study, Marine Environ. Res., *2006*, 62, 287–291

[11] MARTINS M., COSTA P.M., RAIMUNDO J., VALE C., FERREIRA A.M., COSTA M.H.: Impact of remobilized contaminants in *Mytilus edulis* during dredging operations in a harbour area: Bioaccumulation and biomarker responses, Ecotoxicology Environ. Safety, *2012*, 85, 96–103

[12] QUILLARDET P., HOFNUNG M.: The SOS Chromotest, a colorimetric bacterial assay for genotoxins: procedures, Mutation Res., *1985*, 147, 65–78

[13] QUILLARDET P., HOFNUNG M.: The SOS chromotest: A review, Mutation Res., *1993*, 297(3), 235–279

[14] HOFNUNG M., QUILLARDET P., GOERLICH O., TOUATI E.: SOS chromotest and the use of bacteria for the detection and diagnosis of genotoxic agents, Trends in Genetic Risk Assessment Academic Press, London, *1989*, pp. 125–136

[15] AMES B.N., LEE F.D., DURSTON W.E.: An Improved Bacterial Test System for the Detection and Classification of Mutagens and Carcinogens, PNAS USA, *1973*, 70(3), 782–786

[16] MORTELMANS K., ZEIGER E.: The Ames Salmonella/microsome mutagenicity assay, Mutation Res., *2000*, 455(1–2), 29–60

[17] JOMINI S., LABILLE J., BAUDA P., PAGNOUT C.: Modifications of the bacterial reverse mutation test reveals mutagenicity of TiO_2 nanoparticles and byproducts from a sunscreen TiO_2-based nanocomposite, Toxicology Lett., *2012*, 215, 54–61

[18] LE CURIEUX F., GILLER S., GAUTHIER L., ERB F., MARZIN D.: Study of the genotoxic activity of six halogenated acetonitriles, using the SOS chromotest, the Ames-fluctuation test and the newt micronucleus test, Mutation Res., *1995*, 341, 289–302

[19] QUILLARDET P., DE BELLECOMBE C., HOFNUNG M.: The SOS Chromotest, a colorimetric bacterial assay for genotoxins: validation study with 83 compounds, Mutation Res., *1985*, 147, 79–95

[20] BRAMS A., BUCHET J.P., CRUTZEN-FAYT M.C., DE MEESTER C., LAUWERYS R., LÉONARD A.: A comparative study, with 40 chemicals, of the efficiency of the Salmonella assay and the SOS Chromotest (kit procedure), Toxicology Lett., *1987*, 38, 123–133

[21] ZOLL-MOREUX C.: Consequences of the contamination of the aquatic environment by mercury, benzo(a)pyrene, and organochlorine pesticides for two amphibians *Pleurodeles waltl* and *Xenopus laevis*, PhD Thesis, Paul Sabatier University Toulouse, 1991, Toulouse, *1991* (in French)

[22] DAS R.K., NANDA N.K.: Induction of micronuclei in peripheral erythrocytes of fish *Heteropneustes fossilis* by mitomycin C and paper mill effluent, Mutation Researches, *1986*, 175, 67–71

[23] BOLOGNESI C., BUSCHINI A., BRANCHI E., CARBONI P., FURLINI M., MARTINO A., MONTEVERDE M., POLI P., ROSSI C.: Comet and micronucleus assays in zebra mussel cells for genotoxicity assessment of surface drinking water treated with three different disinfectants, Sci Total Environ., *2004*, 333(1–3), 127–136

[24] SCARPATO R., MIGLIORE L., BARALE R.: The micronucleus assay in *Anodonta cygnea* for the detection of drinking water mutagenicity, Mutation Res., *1990*, 245, 231–237

[25] DOPP E., BARKER C.M., SCHIFFMANN D., REINISCH C.L.: Detection of micronuclei in hemocytes of *Mya arenaria*: association with leukemia and induction with an alkylating agent, Aquatic Toxicology, *1996*, 34, 31–45

[26] GUSTAFSON L.L., STOSKOPF M.K., BOGAN A.E., SHOWERS W., KWAK T.J., HANLON S., LEVINE J.F.: Evaluation of a nonlethal technique for hemolymph collection in *Elliptio complanata*, a freshwater bivalve (Mollusca: Unionidae), Diseases of Aquatic Organisms *2005*, 65,159–165

[27] FENECH M., NEVILLE S.: Conversion of excision-repairable DNA lesions to micronuclei within one cell cycle in human lymphocytes, Environ. Mol. Mutagenesis, *1992*, 19(1), 27–36

[28] OECD Guidelines No. 471: Bacterial Reverse Mutation Test, *1977*

[29] KRIFATON CS.: Development of biomonitoring systems for detecting aflatoxin-B1 and zearalenon. PhD Thesis, Szent István University, Gödöllő, *2012* (in Hungarian)

[30] HUBBARD S.A., GREEN M.H.L., GATEHOUSE D., BRIDGES J.W.: The fluctuation test in bacteria, Handbook of Mutagenicity Test Procedures, *1984*, pp. 141–160

[31] Association française de normalisation (AFNOR) Standard NFT90-325. Water quality. Evaluation of genotoxicity using amphibian larvae *(Xenopus laevis*, *Pleurodeles waltl)*, *2000* (in French)

[32] MOUCHET F., GAUTHIER T.L., MAILHES C., JOURDAIN M.J., FERRIER V., TRIFFAULT G., DEVAUXE A.: Biomonitoring of the genotoxic potential of aqueous extracts of soils and bottom ash resulting from municipal solid waste incineration, using the comet and micronucleus tests on amphibian *(Xenopus laevis)* larvae and bacterial assays (Mutatox® and Ames tests), Sci. Total Environ., *2006*, 355, 232–246

[33] LE CURIEUX F., MARZIN D., FRANÇOISE E.: Comparison of three short-term assays: results on seven chemicals. Potential contribution to the control of water genotoxicity, Mutation Res., *1993*, 319, 223–236

[34] USEPA: Method Guidance and Recommendations for Whole Effluent Toxicity (WET) Testing (40 CFR Part 136). EPA 821-B-00-004, U.S. Environmental Protection Agency, Office of Water, *2000*

HUNGARIAN JOURNAL OF INDUSTRY AND CHEMISTRY

HJIC

Advertise upcoming meetings,

conferences and workshops;

make public announcements;

introduce your research laboratory;

a new product or a service

on the pages of the

Hungarian Journal of Industry and Chemistry

Please contact us if interested!

EDITORIAL OFFICE: UNIVERSITY OF PANNONIA
P.O. BOX 158, VESZPRÉM H-8201 (HUNGARY)
Tel.: +36 (88) 624-746, E-mail: hjic@almos.uni-pannon.hu;
web: hjic.mk.uni-pannon.hu
Felelős szerkesztő: Szilágyi Róbert, PhD
Kiadja: Pannon Egyetem, 8200 Veszprém, Egyetem u. 10.
Levélcím: H-8201 Veszprém, Postafiók 158, Tel.: (88) 624-000

HUNGARIAN JOURNAL
OF INDUSTRIAL CHEMISTRY
VESZPRÉM
Vol. 42(1) 7–12 (2014)

IMPROVING THE INTERFACIAL PROPERTIES OF GLASS FIBRE REINFORCED AND UNREINFORCED WASTE SOURCED LOW DENSITY POLYETHYLENE/ACRYLONITRILE BUTADIENE STYRENE/POLYSTYRENE COMPOSITES

JÁNOS SÓJA,[1] VLADIMIR SEDLARIK,[2] PAVEL KUCHARCZYK,[2] AND NORBERT MISKOLCZI[1]✉

[1] MOL Department of Hydrocarbon & Coal Processing, Institute of Chemical Engineering and Process Engineering, Faculty of Engineering, University of Pannonia, Egyetem u. 10, Veszprém, H-8200, HUNGARY
[2] Centre of Polymer Systems, University Institute, Tomas Bata University in Zlin, Nad Ovcirnou 3685, Zlín, 76001, CZECH REPUBLIC
✉E-mail: mnorbert@almos.uni-pannon.hu

This work is focused on compatibilization of immiscible waste sourced low density polyethylene (LDPE), acrylonitrile butadiene styrene (ABS), and polystyrene (PS) blends by different surface modifying routes. To reach better mechanical properties of the given reused waste blends 20% glass fibre was used. The ratio of waste LDPE/ABS/PS was 3.6/2.0/1.0 both in the presence and absence of glass fibre, while the applied concentration of the surface modifying routes was 1% in each case. Blends of raw materials had been manufactured by two roll mill, and specimens were obtained by the press moulded plates. The properties of samples were studied by mechanical testing. Results show that blending of the three kinds of waste polymers without compatibilizers resulted immiscible blends with poor mechanical properties. This could be significantly improved by the application of the commercial and synthetic surface treatment additives. Generally, favourable properties were found in the presence of 20% glass fibre. Especially AD-1 and AD-2 experimental and commercial γ-aminopropylsilane additives showed the best results.

Keywords: immiscible, compatibilizer, waste mechanical recycling, tensile strength

Introduction

Owing to the increasing application of polymers, the utilization of wastes plastics causes serious challenges. According to reports the energetic utilization of polymer wastes were mainly investigated, such as incineration, chemical recycling, and/or mechanical recycling [1–7]. It is also well known that the industrially used plastics are not exchangeable with other constructional materials (glass, metals, etc.). Excess energy use and/or more greenhouse gas emissions would be incurred upon replacement of plastics with other materials. Therefore most of the key industrial segments, such as transportation, aviation, packaging, civil engineering, cannot function without polymers. From the 50s' the plastic industry went through a significant development, which is a reason for their wide-spread and diverse applications often for highly specific purposes. In the case of plastic composites, they provide alternative solutions to problems of increasing strength, maintaining compatibility and malleability [2, 4, 6–14].

The mechanical recycling of polymers is a reshaping process using waste polymeric materials or even the mixtures of unused and waste polymers. Basically the waste polymer can be originated from two sources. In "closed-loop" recycling, the same product is manufactured from the same recycled components. For instance, the material of bottles (in some cases) can be recycled. In contrast, there is a recycling route, when the repeated remanufactured products are becoming less valuable [10–12, 15, 16]. A major challenge in mechanical recycling of polymers is immiscibility that leads to phase separation causing significant reductions in mechanical properties of the polymer mixtures. There are specific kinds of polymers that are immiscible with each other, such as polyolefin-PA, polyolefin-ABS, polyolefin-PET. Therefore, polymer blends may contain two phases, such as disperse and continuous.

Generally, the difference in chemical and physical properties of phases are the source of the above mentioned immiscibility problem. Therefore, coupling agents with special chemical structure can be used to create adequate chemical/physical interaction between the constituents of polymer mixtures. For this purpose grafted-MA or silane based compounds are widely used. These compatibilizers are able to increase the interfacial tension in boundary layer of polymer blends, which results in better chemical/physical interactions [17, 18].

Table 1: The main properties of waste polymers

	LDPE	ABS	PS
tensile strength, MPa	15.8±1.4	34.4±2.5	25.6±1.9
tensile modulus, MPa	420±33	1750±88	1720±95
elongation, %	351.5±35.5	4.7±0.3	189.6±10.2
flexural strength, MPa	-	29.0±2.2	21.0±1.7
flexural modulus, MPa	-	1820±79	1140±73
CHARPY strength, kJ mm^{-2}	3.8±0.4	10.5±1.1	5.9±0.4

Table 3: Sample compositions without glass fibre in weight %

Sample No.	1	2	3	4	5	6	7	8
LDPE	55	54	54	54	54	54	54	54
ABS	30	30	30	30	30	30	30	30
PS	15	15	15	15	15	15	15	15
C-1	-	1	-	-	-	-	-	-
C-2	-	-	1	-	-	-	-	-
AD-1	-	-	-	1	-	-	-	-
AD-2	-	-	-	-	1	-	-	-
AD-3	-	-	-	-	-	1	-	-
AD-4	-	-	-	-	-	-	1	-
Peroxide	-	-	-	-	-	-	-	1

In this work, the feasibility of mechanical recycling of automotive industry waste mixtures of low-density polyethylene (LDPE), acrylonitrile butadiene styrene (ABS), and polystyrene (PS) were studied. The effects of various compatibilization techniques on mechanical properties of the prepared ternary ABS/LSPE/PS systems were studied.

Materials and Methods

Raw Materials

Waste polymers used as raw materials in our experimental work were selectively collected directly from automotive industry. The main properties of the plastic wastes are summarized in *Table 1*. The LDPE has the lowest tensile strength (15.8 MPa), which is followed by the polystyrene (25.6 MPa), and the ABS (34.4 MPa). Tensile modulus showed similar order as well. Due to the chemical structure of plastics, the LDPE had the highest elongation (351.5%), while ABS the lowest (4.7%). The average particle size for each tested plastic wastes were in the range of 4–5 mm, with moisture content of 0.7–0.8 %. Moreover, significant differences were noticed in the CHARPY impact strength of samples; because the maximum value was measured in the case of ABS (10.5 kJ mm^{-2}), while the smallest regarding LDPE (3.8 kJ mm^{-2}).

Table 2: The main of experimental coupling agents

	AD-1	AD-2	AD-3	AD-4
appearance	solid	dense liquid	solid	solid
side chain	C_{16}-C_{18}	polyisobutylene	styrene	C_{20}-C_{22}

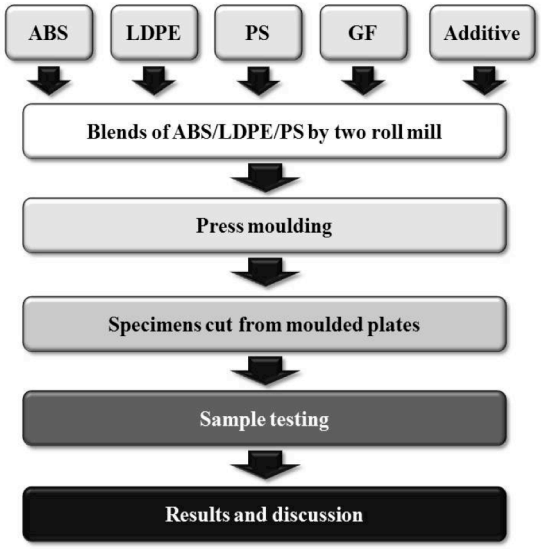

Figure 1: Sample preparation and testing

As known, blends of ABS and LDPE are immiscible phases in the most cases. Therefore, the mechanical properties of ABS and LDPE blend are significantly worse than that of the constituents, either ABS or LDPE. In order to enhance their properties, the interfacial forces must be improved between the constituents. In our work, different commercial and synthetic compatibilizers were used for improving the interfacial properties and decrease the interfacial tension of composites. Two commercially available compounds of γ-aminopropyl silane (C-1) (Aldrich Chemistry), and polyethylene grafted with maleic anhydride (C-2) (Viba Spa) were used as compatibilizer agents. The synthetic agents were maleic anhydride intermediates made from different olefins at the Department of MOL Hydrocarbon and Coal Processing, University of Pannonia with significantly different physical and chemical properties. The main properties of the four additives are summarized in *Table 2*.

Sample Preparation

Blends of waste LDPE/ABS/PS were prepared by two roll mill. Then sample plates were manufactured by press moulding. *Fig.1* demonstrates the flow of the experimental work.

For composite manufacturing a Labtech two roll mill (Labtech ltd, Thailand) was used. The temperatures of the rolls were 170 °C and 190 °C with friction ratio of 0.5. The compositions of samples are summarized in *Tables 3* and *4*.

In selected cases E-type unsized glass fibre with 4–5 cm average length was also added to the composites in its 20%. The E-type GF was produced by Ovens

Table 4: Sample compositions with glass fibre in weight %

Sample No.	**10**	**11**	**12**	**13**	**14**	**15**	**16**
LDPE	43	43	43	43	43	43	43
ABS	24	24	24	24	24	24	24
PS	12	12	12	12	12	12	12
GF	20	20	20	20	20	20	20
C-1	1	-	-	-	-	-	-
C-2	-	1	-	-	-	-	-
AD-1	-	-	1	-	-	-	-
AD-2	-	-	-	1	-	-	-
AD-3	-	-	-	-	1	-	-
AD-4	-	-	-	-	-	1	-
Peroxide	-	-	-	-	-	-	1

Corning and it contained mainly SiO_2, CaO and Al_2O_3. The ratio of waste LDPE/ABS/PS was 3.6/2/1 both in the presence and absence of glass fibre, while the applied concentration of the additives was 1% in each case. The additives were directly added to the molten polymer during the sample sheet manufacturing. In two cases organic peroxide (di-*tercier*-butyl-peroxide) was used to modify the interfacial surface of composites.

The sample blending composites were press moulded at 180 °C using 6.8 ton loading and then specimens with dimension of 1 mm x 10 mm x 100 mm were cut from the composite plates.

Determination of Tensile Strength

The tensile properties of the composites were determined by Instron 3345 universal tensile machine using 90 mm/min crosshead displacement rate. During the tests, the ambient temperature was 23 °C, and the relative humidity was 35 % in all cases. Preloading was not applied.

Determination of Flexural Strength

The three point flexural tests were performed by also the before mentioned Instron 3345 universal tensile tester. The crosshead displacement rate was 20 mm min^{-1} in all cases.

Determination of Charpy Impact Properties

A CEAST Resil IMPACTOR was used for determination of Charpy impact strength. The machine was equipped with a 4J hammer, while the specimens were cut.

Results and discussion

Tensile properties

Fig.2 compares the tensile strength of samples. It can be seen that the tensile strength has changed in the range of

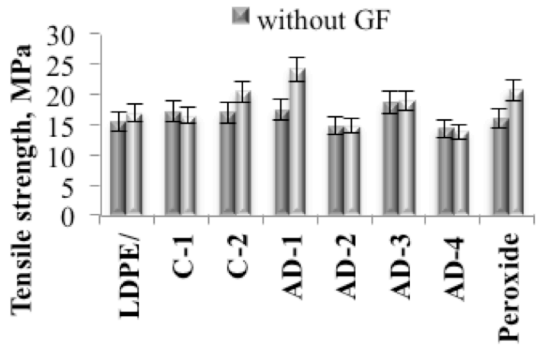

Figure 2: Tensile strength of samples

13.8 and 24.1 MPa. However, the reinforced composites

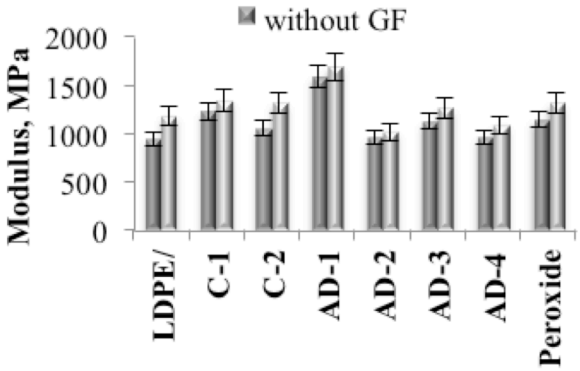

Figure 3: Tensile modulus of LDPE/ABS/PS samples

have significantly better resistance against constant tensile loading (13.8–24.1 MPa), than that of unreinforced (14.2–18.5 MPa). According to data the highest values were obtained in the case sample containing A-1 surface modifier agent in the presence of GF (24.1 MPa), while that was the highest in using AD-3 additive without GF (18.5 MPa).

From *Table 1*, the raw materials had 34.4 MPa (ABS), 25.6 MPa (PS) and 15.8 MPa (LDPE) tensile strength. On the contrary, the untreated LDPE/ABS/PS composites have tensile strength of 15.3 MPa without fibres, and 16.8 MPa in the presence of 20% glass fibre. It means that presumably owing to the immiscible phases the LDPE/ABS/PS composites without surface modifying additive has lower strength than its constituents. In three samples (C-1, AD-2, and AD-4) the tensile strength of glass fibre free, but treated composites was lower than that of untreated. This is probably due to the reason of the additive has been disadvantageously altered in surface characteristics of the plastic mixture. The largest increase in the tensile strength occurred for AD-1 (+12%) and AD-3 (+21%) additives without GF, while the peroxide (+23%), and AD-1 (43%) samples have resulted the best properties using 20% glass fibre, as well.

The Young's modulus, as the measure of the elastic property of sample, changed in the range between 1015 and 1685 MPa in the presence of glass fibre, while the values were between 937 and 1579 MPa without GF reinforcing *(Fig.3)*. The maximum value of tensile modulus was found by the using AD-1 surface treating agent both presence and absence of GF (1579 MPa and

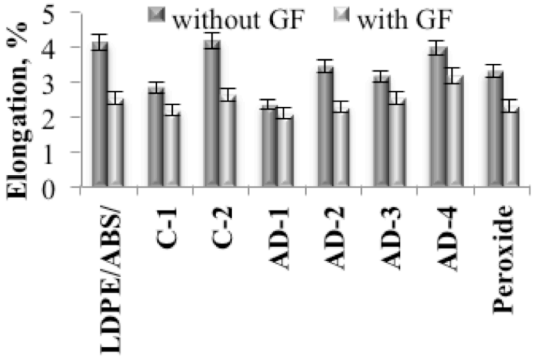

Figure 4: Elongation of samples measured at tensile test

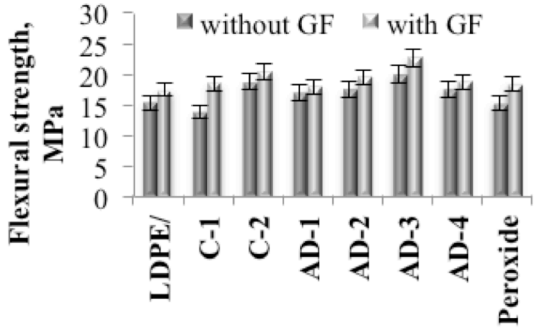

Figure 5: Flexural strength of LDPE/ABS/PS samples

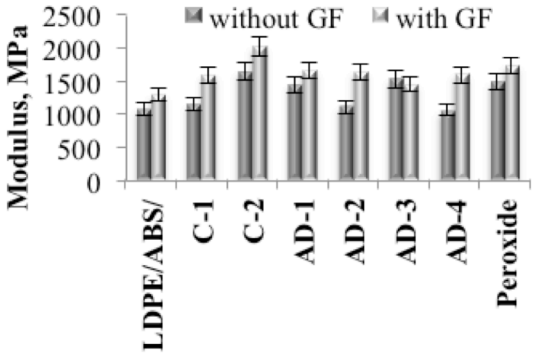

Figure 6: Flexural modulus of ABS/LDPE/PS samples

1685 MPa). On the basis of data in *Table 1*, the tensile modulus of LDPE, ABS and PS raw materials were 420, 1750 and 1720 MPa, respectively. The untreated LDPE/ABS/PS samples had significantly lower tensile moduli with 937 MPa and 1173 MPa in the presence and absence of GF, respectively. Presumably it was the consequence of the phase separation occurring the immiscible polymers. The compatibility of immiscible polymer blends could be significantly improved by the above mentioned additives, because not only the tensile strength, but also the tensile modulus was significantly increased e.g. by the application of AD-1 additive (+44 % with GF and +69% without GF). In general, the tensile modulus was higher in the presence of glass fibre than without that.

The relative elongation refers to the change in sample length during the tensile tests. Rigid materials (polyamide, ABS, etc.) have low value of elongation, while that of significantly higher in case of soft or rubber like elastic polymers (polyethylene, PP, PS, rubber, etc.).

The relative elongation *(Fig.4)* follows the opposite trends than tensile strength or modulus. It is changed in the range of 2.33 and 4.29% without GF, or 2.09 and 3.16% with GF. It means that the glass fibre presence resulted lower values of relative elongation. The surface treating agents have only slight effect to the elongation apart from AD-1 sample, because the difference between the treated and untreated samples was 63% in case of AD-1. In any other cases this value was less than 20%.

Flexural Properties

Results from flexural tests are summarized in *Figs.5* and *6*. The flexural strength was in the range of 17.3 and 22.6 MPa in case of GF reinforced LDPE/ABS/PS composites and between 13.7 and 19.9 MPa in case of unreinforced specimens. The best result was found when the interfacial surface of LDPE/ABS/PS composite and/or the glass fibre surface were modified by AD-3 additive (22.6 MPa). In the presence of AD-3 additive the unreinforced LDPE/ABS/PS blend had 19.9 MPa flexural strength value. Generally, the tensile properties were favourable in case of reinforced, than that of unreinforced samples. According to *Table 1*, the waste ABS and PS raw materials had flexural strength of 29.0 MPa and 21.0 MPa, respectively. On the other hand, the flexural strength of unreinforced LDPE/ABS/PS was 15.3 MPa, which can be increased to 17.3 MPa in the presence of GF. It means that the flexural strength was below the lowest value of constituent (PS, 21.0 MPa) even in the presence of GF. Co MParing tensile and flexural strength, it can be concluded that the effect of the surface modifying agents were more significant to the tensile than to the flexural properties. The negative effect of surface modifying agents was observed in some cases. For instance, flexural strength was reduced in case of C-1 and peroxide additives. Regarding the flexural strength the largest increase occurred in the presence of AD-3 (+30%) and C-2 (+22%) additives without glass fibre reinforcements. The increasing in flexural strength was 30% (without GF) and 31% (with GF) in case of AD-3 additive, while that of was 22% (without GF) and 17% (with GF).

Regarding flexural modulus, similar results were obtained as discussed above. ABS and PS raw materials have 1820 and 1140 MPa flexural modulus, respectively. According to *Fig.6*, the flexural modulus was 1080 MPa and 1285 MPa in case of unreinforced and reinforced LDPE/ABS/PS composite without surface treating agents. The flexural modulus indicates the rigidity. Higher modulus means greater rigidity. Results demonstrate that the flexural modulus changes in the range 1285 and 2015 MPa in the presence of GF, whereas values were between 1040 and 1637 MPa in case of the non-reinforced composites. The maximum value of flexural modulus was given specimens

containing C-2 surface treating additives both with and without glass fibres.

CHARPY Impact Strength

The CHARPY impact test determines the amount of energy absorbed by a material during fracture. *Fig.7* summarizes the CHARPY impact strength of samples as a function of surface treatment additives. The impact strength of the samples ranged from 4.7 to 9.1 kJ mm^{-2}, in which reinforced composite materials was between the higher range of 5.9 and 9.1 kJ mm^{-2}. The highest value was in a sample including AD-1 surface modification agent, and glass fibre (9.1 kJ mm^{-2}). In case of the same additive without reinforced fibre the impact strength was 7.1 kJ mm^{-2}.

Results show that the impact strength could be increased in each case due to surface treatment. The impact strength of LDPE/ABS/PS composite was 4.7 kJ mm^{-2} without reinforced and 6.8 kJ mm^{-2} in reinforced by glass fibres. The largest growth was observed in the case of the sample containing C-2 (+53%) and AD-1 (+51%) additives for samples without glass fibres. Contrary, the least growth was observed in the case of the sample containing AD-2 (+4%) additives. Regarding the GF reinforced samples, the largest growth was observed when the AD-1 (+34%) and C-2 (+29%) additive were used. Only the AD-2 additive resulted in lower impact strength, than ABS/LDPE/PS excluding any additive (-13%).

Conclusion

In this paper the efficiency of different compatibilizers in waste sourced LDPE/ABS/PS composite were investigated both in absence and presence of 20% E-type glass fibre. It was found that both the tensile and flexural properties of samples could be significantly improved by both synthetic and commercial coupling agent. The tensile strength and elastic modulus were the best when AD-1, a C_{16}-C_{18} olefin containing polyakenyl polymaleic anhydride compatibilizers and 20% GF were applied. Thus, compared to the LDPE/ABS/PS composite without glass fibre and surface modifying additives, the tensile strength showed 58 %, and the elastic modulus showed an 80 % increase. Regarding flexural properties similar result were observed, but not with AD-1, rather than AD-3, a polyakenyl polymaleic anhydride additive that resulted in the best properties, such as increase of 22.6 MPa in flexural strength. CHARPY impact strength increase was the largest (9.1 kJ mm^{-2}) in a sample containing AD-1 agent in the presence of glass fibres, which converts to about 90% increase relative the LDPE/ABS/PS blend without GF and compatibilizing additives. Synergistic effect of glass fibres and some of the compatibilizers can lead to increase of CHARPY impact strength by 94% in comparison to unmodified LDPE/ABS/PS sample.

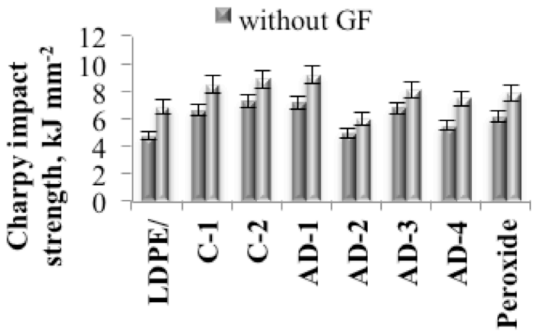

Figure 7: Charpy impact strength of LDPE/ABS/PS samples

Acknowledgements

V.S. and P.K are thankful for support from the project of Operational Programme Research and Development for Innovations co-funded by the European Regional Development Fund (project CZ.1.05/2.1.00/03.0111).

REFERENCES

[1] LAI S.-M., LI H.-C., LIAO Y.-C.: Properties and preparation of compatibilized nylon 6 nanocomposites/ABS blends: Part II – Physical and thermal properties, Eu. Polymer J., *2007*, 43(5), 1660–1671

[2] MAJUMDAR B., KESKKULA H., PAUL D.R.: Morphology of nylon 6/ABS blends compatibilized by a styrene/maleic anhydride copolymer, Polymer, *1994*, 35(15), 3164–3172

[3] HALE W., KESKKULA H., PAUL D.R.: Compatibilization of PBT/ABS blends by methyl methacrylate-glycidyl methacrylate-ethyl acrylate terpolymers, Polymer, *1999*, 40(2), 365–377

[4] KUDVA R.A., KESKKULA H., PAUL D.R.: Properties of compatibilized nylon 6/ABS blends: Part II. Effects of compatibilizer type and processing history, Polymer, *2000*, 41(1), 239–258

[5] HUSSEIN I.A., HAMEED T., SHARKH B.F.A., MEZGHANI K.: Miscibility of hexene-LLDPE and LDPE blends: influence of branch content and composition distribution, Polymer, *2003*, 44(16), 4665–4672

[6] ZAINAL Z., ISMAIL H.: The Effects of Short Glass Fibre (SGF) Loading and a Silane Coupling Agent on Properties of Polypropylene/Waste Tyre Dust/Short Glass Fibre (PP/WTD/SGF) Composites, Polymer-Plastics Techn. Engng., *2011*, 50(3), 297–305

[7] LI Y., SHIMIZU H.: Improvement in toughness of poly(l-lactide) (PLLA) through reactive blending with acrylonitrile–butadiene–styrene copolymer (ABS): Morphology and properties, Eu. Polymer J., *2009*, 45(3), 738–746

[8] LIM J.C., CHO K.Y., PARK J.-K.: Weld line characteristics of PC/ABS blend. II. Effect of reactive compatibilizer, J Appl. Polymer Sci., *2008*, 108(6), 3632–3643

[9] SUN S., TAN Z., ZHOU C., ZHANG M., ZHANG H.: Effect of ABS grafting degree and compatibilization on the properties of PBT/ABS blends, Polymer Composites, *2007*, 28(4), 484–492

[10] SUPRI A.G., ISMAIL H.: Effect of Vinyl Alcohol-Phthalic Anhydride on Properties of Low Density Polyethylene (LDPE)/Tyre Dust (TD) Composites, *2012*, 51(6), 549–555

[11] SUPRI A.G., ISMAIL H.:: The Effect of Isophorone Diisocyanate-Polyhydroxyl Groups Modified Water Hyacinth Fibers (Eichhornia Crassiper) on Properties of Low Density Polyethylene/ Acrylonitrile Butadiene Styrene (LDPE/ABS) Composites, Polymer-Plastics Techn. Engng., *2011*, 50(2), 113–120

[12] GHANI S.A., TAN S.J., YENG T.S.: Properties of Chicken Feather Fiber-Filled Low-Density Polyethylene Composites: The Effect of Polyethylene Grafted Maleic Anhydride, Polymer-Plastics Techn. Engng., *2013*, 52(5), 495–500

[13] VILAPLANA F., KARLSSON S.: Quality Concepts for the Improved Use of Recycled Polymeric Materials: A Review, Macromol. Mater. Engng., *2008*, 293(4), 274–297

[14] ZURALE M.M., BHIDE S.J.: Properties of fillers and reinforcing fibers, Mech. Composite Mater., *1998*, 34(5), 463–472

[15] PÉREZ R., ROJO E., FERNÁNDEZ M., LEAL V., LAFUENTE P., SANTAMARÍA A.: Basic and applied rheology of m-LLDPE/LDPE blends: Miscibility and processing features, Polymer, *2005*, 46(19), 8045–8053

[16] SHIEH Y.-T., LIU C.-M.: Silane grafting reactions of LDPE, HDPE, and LLDPE, J. App. Polymer Sci., *1999*, 74(14), 3404–3411

[17] TRIACCA V.J., ZIAEE S., BARLOW J.W., KESKKULA H., PAUL D.R.: Reactive compatibilization of blends of nylon 6 and ABS materials, Polymer, *1991*, 32(8), 1401–1413

[18] ARAÚJO E.M., HAGE E. JR., CARVALHO A.J.F.: Thermal properties of nylon6/ABS polymer blends: Compatibilizer effect, J. Mat. Sci., *2004*, 39(4), 1173–1178

HUNGARIAN JOURNAL OF
INDUSTRY AND CHEMISTRY
VESZPRÉM
Vol. 42(1) pp. 13–18 (2014)

APPLICATION OF ONLINE AND LABORATORY METHODS FOR THE INVESTIGATION OF SURFACE WATERS

JANKA BOBEK,[1]✉ ZSÓFIA KOVÁCS,[1] AND ZOLTÁN ZSILÁK[2]

[1] Institute of Environmental Engineering, University of Pannonia, Egyetem Str. 10, Veszprém H-8200, HUNGARY
[2] Department of General and Inorganic Chemistry, University of Pannonia, Egyetem Str. 10, Veszprém H-8200, HUNGARY
✉E-mail: bobek.janka@gmail.com

Pollutions in surface waters run down quickly, so the pollution waves cannot be detected by traditional point sampling. Remote controlled online monitoring methods can make the tracking of pollutants possible. These solutions ensure that we can immediately access up-to-date information. The goal of our paper was to compare online monitoring and laboratory measurement techniques. During our work, we investigated the chemical and physical properties of the Séd creek in Veszprém with two different online monitoring systems. Furthermore, we made parallel laboratory measurements of samples taken weekly to evaluate the measurement results of online methods. We discuss the difficulties of installation and operation of online systems and problems arising during emergencies caused by weather.

Keywords: Séd creek, on-line monitoring systems, comparing measurement techniques

Introduction

The 2000/60/EC EU Water Framework Directive (WFD) prescribes that by 2015 all surface water bodies have to reach a good ecological and chemical status. To ensure this, we need to have information about the status of water quality. A desirable feature would be the possibility of continuously track the status of our water bodies with a cost effective monitoring system.

The goal of our work was to introduce online monitoring systems and laboratory methods used to measure the physical-chemical parameters of the Séd creek in Veszprém. In order to continuously monitor water quality, two online monitoring systems were installed, which operate on different principles. The majority of our work was to test the Mobile Monitoring Station (No. 1), which was developed at the Environmental Engineering Institute of the University of Pannonia. In addition, we had the opportunity to follow up the operation of a more complex Mobile Monitoring Station (No. 2), which was manufactured by Combit IT Ltd. The two monitoring stations were placed strategically that the effect of the town of Veszprém on the stream could be measured. With the help of measurements made online and control measurements made in the laboratory, we mapped the loads effecting the Séd creek and to detect pollutant waves travelling down the stream.

Materials and Methods

The investigated water body is the middle section of Séd creek. The water body belongs to the Danube catchment and in it to the Northern-Mezőföld and Eastern-Bakony subunit. The Séd originates in the Bakony, then flows through the city of Veszprém, and joins Nádor Canal at Ősi. The total length of Séd-Sárvíz-mill canal is 71.82 km. Point pollutions are caused on the territory by communal and industrial wastewater inlets. Intensive agriculture and husbandry are characteristic. Because of the side-point sources, we also have to focus on the investigation of diffuse pollutions [4].

Description of Installed Online Monitoring Stations

Two online water quality Mobile Monitoring Stations were installed on the middle section of Séd creek. The evaluated period of continuous measurement was between the August 4, 2013 and October 11, 2013. The two stations were different with respect of place of installation, power source, size, security, sampling, measured physical-chemical parameters, as summarized in *Table 1*. Mobile Monitoring Station 1 *(Fig.1)* was located at the section of Séd creek, where it enters Veszprém, while Mobile Monitoring Station 2 is at the exit point from the city *(Fig.1)*.

Figure 1: Location of installed Mobile Monitoring Stations

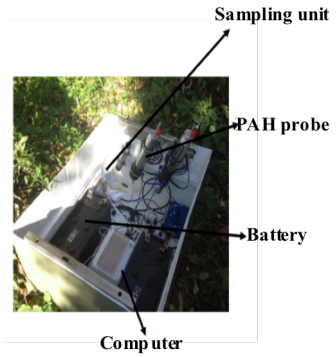

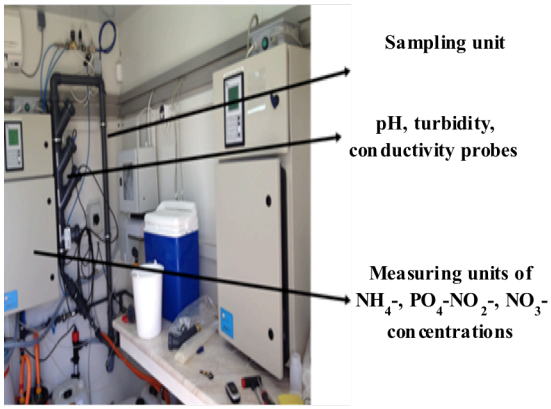

Figure 2: Structure of Mobile Monitoring Station 1 and 2

Results and Discussion

Online Measurements

During the period of August 4, 2013 and October 11, 2013, a tendency was observed for every measured parameter. In *Fig.3*, the pH measured at the examined section of Séd was between 7.3–8.0. The average value of conductivity is 720 µS cm^{-1}, the value of turbidity is 30 NTU. Differences and jumps compared to the baseline indicate pollution, heavy rain or malfunction.

Owing to the placing of the Mobile Monitoring Stations changes could be detected in the pH values between the two sampling points. At Mobile Monitoring Station 1 pH value was in average 0.4–0.5 points higher (7.85) than at Mobile Monitoring Station 2 (7.45) *(Fig.4)*. There are numerous karst water inflows into the Séd as it flows through the city, which causes the lowering of pH. Possible acidic pollutants from roadways, rainwater inlets and industrial areas can also add to the mild acidification of the water body.

In the case of measured ionic concentrations *(Fig.5)* it was observed that all components have a background baseline with a well-defined average concentration. The differences from the baseline appear as peaks that can indicate pollutants or rainy weather. The baseline concentrations are 0.09, 0.03, 0.02, and 4.5 mg dm^{-3} for PO_4^{3-}-P, NH_4^+-N, NO_2^--N, and NO_3^--N, respectively from their average values.

When evaluating the timecourse of all chemical parameters, salient values can be identified and associated with some kind of an event. If we compare *Figs.3* and *5* carefully, we can see that peaks appear at the same time for all components. During the evaluation of data, we identified pollutants, which were washed into the creek due to precipitation.

Table 1: Properties of Mobile Monitoring Stations

	Monitoring Station No.1	Monitoring Station No.2
location of installation	entry point into Veszprém in inner defense area of the waterworks	exit point from Veszprém on an industrial area
size	85×85×85 cm outer size monitoring station made of hardened plastic	2.4×2.4 m base area, 2.5 m height monitoring station
transportation	car	truck with crane
power source	2 pcs of 12 volt lead battery	line power (220V)
measured parameters	pH [11] turbidity [9] conductivity [8] water temperature [11] dissolved oxygen concentration [10] polyaromatic hydrocarbon concentration [17]	pH [12] turbidity [3] conductivity [2] NH_4^+-N concentration [13] PO_4^{3-}-P concentration [16] NO_3^--N concentration [14] NO_2^--N concentration [15]
sampling	every 15 minutes	every hour
maintenance	weekly battery replacement cleaning of the probes	changing reagents and blind reagent calibration (biweekly) supplying distilled water (biweekly) cleaning of sample dispenser vessel sampling tubes

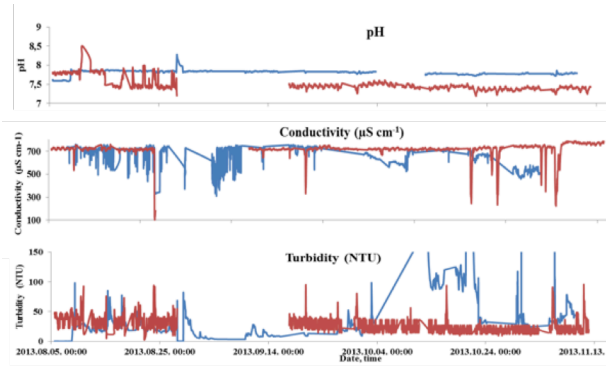

Figure 3: Results of physical parameters measured (blue: Station1, red: Station 2)

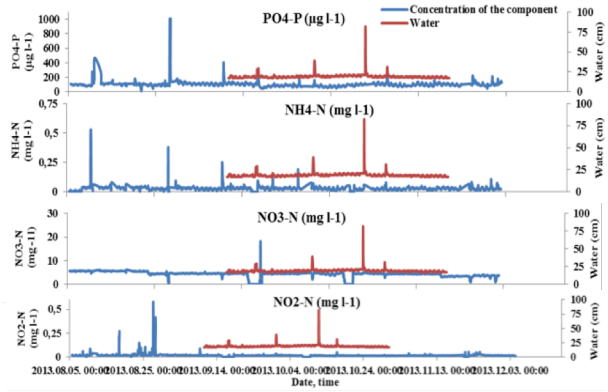

Figure 5: Change of concentration of measured ions

In addition, we detected pollution waves in two occasions. As can be expected, point sampling cannot give detailed information about the status of a water body. The advantage of online methods is clear due to their continuous monitoring, even if they are only operated for a short period of time. Thus, we will get a more holistic picture about the status of a water body toward implementing efficient measures for water quality protection.

Pollutant Leaching from Precipitation

To identify events, we used data from Measurement Station 2. In addition, water level data were downloaded from the water management web page of the Ministry of Interior, Hungary. The water level of Séd is at an average of 20 cm. From the time points in *Figs.3–5*, we select an event occurred on September 30, 2013.

Around the time of the event, the water level started rising, the concentrations of physical-chemical parameters have also started to change. The pollutant downwash was detected between 04:00 and 06:00 according to the results; the concentration peak appeared at 05:00. Viewing physical parameters (*Fig.6*) the value of turbidity has risen, and after reaching the positive peak (14.6 NTU) it started to decrease. Other physical parameters were seen as negative troughs. In the falloff phase all parameters moved back to the average value. Looking at the chemical components *(Fig.6)* as an effect of the rising water level, NH_4^+-N, PO_4^{3-}-N and NO_2^--N concentrations have risen, while NO_3^--N concentration appeared as a negative trough. Outstanding physical-chemical parameters (e.g. PO_4^{3-}-P

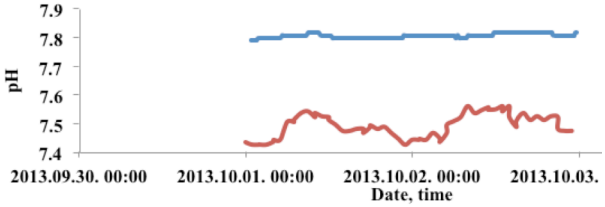

Figure 4: Variation of pH value as a result of discharge from the city (blue: Station1, red: Station 2)

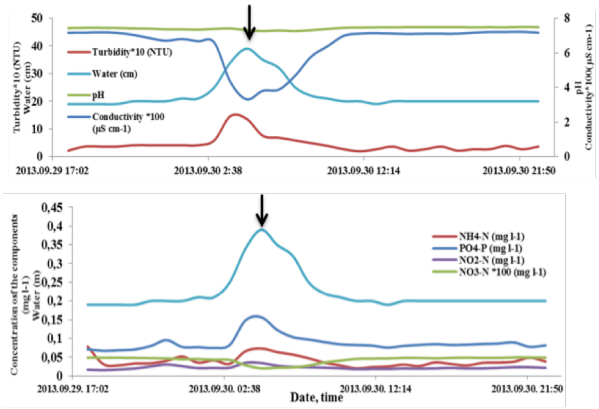

Figure 6: Effect of precipitation on the physico-chemical components

at 0.15 mg dm^{-3} level) measured as an effect of pollutants washed in during precipitation. Afterwards, the PO_4^{3-}-P level moved back to its near average range of 50 µg dm^{-3}.

Detecting Pollutants

Pollutant waves were identified as events, when water level rise did not support the deviations of data points from their expected average values. Alternatively, as a result of precipitation, water level of Séd doubled relative to its average value without the presence of in pollutant waves.

As an example, we analyze here the effect of a pollution wave appeared on September 26, 2013. The pollution was detected between 17:00 and 19:00 with reaching its peak at 18:00. Looking at physical parameters *(Fig.7)* turbidity values doubled relative to the average of 60 NTU. Conductivity decreased significantly from 700 µS cm^{-1} to 640 µS cm^{-1}. The pH decreased by 0.1 unit to 7.3. When we look at ion concentrations in *Fig.7*, NH_4^+-N concentration rose fourfold compared to the baseline (0.19 mg dm^{-3}). PO_4^{3-}-P and NO_2^--N concentrations also showed significant rise (30–180 µg dm^{-3}). NO_3^--N displayed a negative trough at 40 µg dm^{-3}, but this component was the least sensitive to the change.

Measurement of Polyaromatic Hydrocarbons

Based on the data points taken every 15 minutes by the polyaromatic hydrocarbon (PAH) probe (TRIOS) at Measuring Station 1 *(Fig.8)* a PAH pollutant wave was not detected during the investigated period. The baseline of PAH compounds was measured to be 6–7 µg dm^{-3} and 13–15 µg dm^{-3}. Values significantly differing from

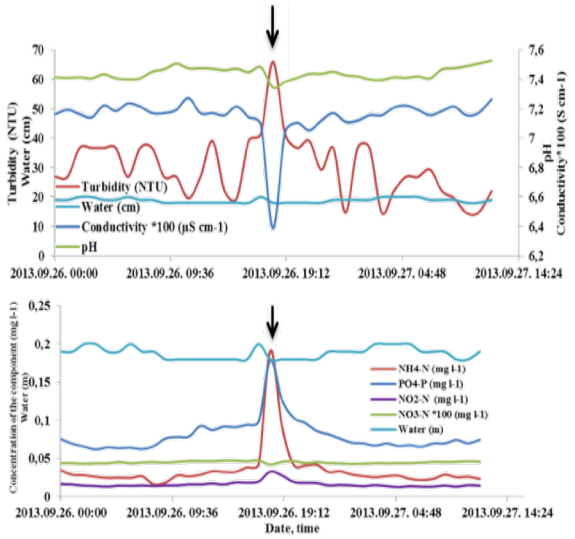

Figure 7: Effects of a pollutant wave on the physical-chemical parameters components

the baseline (35 µg dm^{-3}) can be counted as measurement errors.

Evaluation of Laboratory Measurement Results

In the duration of the investigation, we have taken point samples at the two measurement sites 13 times. The samples were always taken according to standard MSZ ISO 5667–1:2007 [6] in the same time when the monitoring stations recorded data. The samples were transported in a cooler according to standard MSZ EN ISO 5667–3:2004 [7], and were analyzed on the day of sampling. *Table 2* summarized the type of instruments used for measurements.

We compared the data obtained at Measurement Station 2 with the results of laboratory measurements *(Fig.9)*. Correlation can be found for the outliers measured at the monitoring station (250 µg dm^{-3} PO_4^{3-}-P) and in the laboratory (310 µg dm^{-3} PO_4^{3-}-P). However, difference was found in the NO_3^--N concentrations between the laboratory and measurement station results showing around half values for the laboratory measurements than those from the measurement stations. Based on these observations we proposed that the analyzer at the Mobile Monitoring Station measures higher concentration than the real concentration.

The Effect of the City of Veszprém on Séd

Using laboratory measurements, the effect of the city of Veszprém on the creek's water quality was measured. The results obtained for averages of 13 samples are shown in *Fig.10*. It can be seen that there was no significant change in the concentration of NH_4^+-N (26.4–27.3 mg dm^{-3}) between the entry and exit points of the creek with respect of the city. Jumps in the concentration of NH_4^+-N are characteristic during pollutant waves and precipitation. Decrease in concentration of PO_4^{3-}-P is notable (131–100 µg dm^{-3}) at the exit section. At the entry section, Séd flows near to agricultural areas, backyard gardens. We correlate the

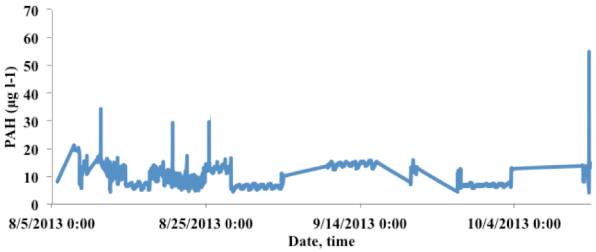

Figure 8: Change in PAH concentration in the investigated timeframe

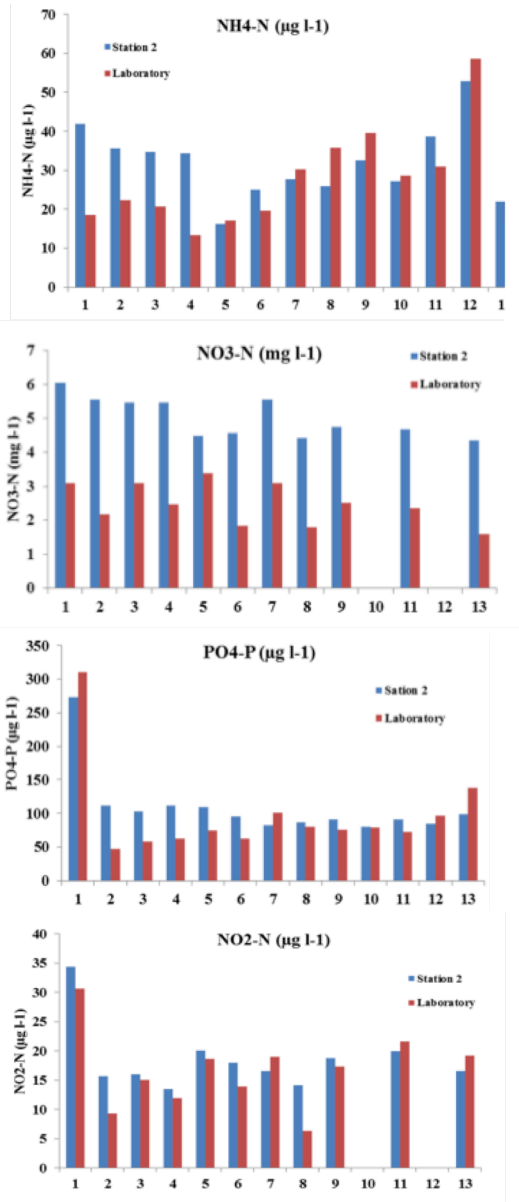

Figure 9: Comparing mobile Monitoring Station 2 and laboratory results

decrease of phosphate concentration within city limits with the presence of pure karst water inflows resulting in significant dilution effect.

In the case of NO_3^--N and NO_2^--N concentrations *(Fig.10)* an obvious increase can be seen (1.3–2.6 mg dm^{-3}; 4.3–5.6 mg dm^{-3}), which is related to the high nitrate content of the incoming karst water. The discharges from rainwater drains, backyard gardens, the canal of the zoo, and inflow from roads add to the increase of these concentrations.

Table 2: Devices used to measure physical and chemical properties of water samples

	Mobile Monitoring Station 1	Mobile Monitoring Station 2	Laboratory
pH	NEOTEK-PONSEL, PHEHT	SENTEK PI11	Consort C902
conductivity	NEOTEK-PONSEL, C4E	Endress+Hauser InduMaxP CLS 50	Consort C902
turbidity	NEOTEK-PONSEL, NTU sensor	Endress+Hauser TurbiMax W CUS41/CUS41-W	-
PO_4^{3-}-P NH_4^+-N NO_3^--N NO_2^--N	-	µMAC C	Lovibond PC Spectro
PAH	Trios, eviroFlu-HC	-	-

Table 3: Comparison of laboratory and online measurement results

	EnviroFlu (µg dm^{-3})	Laboratory (µg dm^{-3})
sample form Séd	13.01	0.13
Séd + 20 µg dm^{-3} PAH mix	25.27	13.7
Séd +100 µg dm^{-3} naphtaline-disulphonate	21.03	0.15

Table 4: Monthly average values for water quality parameters

	August	September	October
pH	7.64	7.45	7.43
Conductivity, µS cm^{-1}	711.22	707.16	720.74
Oxygen saturation, %	84.15	93.4	77.32
Dissolved oxygen, mg dm^{-3}	9.39	10.28	8.73
NH_4^+-N, µg dm^{-3}	33	31	26
NO_2^--N, µg dm^{-3}	31	17	15
NO_3^--N, mg dm^{-3}	5.12	4.02	4.14
PO_4^{3-}-P, µg dm^{-3}	113.79	96.58	92.04

Measurement of Polyaromatic Hydrocarbon Concentrations

The two goals of the measurements were the testing the reliability of the results by EnviroFlu and evaluating whether the probe can detect other PAH compounds that are not fluorescent. To check reliability, we used the addition method with EPA TCL Polynuclear Hydrocarbons Mix chemical from Sigma-Aldrich. Furthermore, we also used naphtaline-disulphonate compound for inducing disturbing effect. We measured three solutions as shown in *Table 3* with probe and we have taken emission spectra. Laboratory control measurements (MSZ 1484-6) [5] were done by ELGOSCAR 2000.

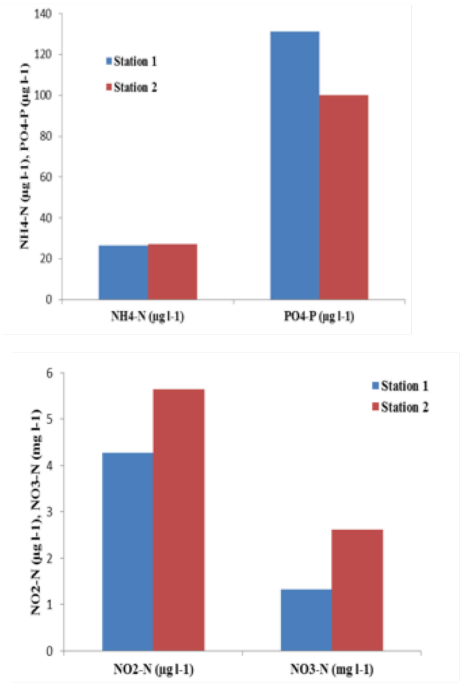

Figure 10: The effect of the city of Veszprém on the investigated section of Séd creek

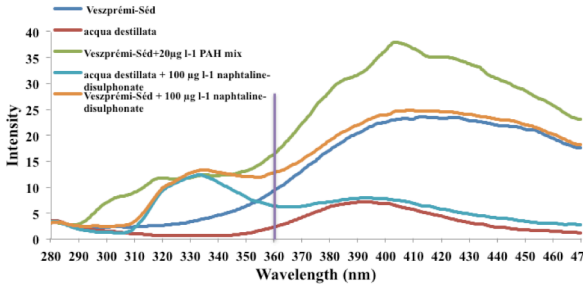

Figure 11: Emission spectra taken with fluorimeter

Comparison of the laboratory and probe results showed significant difference *(Table 3)*. If we deduct the values obtained for the sample from Séd creek as base values, we get similar results. The reliability of results obtained this way was confirmed by spectra taken by a Perkin Elmer LS50B type fluorimeter *(Fig.11)* [1]. The EnviroFlu probe detects fluorescent light at 360 nm. When looking at the curves at 360 nm, we can see that the proportions of intensity differences between the spectra of a sample from Séd and artificially polluted samples correspond to the concentration differences. The significant difference between the laboratory and probe results comes from the fact that the probe senses all compounds giving fluorescence at a given wavelength. This was further elaborated by the significant concentration difference when the sample contained naphtaline-disulphonate.

Water Quality According to Water Framework Directive

The middle section of Séd belongs to Type 3, or alpine, calcic-rough bed material, medium catchment water flow according to Water Management Plan [18] on the basis of Water Framework Plan [19.] We have prepared

water qualification in the observed timeframe in monthly divisions. For dissolved oxygen and oxygen saturation values we used the results of Mobile Monitoring Station 1 and for other components the results of Mobile Monitoring Station 2.

We have calculated monthly average values of water quality parameters *(Table 4)*. In addition, we classified each component on a five-level scale and then made class averages. The class minimums provided classifications for each month. The minimum of class average for August, September, and October were 2.5, 3, and 3, respectively; which resulted in water quality that did not reach a good status.

Conclusions

The advantage of online measurement methods was demonstrated due to the possibility of continuously monitoring the quality of the examined creek. With online devices events can be detected that can be missed by point sampling, such as daily fluctuations, pollution waves in extreme time points.

Another advantage of online methods is the remote controllability, which does not require personnel except for maintenance. A drawback of the larger and more complex Mobile Monitoring Station 2 compared to more portable Mobile Monitoring Station 1 is the need for significant chemical, distilled water and maintenance time.

The measurement stations can reveal trends, the results provided by them are in the same magnitude, but it cannot compete with the accuracy of an accredited laboratory. The goal of online measurements is to detect pollutant waves and extreme values. In order to enhance the accuracy of online measurements follow up laboratory control measurements is needed.

In addition to the entry and the exit sections of the Séd creek, the Catchment Management Plan requires monitoring the physical and chemical parameters of the middle section of Séd that are missing. The results presented in the given paper may help in the drafting of the measurement plans.

Acknowledgements

This work was supported by the European Union and co-financed by the European Social Fund in the frame of the TÁMOP-4.2.2/B-10/1-2010-0025.

REFERENCES

[1] KRISTÓF J.: Chemical Analysis II. (Instrumental Analysis), VE 13/2000. Veszprém, Pannon Egyetemi Kiadó, *2000* (in Hungarian)

[2] Endress+Hauser Conductivity Sensor InduMaxP CLS 50: Technical Information (TI 182C/07,en, No 51517565), Endress+Hauser in Germany, *2007*

[3] Endress+Hauser Solids Content Sensor Turbimax W CUS 41/CUS 41-W: Technical Information (TI 177C/07,en, No 51517577), Endress+Hauser in Germany, *2007*

[4] Water Management of Central Transdanubia: Significant Water Management Issues 1–13; Northern and Eastern Bakony field land planning sub-unit, Székesfehérvár, *2007* (in Hungarian)

[5] MSZ 1484-6:2003: Testing of waters. Determination of policyclic aromatic hydrocarbons (PAH) content gas chromatographic-mass spectrometry, Hungarian Standards Institution Standards Bulletin, *2003* (in Hungarian)

[6] MSZ ISO 5667-1:2007: Water Quality. Sampling; Part 1: Guidance on the design of sampling programmes and sampling techniques, Hungarian Standards Institution Standards Bulletin, *2007* (in Hungarian)

[7] MSZ EN ISO 5667-3:2004: Water Quality. Sampling; Part 3: Guidance on preservation and handling of water samples, Hungarian Standards Institution Standards Bulletin, *2004* (in Hungarian)

[8] NEOTEK-PONSEL Digital sensorC4E: Conductivity/Salinity Datasheet, NEOTEK-PONSEL in France, *2009*

[9] NEOTEK-PONSEL Digital sensor Nephelometric Turbidity Datasheet, NEOTEK-PONSEL in France, *2009*

[10] NEOTEK-PONSEL Digital sensor ODOT: Optical Dissolved Oxygen Datasheet, NEOTEK-PONSEL in France, *2009*

[11] NEOTEK-PONSEL Digital sensor PHEHT: pH, Redox, Temperature Datasheet, NEOTEK-PONSEL in France, *2009*

[12] SENTEK Electrochemical Sensor Specialists PI 11 pH elektrode manual, SENTEK in UK, *2008*

[13] SYSTEA S.p.A: Ammonia in water 0–0.4 ppm $N\text{-}NH_3$ (LFA-NH3-05 rev.1 common.609) , Systea S.p.A., Italy, *2000*

[14] SYSTEA S.p.A: Nitrate in water DTPA UV reduction 0–100 mg dm^{-3} $N\text{-}NO_3^-$+$N\text{-}NO_2^-$ (LFA-NO3DTPA-02 rev.1 comm. 896) Systea S.p.A., Italy, *2000*

[15] SYSTEA S.p.A: Nitrite in water and seawater 0–5 ppm $N\text{-}NO_2^-$ (LFA-NO2-01 rev2.comm. 896) Systea S.p.A., Italy, *2000*

[16] SYSTEA S.p.A: Orthophosphate in water and seawater 0–20 ppm (LFA-PO4-02 rev.1 comm.896) Systea S.p.A., Italy, *2000*

[17] TriOS GmbH: Trios Optical Sensors enviroFlu-HC manual submersible fluorimeter for the detection of polycyclic aromatic hydrocarbons (PAHs) in water, TriOS GmbH in Germany, 2004

[18] Directorate for Water and Environmental Protection: Water Management Plan for the Danube River Basin in Hungary, *2009* (in Hungarian)

[19] EU Water Framework Directive: The European Parliament and of the Council, Water Framework Directive (2000/60/EC), OJL 327, 22 December *2000*, 1–73

HUNGARIAN JOURNAL
OF INDUSTRY AND CHEMISTRY
VESZPRÉM
Vol. 42(1) pp. 19–23 (2014)

ADSORPTION AND INTERCALATION OF SMALL MOLECULES ON KAOLINITE FROM MOLECULAR MODELLING STUDIES

ATTILA TÁBOROSI,[1]✉ RÓBERT KURDI,[1] AND RÓBERT K. SZILÁGYI[2]

[1] Surfaces and Nanostructures Laboratory, Institute of Environmental Engineering, University of Pannonia, Veszprém, H-8201, HUNGARY
[2] Department of Chemistry and Biochemistry, Montana State University, Bozeman, MT 59717, U.S.A.
✉E-mail: taborosia@almos.uni-pannon.hu

Kaolinite is an abundant natural material with considerable industrial potential. Despite its simple composition ($Al_2Si_2O_5(OH)_4$ and layered structure being a phyllosilicate), it is notable that only little known about the interaction of kaolinite sheets with small organic reagents at the molecular level. These assumed to govern intercalation, delamination, and then the complete exfoliation processes. A common methodology to model the molecular structure of kaolinite is the employment of periodic boundary conditions. The application of molecular cluster models gained importance nowadays by capitalizing on the availability of wide range of theoretical tools for describing structural features and reaction mechanisms. In this study, we present our results using theoretical methodologies and modelling strategies from literature that are applied for adsorption and intercalation of urea, ethylene glycol, and potassium acetate.

Keywords: kaolinite, intercalation, adsorption, hydrogen bonding, molecular cluster model

Introduction

A significant hindrance in the design, optimization, and execution of experimental research involving clay minerals is the lack of our understanding of molecular level processes occurring at the outer (adsorption) or at the inner surface (intercalation) of layers of clay. Molecular modelling approaches have the potential to aid experimental design, mitigating cost of chemicals used, rationalizing unsuccessful trial-and-error experiments, and thus contributing to tailored utilization of clay minerals as industrial raw materials.

Given the periodic nature of the crystalline clay minerals, a common approach in modelling is the use of periodic boundary conditions [1–4]. A competitive approach is based on molecular cluster models [5–9]. An advantage of using the latter is the availability of a broad range of quantum chemical tools for studying the local chemical environment of the site(s) of adsorption and/or intercalation.

In the given study, we have utilized kaolinite, which is a member of the 1:1 class of clay minerals. This implies that the layers of this simplest phyllosilicate are composed of octahedral (O) and tetrahedral (T) sheets. The O-sheet contains hexacoordinate Al^{3+} ions, while the T-sheet has tetracoordinate Si^{4+} ions. The O- and T-sheets are connected *via* tricoordinate oxide anions, while the separate OT or 1:1 layers are connected through hydrogen bonds (H-bonds) *(Fig.1)*.

Computational Methods

The computational models were created from the unit cell of the experimental X-ray diffraction structure of crystalline kaolinite [10]. We will discuss results here for models for separate O- and T-sheets with

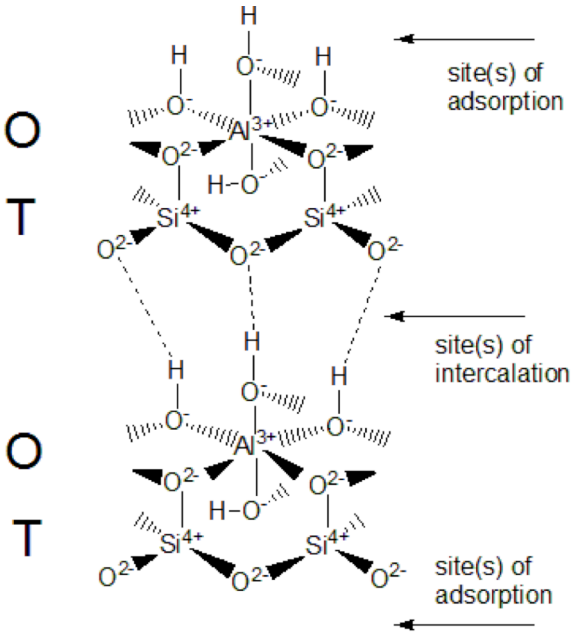

Figure 1: Schematic presentation of adjacent OT layers of delaminated kaolinite

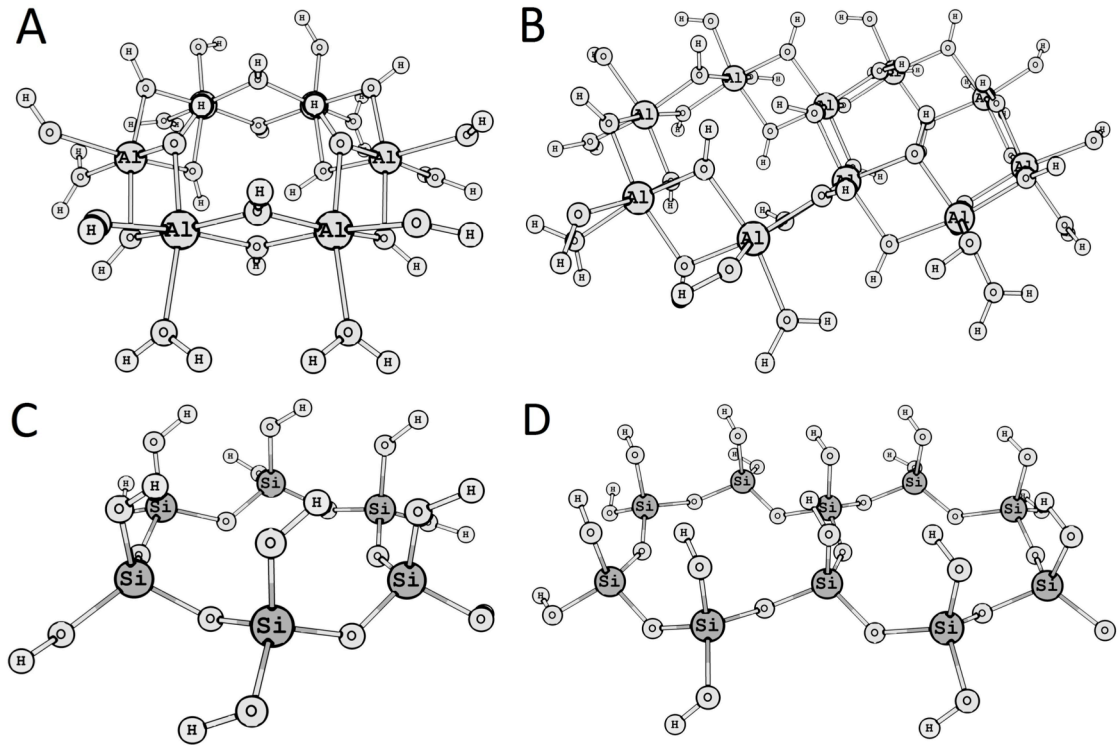

Figure 2: Computational models for the hexagonal honeycomb-like units of [6Al] (A) and [10Al] (B) octahedral, [6Si] (C) and [10Si] (D) tetrahedral cluster models for O- and T-sheets of kaolinite, respectively

stoichiometry of $Al_6O_{24}H_{30}$ and $Si_6O_{18}H_{12}$, respectively *(Figs.2A and C)*. These are the smallest possible cluster models for the hexagonal, honeycomb like units of the O- and T-sheets. In addition, two larger models of $Al_{10}O_{38}H_{46}$ and $Si_{10}O_{29}H_{18}$ were also considered *(Figs.2B and D)* for the larger intercalating agents (ethylene glycol, potassium acetate). The unit cell of kaolinite was multiplied in all crystal dimensions to create a super-cell. This was then truncated to the cluster models presented above. The charge neutrality was achieved by terminating dangling bonds with protons at the periphery of the models. The initial positions of the adsorbent reagents were set at the centre of the hexagonal honeycomb-like unit of both O- and T-sheets and it was allowed to fully relax during optimizations.

Given that the computational models shown in *Fig.2* are simplifications of the experimental crystal structure environment, structural constrains were applied during geometry optimizations. In all calculations, the atoms of the organic reagents, the surface hydroxide groups (*s*-HO^-) of the O-sheet, and the bridging oxide groups (*b*-O^{2-}) of the T-sheets were allowed to move, while the positions of the rest of the atoms were kept fixed. After structural optimizations, the positions and relative arrangements of the organic reagents with respect of the outer and inner surfaces, the shortest distances of possible ion/dipole interactions or H-bonds were noted. For computational models of T…reagent…O intercalation, the basal spacing was set at the beginning of calculations to the experimental values of 10.7, 9.5, 11.5 Å, and 14.2 Å for urea [11], ethylene glycol [12], and potassium acetate in the absence or in the presence of water [13], respectively.

The calculations were carried out using the B3LYP hybrid density functional [14,15] with LANL2DZ basis set [16] as implemented in Gaussian09 [17]. The interaction energies were not considered in this work due to the modest level of theory and lack of consideration of explicit or implicit solvation shell. The main focus of the given work is to establish initial structural models for rationalizing experimental observations and prepare for more advanced computational modeling. The optimized structures presented in this work were made available at computational.chemistry.montana.edu/SI.

Results and Discussions

Kaolinite-Urea Interactions

The lowest energy, optimized structure for the adsorbed urea on O-sheet can be characterized by two short O(urea)…*s*-HO^- distances of 1.92 and 1.95 Å, while one of the amide groups approaches the opposite *s*-HO^- group within 1.73 Å as shown in *Fig.3A*. The presence of both donor and acceptor interactions for the same reagent molecule result in a tilted orientation of the urea. An alternative orientation in which only the carbonyl group is interacting with three *s*-HO^- groups (see below for intercalation model) was not found to be a stationary structure at this level of theory. *Figs.3B* and *C* illustrate the two different orientations of the urea at the T-sheet, where the amide groups are H-bonded to the *b*-O^{2-} groups of the same Si^{4+} ion *(geminal)* with NH…*b*-O^{2-} distances of 2.03 and 2.12 Å or two different Si^{4+} ions *(vicinal)* with 2.02 and 2.08 Å

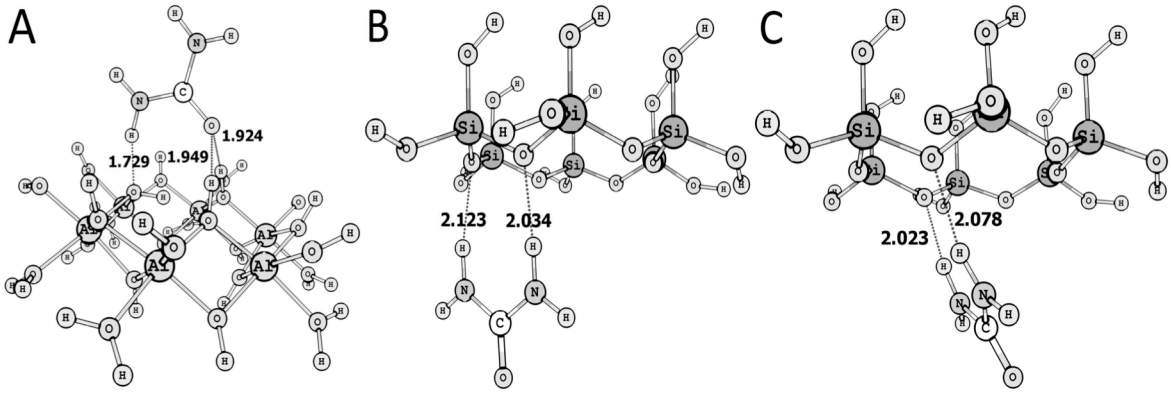

Figure 3: Computational models for urea absorption at O- (A) and T-layers in *geminal* (B) and *vicinal* (C) arrangements

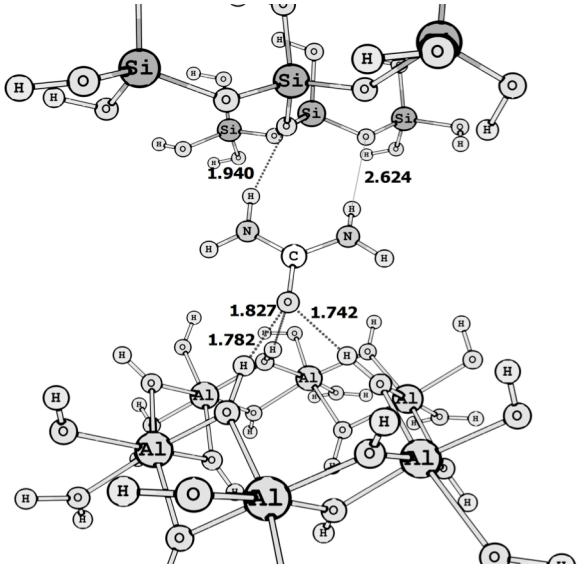

Figure 4: Computational model for intercalation of urea in kaolinite

distances. The energetic difference between the germinal and vicinal coordination is not significant (less than 10 kJ mol^{-1}) at this level of theory.

When the adsorption of urea considered simultaneously at both the O- and T-sheets, a model can be obtained for a plausible structure of the urea intercalated between two OT-layers *(Fig.4)*. In this computational model, the carbonyl group of urea forms three H-bonds at 1.74, 1.78, and 1.83 Å distances with three *s*-HO$^-$ groups of the hexagonal O-sheet cross from each other. At the same time, the intercalated urea forms two H-bonds with the *geminal b*-O^{2-} groups at 1.94 and 2.62 Å distances. The tilted orientation of the urea is the consequence of the experimental basal spacing of 10.7 Å, which was kept fixed during the structural optimizations. It is important to recognize that according to our computational model, there is not enough room between the expanded layers of kaolinite to accommodate urea perpendicular to the basal planes or with parallel carbonyl groups to the crystallographic 'c' axis.

Kaolinite-Ethylene Glycol Interactions

Ethylene glycol is generally used in exchange-intercalation as a step followed by initial dimethyl

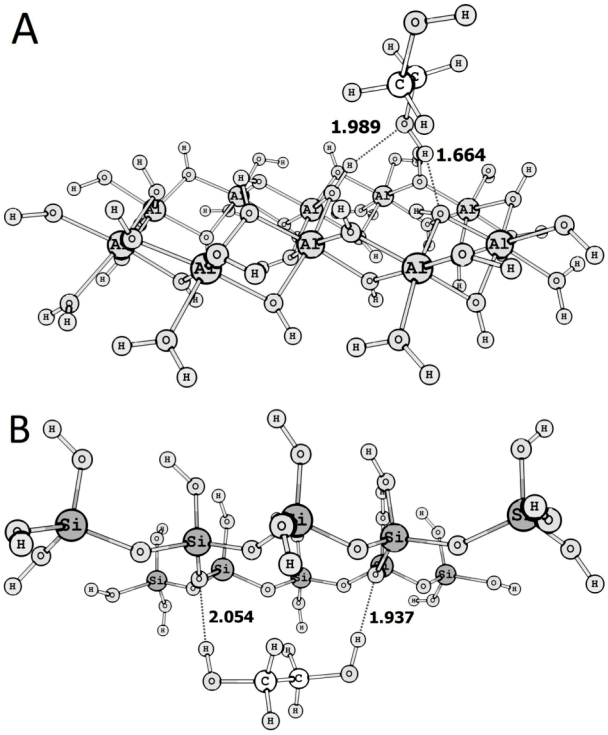

Figure 5: Computational models for the adsorption of ethylene glycol at the (A) O- and (B) T-sheets

sulfoxide or potassium acetate intercalation. As shown in *Fig.5A*, the donor interaction between the reagent hydroxyl group and the Al^{3+} bound *s*-HO$^-$ is much shorter (1.66 Å) than those seen for urea adsorption (1.73 Å), while the acceptor interaction is slightly longer (1.99 Å). Given that the *b*-O^{2-} groups of the T-sheet can only act as H-bond acceptors with ethylene glycol, the reagent spans the entire hexagonal honeycomb-like unit of the T-sheet by forming longer (2.05 and 1.94 Å), thus weaker H-bond interactions than with the O-sheet.

The complementarity of the O- and T-sheets with respect of being H-bond donor and acceptor, respectively, allows for an ideal orientation of the functional groups of ethylene glycol for maximizing the strength of H-bond interactions. The O-sheet forms a short (1.61 and 1.79 Å) interaction between the O(glycol)…*s*-HO$^-$ groups. The T-sheet accepts the HO groups of the ethylene glycol at 1.73 and 1.88 Å distances. Comparison of the urea *(Fig.5)* and ethylene

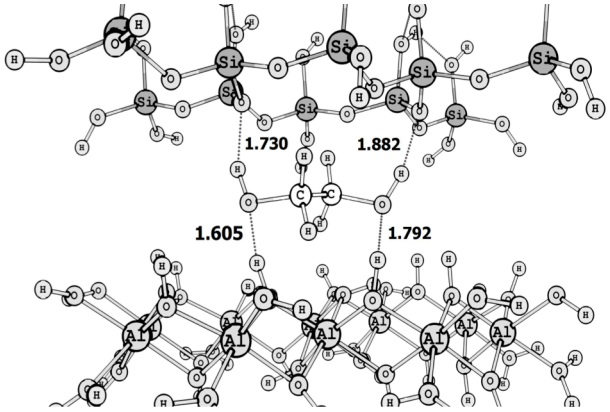

Figure 6: Computational model for ethylene glycol intercalation in kaolinite

glycol *(Fig.6)* intercalated models, the network of interactions between the layers and reagents parallel well the different experimental basal spacing (10.7 vs. 9.5 Å, respectively). While the urea opens the interlayer space more; however, it anchors the two layers with a stronger set of interactions than ethylene glycol. This can be correlated with the limited reactivity of urea/kaolinite complex in exchange intercalation; while ethylene glycol often provides the last step before complete delamination and exfoliation of clays.

Kaolinite-Potassium Acetate Interactions

A limitation of the *in vacuo* models used in this study greatly hinders the dissociation of the potassium ion from acetate and thus in both adsorption models the cation remained at the centre of the hexagonal honeycomb-like model for the O- and the T-sheets in the vicinity of the anion acetate. In addition, the ionized carboxylic group of the reagent form two short and thus strong H-bonding interactions at 1.65 and 1.89 Å distances with two germinal *s*-HO^- groups of the O-sheet. The shortest acetate C-H…*b*-O^{2-} distance in *Fig.7B* is 2.95 Å, which indicates the presence of weak

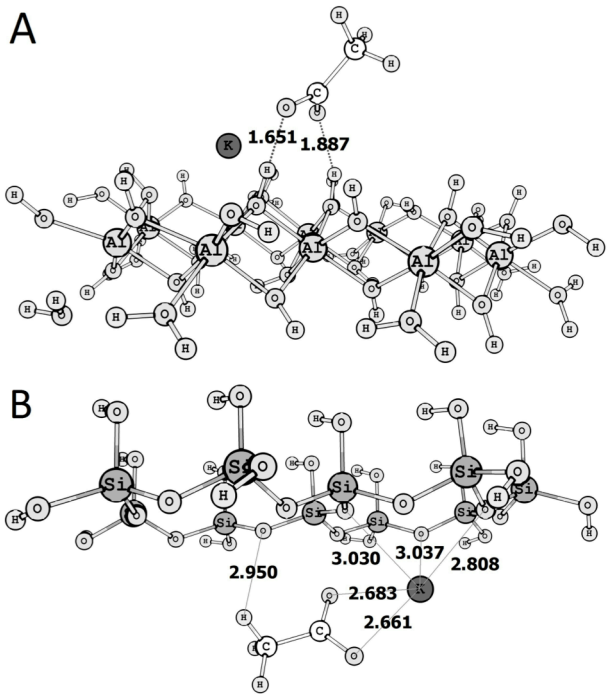

Figure 7: Computational models for the adsorption of potassium acetate on (A) O- and (B) T-sheets

interactions between the methyl group and the *b*-O^{2-} groups. In the adsorption model for the T-sheet, the acetate appears to be held in place by the cation at about 2.66 and 2.68 Å.

Some of the plausible structures for the intercalation of potassium acetate were obtained from simulations in the absence *(Fig.8A)* and presence *(Fig.8B)* of solvent water. Similarly to the other models the values of basal spacing were set to their corresponding experimental values of 11.5 and 14.2 Å, respectively. The 2.7 Å difference allows for the accommodation of a water molecule as shown in *Fig.8B*. In agreement with the absorption models in *Fig.7*, we found short H-bond distances between the carboxylate group and the *s*-HO^- of the O-sheet at 1.59 and 1.83 Å distances. When water

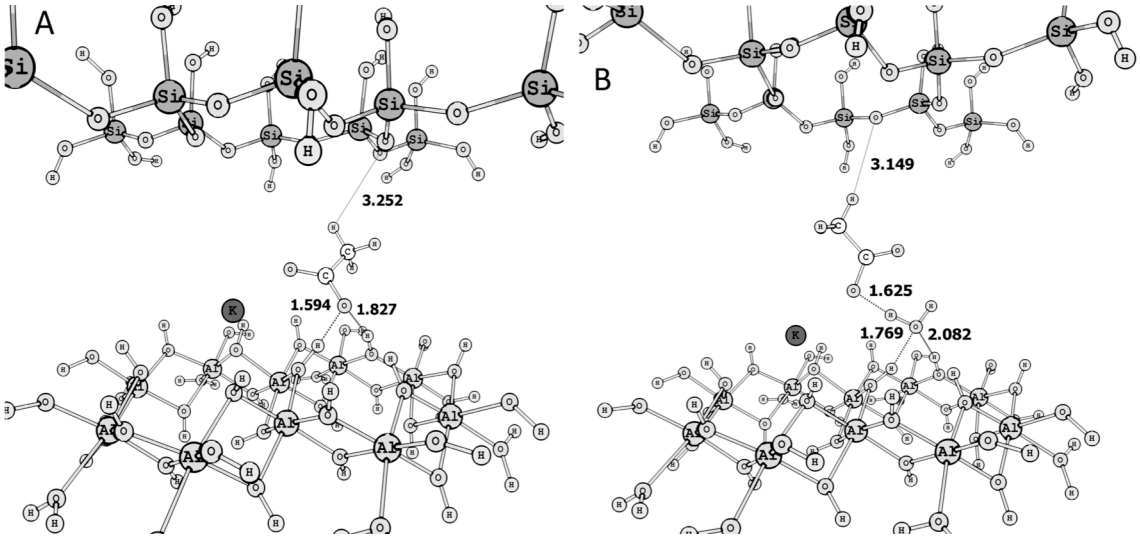

Figure 8: Computational models for potassium acetate intercalation in the (A) absence and (B) presence of solvent water

is present, it is likely to solvate the negatively charged end of the acetate ion with a characteristic -COO^-…H-OH distance of 1.63 Å. The interaction of the water and the O-sheet is asymmetrical with 1.77 and 2.08 Å O(water)…*s*-HO^- distances.

Given the energetic preference of the O-H…OH^- H-bonding interaction, the methyl group of the acetate will only interact with anionic groups of the T-sheet with representation C-H…*b*-O^{2-} distances of 3.15 and 3.25 Å. The lack of a representative solvent environment is of less importance for the position of the potassium ion in the intercalation models, since the inner environment of this model will likely be only exposed to bulk solvent only to a limited extent.

Conclusions

We have started with a few notable preliminary results the establishment of a structural database for reference models related to the adsorption and intercalation of small molecules and kaolinite. We found that even a modest level of theory with respect of the basis set can provide reasonable structures. These results allow us for visualizing molecular structures in order to rationalize experimental observables and generate new ideas for research directions. Furthermore, these models can be considered as initial structures for higher-level calculations that are currently in progress in our laboratory.

Acknowledgement

This research was supported by the European Union and the State of Hungary, co-financed by the European Social Fund in the framework of TÁMOP 4.2.4.A/2-11-1-2012-0001 ‘National Excellence Program’ (RKS and AT) and TÁMOP-4.2.2.A-11/1/KONV-2012-0071 (RK). The authors acknowledge the helpful discussions with Prof. JÁNOS KRISTÓF and Prof. ERZSÉBET HORVÁTH. We acknowledge the use of the computational facilities at Montana State University, Bozeman, MT.

REFERENCES

[1] SMRCOK L., TUNEGA D., RAMIREZ-CUESTA A.J., IVANOV A., VALUCHOVA J.: The combined inelastic neutron scattering and solid-state DFT study of hydrogen-atoms dynamics in kaolinite-dimethylsulfoxide intercalate, Clays Clay Minerals, *2010*, 58(1), 52–61

[2] MERCIER P.H.J., LE PAGE Y.: Rational *ab initio* modeling for low energy hydrogen-bonded phyllosilicate polytypes, Eu. J. Mineral., *2011*, 23(3), 401–407

[3] GEATCHES D.L., JACQUET A., CLARK S.J., GREENWELL H.C.: Monomer adsorption on kaolinite: modeling the essential ingredients, J. Phys. Chem. C, *2012*, 116(42), 22365–22374

[4] TUNEGA D., BUCKO T., ZAOUI A.: Assessment of ten DFT methods in predicting structure of sheet silicates: Importance of dispersion corrections, J. Chem. Phys., *2012*, 137(11), 114105

[5] HATÓ Z., MAKÓ É., KRISTÓF T.: Water-mediated potassium acetate intercalation in kaolinite as revealed by molecular simulation, J. Mol. Mod. *2014*, 20(3), 1–10

[6] MICHALKOVA A., ROBINSON T.L., LESZCZYNSKI J.: Adsorption of thymine and uracil on 1:1 clay mineral surfaces: comprehensive *ab initio* study on influence of sodium cation and water, PCCP, *2011*, 13(17), 7862–7881

[7] DAWLEY M.M., SCOTT A.M., HILL F.C., LESZCZYNSKI J., ORLANDO T.M.: Adsorption of formamide on kaolinite surfaces: A combined infrared experimental and theoretical study, J. Phys. Chem. C, *2012*, 116(45), 23981–23991

[8] SCOTT A.M., DAWLEY M.M., ORLANDO T.M., HILL F.C., LESZCZYNSKI J.: Theoretical study of the roles of Na+ and water on the adsorption of formamide on kaolinite surfaces, J. Phys. Chem. C, *2012*, 116(45), 23992–24005

[9] SONG K.H., WANG X., QIAN P., ZHANG C., ZHANG Q.: Theoretical study of interaction of formamide with kaolinite, Comp. Theor. Chem., *2013*, 102, 72–80

[10] BISH D. L.: Rietveld refinement of the kaolinite structure at 1.5-K, Clays Clay Minerals, *1993*, 41(6), 738–744

[11] MAKÓ É., KRISTÓF J., HORVÁTH E., VÁGVÖLGYI V.: Kaolinite-urea complexes obtained by mechanochemical and aqueous suspension technics-a comparative study. J. Colloid Inter. Sci., *2009*, 330(2), 367–373

[12] GARDOLINSKI J.E.F.C., LAGALY G.: Grafted organic derivatives of kaolinite: I. Synthesis, chemical and rheological characterization, Clay Minerals, *2005*, 40(4), 537–546

[13] FROST R.L., KRISTÓF J., KLOPROGGE J.T., HORVÁTH E.: Rehydration of Potassium Acetate-intercalated Kaolinite at 298 K. Langmuir, *2000*, 16(12), 5402–5408

[14] LEE C.T., YANG W.T., PARR R.G.: Development of the Colle-Salvetti correlation energy formula into a functional of the electron-density, Phys. Rev. B, *1988*, 37(2), 785–789

[15] BECKE A.D.: Density-Functional thermochemistry 3 The role of exact exchange, J. Chem. Phys. *1993*, 98(7), 5648–5652

[16] DUNNING JR. T.H., HAY P.J., (ED.: SCHAEFER III H.F.): Modern Theoretical Chemistry: Methods of Electronic Structure Theory, Plenum, New York *1976*, Vol. 3, pp. 1–28

[17] FRISCH M.J.T., TRUCKS G.W., SCHLEGEL H.B., SCUSERIA G.E., ROBB M.A., CHEESEMAN J.R.; *et alas*: Revision D.01 ed., Gaussian, Inc., Wallingford CT, 2009

Acknowledgement

The dedicated issue of the Hung. J. Ind. & Chem. and in part the organization of the 2014 Spring Scientific Students' Meeting at University of Pannonia were made possible from support provided by the National Talent Program of the Educational Research and Development Institute and the Human Resource Support Program of the Ministry of Human Resources within the framework of "Support of TDK Workshops Recognized by the Council of National Scientific Students' Association" (NTP-TDK-13)

National Scientific Students' Association

OFI

Köszönetnyilvánítás

Jelen kiadvány és részben a 2014. évi Tavaszi Tudományos Diáknap a Pannon Egyetemen az Emberi Erőforrások Minisztériuma megbízásából az Oktatáskutató és Fejlesztő Intézet és az Emberi Erőforrás Támogatáskezelő által gondozott Nemzeti Tehetség Program „Az Országos Tudományos Diákköri Tanács által elismert TDK-műhelyek támogatása" (NTP-TDK-13) című pályázatának köszönhetően valósult meg.

HUNGARIAN JOURNAL
OF INDUSTRY AND CHEMISTRY
VESZPRÉM
Vol. 42(1) pp. 25-29 (2014)

IMPACT OF SIZE HETEROGENEITY OF CORE-SHELL PACKING MATERIALS ON CHROMATOGRAPHIC SEPARATION OF LARGE BIOMOLECULES

DIÁNA LUKÁCS AND KRISZTIÁN HORVÁTH✉

Department of Analytical Chemistry, University of Pannonia, 8200 Veszprém, Egyetem St. 10., HUNGARY
✉E-mail: raksi@almos.uni-pannon.hu

The effect of particle size heterogeneity of core-shell stationary phases on the efficiency of chromatographic separation of large biomolecules was studied. It was shown that the column efficiency was affected significantly by the breadth of particle size distribution. The chromatographic efficiency decreased as the heterogeneity of particle sizes increased. Although the absolute decrease of separation efficiency was affected by the linear velocity, u, of the eluent, the relative change of HETP was independent of u in the practical range of eluent velocities. The results showed that the affect of particle size distribution was the highest in case of fully porous phases, and it decreased as the diameter of the inner core decreased. It was shown that, in the usual range of particle size heterogeneity of core-shell phase, the peak capacities did not change significantly even at high eluent velocities.

Keywords: high performance liquid chromatography, particle size heterogeneity, separation efficiency, core-shell phases

Introduction

Modern analytical applications of liquid chromatography require efficient stationary phases. Before the introduction of core-shell particles – particles with a porous layer surrounding a solid core (*Fig. 1*) – the use of monolithic silica rods [1, 2], or of sub-2 μm particles offered today the most satisfactory results. Due to their excessive radial heterogeneity, however, the efficiency of monolithic columns currently is lower than that of sub-2 μm particles. Columns packed with fine particles, however, have a low permeability [5–7]. Thus, efficiency of columns packed with core-shell particles similar to the columns packed with sub-2 μm particles, but can be operated with the same instruments as those used for conventional columns. The use of core-shell phases is particularly advantageous in the separation of large biomolecules [8]. Recently, core-shell phases were optimized for the separation of large biomolecules [9, 10]. Besides their unique structure, the high efficiency of core-shell phases is in part due to the very narrow particle size distribution, with a relative standard deviation around 5–10% vs. 20–40% for most totally porous particles [7].

In literature, fairly contradictory information can be found about the effect of particle size distribution, PSD, on the separation efficiency. Some results suggest that the large particle size variance has no influence on the column efficiency, while according to other data the wide PSD decreases the efficiency of chromatographic separation. Halász and Naefe [11] were the first ones who examined the effect of particle size distribution

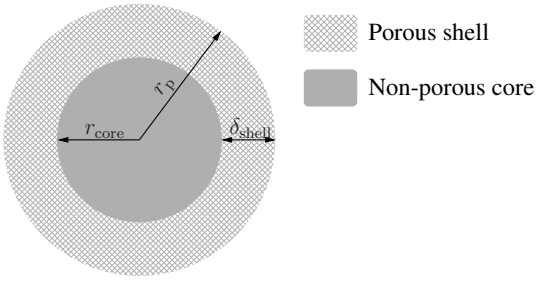

Figure 1: Structure of core-shell particles

on the column efficiency in case of particles that were larger than 50 μm. In their work, no experimental result was found for the change of chromatographic efficiency even in case of wide PSDs ($\sim$ 40%). Two years after Halász's work, significantly smaller, 1-10 μm, particles were tested by Endele *et al.* [12]. No change in the permeability and in the chromatographic efficiency were observed as long as the average particle size remained the same. Dewaele and Verzele prepared columns packed with mixtures of different compositions of reversed phase particles of 3 and 8 μm and investigated the effect of the PSD on the column efficiency [13] with similar results.

Billen *et al.* found that the breadth of the distribution of the stationary phase particles has no effect on the chromatographic efficiency as long as no fines are present. In the presence of fines, the efficiency decreases significantly [14]. They emphasized that

different conclusions can be drawn about the goodness of a chromatographic column depending on the definition used for the particle size distribution.

The effect of the PSD on the chromatographic efficiency of sub-2 μm particles was studied by Cabooter *et al.* by analyzing kinetic plots of these phases [15]. In their work, they showed that not just the PSD is important but also the separation efficiency one wants to achieve. It was concluded that the greater the achievable number of theoretical plates, the more the PSD affects the separation efficiency. In their experiments, the authors obtained better results by using columns with a narrower PSD than by using columns of the same dimensions but packed with particles with broader PSD.

Recently, Gritti *et al.* found that the chromatographic efficiency of the columns can be optimized if a small amount of greater particles is added to the sub-3 μm particles which leads to better bead homogeneity [16]. Manufacturers practice matches these, because on their confession they add a small amount of larger particles to the bathes to optimize the pressure drop along the column.

Experimental study of the effect of PSD on chromatographic efficiency is rather complex, because the column packing procedure is hardly reproducible. It is particularly true when we work with stationary phases which have different PSDs. The quality of column packing also affects the column efficiency significantly. Theoretical models can provide more reliable data on this field because it does not affected by the variability of column packing. The goal of this work is to study the effect of particle size heterogeneity on the chromatographic efficiency of separation of large biomolecules on core-shell stationary phases on a theoretical basis.

Theory

In HPLC, one of the measure of separation efficiency is the height equivalent to a theoretical plate, HETP [17]. The higher the plate height, the less efficient the separation is. The general rate model of chromatography [18] permits the calculation of HETP of columns packed by core-shell phases [8]:

$$H(d_\mathrm{p}) = \frac{2D_\mathrm{L}}{u} + \frac{k_1^2}{1+k_1^2}\left(\frac{\Omega\, u\, d_\mathrm{p}^2}{30FD_\mathrm{p}} + \frac{u\, d_\mathrm{p}}{3Fk_\mathrm{f}}\right), \quad (1)$$

where d_p is the diameter of particles of packing material, u the linear velocity of the eluent in the interstitial volume, k_1 the interstitial retention factor, F the phase ratio, D_L and D_p the axial and pores diffusion coefficients, respectively, and k_f the external mass transfer coefficient. Ω is given by the relationship

$$\Omega = (1-\rho)\,\frac{1+3\rho+6\rho^2+5\rho^3}{\left(1+\rho+\rho^2\right)^2}, \quad (2)$$

where ρ represents the ratio of the radius of the inner solid core, r_core, to the radius of the particle, r_p (see *Fig. 1*):

$$\rho = \frac{r_\mathrm{core}}{r_\mathrm{p}}. \quad (3)$$

Accordingly, ρ is zero for fully porous particle and one for non-porous particle.

For a core-shell particle, the interstitial retention factor is

$$k_1 = \frac{(1-\varepsilon_\mathrm{e})\,(1-\rho^3)}{\varepsilon_\mathrm{e}}\left[K_\mathrm{a}(1-\varepsilon_\mathrm{p})+\varepsilon_\mathrm{p}\right], \quad (4)$$

where ε_e is the external bed porosity, ε_p is the porosity of the porous shell, and K_a is the adsorption equilibrium constant (Henry constant).

The particle size distribution is usually described by log-normal distribution [19]. The PSD of a packing material with mean μ and variance σ^2 is

$$f_{d_\mathrm{p}} = \frac{1}{d_\mathrm{p}\sqrt{2\pi\theta}}\exp\left(-\frac{\left(\ln\frac{d_\mathrm{p}}{\mu}+\frac{1}{2}\theta\right)^2}{2\theta}\right), \quad (5)$$

where

$$\theta = \ln\left(\frac{\sigma^2}{\mu^2}+1\right). \quad (6)$$

On the basis of the equations above, the probability density function of local HETPs, f_H, can be derived by applying the change-of-variables rule [20]:

$$f_H = \left|\frac{\mathrm{d}}{\mathrm{d}H}d_\mathrm{p}(H)\right| f_{r_\mathrm{p}}\left(d_\mathrm{p}(H)\right), \quad (7)$$

where $d_\mathrm{p}(H)$ is the inverse function of $H(d_\mathrm{p})$ (see *Eq. (1)*).

The observable HETP of the column is the first moment of *Eq. (7)*:

$$H_\mathrm{col} = \int_0^\infty H\, f_H\, \mathrm{d}H. \quad (8)$$

Methods of Calculations

For the calculation of H_col (*Eq. (8)*) a software written in C++ language, using the adaptive quadrature routine provided by GNU Scientific Library (GSL, v. 1.15) [21]. The integration region was divided into subintervals, and on each iteration the subinterval with the largest estimated error was bisected. As a result, the overall error reduced rapidly, as the subintervals became concentrated around local difficulties in the integrand. These subintervals were managed by the GSL library, which handled the memory for the subinterval ranges, results and error estimates too. The relative error of integration was set to 10^{-10}. The source code of the program was compiled by g++ shipped by GNU

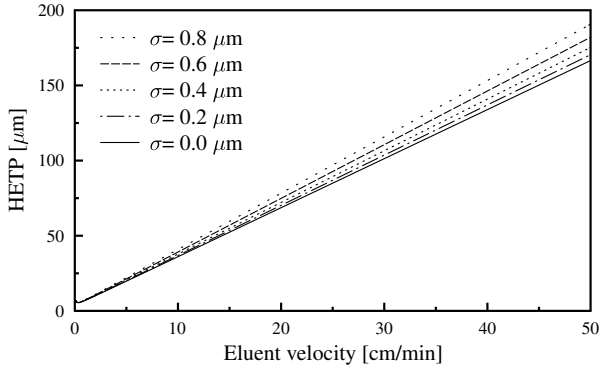

Figure 2: Van Deemter plots of large biomolecules in case of different standard deviations of particle size distributions of 2.6 μm core-shell stationary phases

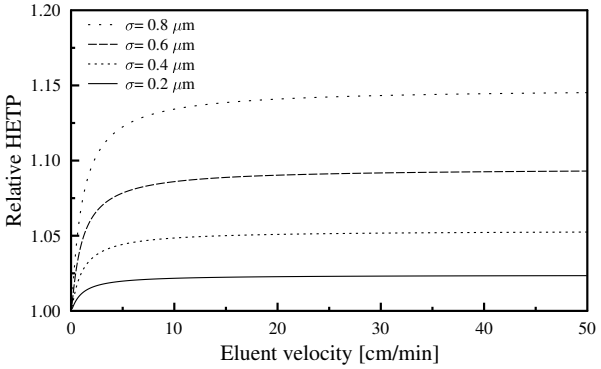

Figure 3: Relative van Deemter plots of large biomolecules in case of different standard deviations of particle size distributions of 2.6 μm core-shell stationary phases

Compiler Collection ver. 4.7.2 using O1 optimization. The calculations were performed on a Pentium IV computer (2.80 GHz) running GNU Linux operating system (Debian Wheezy).

The function f_H (*Eq. (7)*) for the numerical integration was derived symbolically by Mathematica 8.0 (Wolfram Research, Inc.). H (*Eq. (1)*) was calculated as it is described in Ref. [8]. The internal (ε_p) and external column porosities (ε_e), were 0.05 and 0.4, respectively. The distribution coefficient of the compounds were set to 3. The ratio of the molecule size and the average pore diameter were assumed to be 0.68. The molecular diffusivity was 2.5×10^{-5} cm^2/min. The value of "eddy" diffusion term, the internal and external obstruction factors were 1.3, 0.31 and 0.6, respectively. The linear velocity of the eluent was varied between 0.1 and 50 cm/min. The average pore size was 80 Å. It was assumed that the quality of the column packing remained identical in all cases.

Results and Discussion

In *Fig. 2* the calculated van-Deemter curves of large biomolecules separated on 2.6 μm core-shell phases can be seen. The ratio of the radius of the inner solid core to the radius of the particle, ρ, is 0.7 representing the typical core size of commercial core-shell phases. The standard deviation of particle size distribution is varied between 0.0–0.8 μm that corresponds to 0–30% relative standard deviation. Close examination of *Fig. 2* highlights that the HETP values of large biomolecules are approximately directly proportional to the eluent velocity.

Fig. 2 shows that the heterogeneity of particle sizes has a significant effect on the separation efficiency of large biomolecules. The separation efficiency is the highest when the variance of particle size distribution is zero (solid black line). Increasing breadth of particle size distribution decreases the efficiency of separation. The decrease in the efficiency is more significant at higher eluent velocities. At 10 cm/min, the difference between the two extremes ($\sigma = 0$ and $\sigma = 0.8$) is less than 5 μm that is approximately 15% of the total plate height at this eluent velocity in ideal case ($\sigma = 0$). In case of 30, 40, and 50 cm/min the differences are significantly larger: $\sim$15, $\sim$20, and $\sim$25 μm, respectively. Note, however, that the relative increase is $\sim$15% in each case suggesting that the relative change of HETP is independent from the eluent velocity.

In *Fig. 3* the relative HETP, H_rel, values of large biomolecules can be seen as a function of eluent velocity. H_rel were calculated as

$$H_\mathrm{rel} = \frac{H_\sigma}{H_0}, \tag{9}$$

where H_σ and H_0 are HETP values at σ^2 and 0 variance of PSD.

In *Fig. 3*, it can be seen that raising eluent velocity increases the relative HETP. Above $\sim$8 cm/min, however, a plateau is reached and the change of relative HETP becomes negligible. It suggests that, at low eluent velocities, the interstitial dispersion is the governing effect in band dispersion. As the velocity of eluent increases, the pore diffusion becomes more and more significant. Accordingly, in practice ($u > 10$ cm/min), it is the dominant effect in band dispersion.

Fig. 4 shows the effect of core size on the chromatographic efficiency at different breadth of core-shell particle distribution. The linear velocity of the eluent was 15 cm/min that is a typical value in chromatographic applications. It can be seen that, as expected from *Eq. (1)*, the efficiency of stationary phase increases as the thickness of porous layer decreases. The effect of width of particle size distribution is less significant at larger ρ values. While in case of fully porous particles, the difference is almost 17 μm between the HETP values of the two extremes ($\sigma = 0$ and $\sigma = 0.8$), it is slightly more than 4 μm at $\rho = 0.8$.

The relative HETPs calculated as in case of *Fig. 3* do not change significantly with the diameter of non-porous core until $\rho = 0.8$ (*Fig. 5*). Above that value,

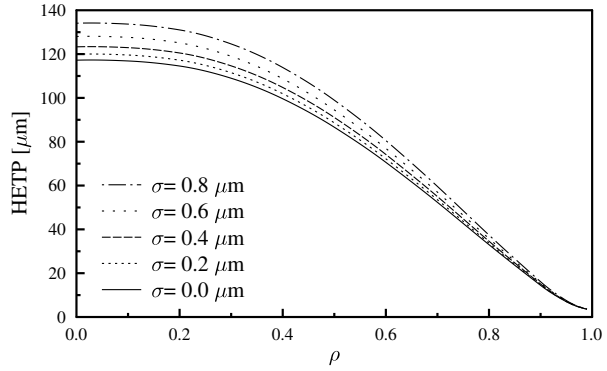

Figure 4: HETP of columns packed with 2.6 μm core-shell particles

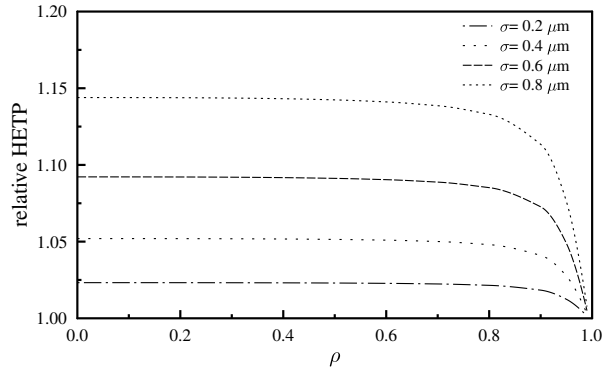

Figure 5: Relative HETPs of columns packed with 2.6 μm core-shell particles

H_{rel}s decrease abruptly, at $\rho = 1$ there is no difference between the cases. It can be explained by considering that the separation efficiency of large biomolecules is affected mainly by the pore diffusion (second term of *Eq. (1)*). As the thickness of porous layer of core-shell particles decrease, the diffusion paths reduce as well. As a result, the impact of pore diffusion on band broadening is less and less significant. The difference between the distinct particles vanishes. Finally, at $\rho = 1$, only the interstitial band spreading (first term of *Eq. (1)*) influences the efficiency of separation. Since D_{L} is not affected by the particle size distribution, H_{rel}s become unity.

Besides the plate heights, the change of peak capacities were also studied. Peak capacity, n_{c}, is a practical measure of separation potential in HPLC. n_{c} is defined as the maximum number of components that can be resolved completely between the peaks of the least and most retained solutes [22]. Several expressions exist for the calculation of peak capacity [23] depending on the mode of chromatography. In case of isocratic mode of separation, n_c can be calculated as

$$n_c = \frac{1}{4}\sqrt{N}\,(t_{\max} - t_{\min}) \ln \frac{t_{\max}}{t_{\min}}, \qquad (10)$$

where $t_{\max}$ and $t_{\min}$ are the retention times of the first and last eluting peaks, and N the number of theoretical plates ($N = L/H$).

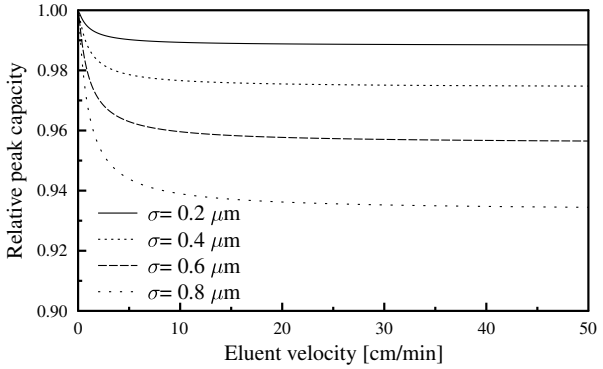

Figure 6: Relative peak capacities of columns packed by 2.6 μm core-shell particles; $L = 10\,\mathrm{cm}$, $t_0 = 10/9$, $t_{\max} = 100/9$

In *Fig. 6* the peak capacities of 2.6 μm core-shell phases can be seen as a function of eluent velocity in case of separation of large biomolecules. The calculated peak capacities were normalized for value that belongs to zero variance of PSD. The figure shows that the achievable peak capacity of a column packed with core-shell particles is affected by the heterogeneity of particle sizes. The decrease of peak capacities, however, is significantly smaller than the decrease of column efficiencies (*Fig. 2*). That is because n_{c} is proportional to the reciprocal square root of H. Accordingly, 15% increase in the plate height results in ∼7% loss of peak capacity that is not significant in practice.

Conclusions

Since their introduction, core-shell stationary phases became very popular for the analysis of large biomolecules. The morphology of these phases results in less band broadening compared to fully porous particles and thus delivers extremely high efficiencies. In this work, the effect of particle size heterogeneity of core-shell stationary phases on the efficiency of chromatographic separation of large biomolecules was studied. The results showed that slopes of van Deemter curves were affected by the breadth of particle size distribution. As a result of widening PSD the column efficiencies decreased significantly. The analysis of peak capacities showed that the maximum number of large biomolecules that can be resolved by core-shell phases was not affected significantly, even if the PSD was wide. Considering that the relative standard deviations of PDSs of core-shell phases are between 0.2–0.4 μm for 2.6 μm particles, it can be concluded that the efficiency of these phases is affected significantly by the size heterogeneity of the particles. Further efforts from column manufacturers in order to improve the PSD do not give any more advantages and are not profitable.

Acknowledgements

This research was supported by the European Union and the State of Hungary, co-financed by the European Social Fund in the framework of TÁMOP-4.2.4.A/2-11/1-2012-0001 'National Excellence Program'. The research infrastructure was supported by the Hungarian Scientific Research Fund (OTKA PD104819) and the Hungarian State and the European Union under the TÁMOP-4.2.2.A-11/1/KONV-2012-0071 project.

REFERENCES

[1] NAKANISHI K., SOGA N.: Phase Separation in Gelling Silica–Organic Polymer Solution: Systems Containing Poly(sodium styrenesulfonate), J. Am. Ceram. Soc., *1991*, 74, 2518–2530

[2] MINAKUCHI H., NAKANISHI K., SOGA N., ISHIZUKA N., TANAKA N.: Octadecylsilylated porous silica rods as separation media for reversed-phase liquid chromatography, Anal. Chem., *1996*, 68, 3498–3051

[3] KIRKLAND J., LANGLOIS T., DESTEFANO J.: Fused core particles for HPLC columns, American Laboratory, *2007*, 39, 18–21

[4] DESTEFANO J.J., LANGLOIS T.J., KIRKLAND J.J.: Characteristics of superficially-porous silica particles for fast HPLC: Some performance comparisons with sub-2-μ m particles, J. Chromatogr. Sci., *2008*, 46, 254–260

[5] GRITTI F., CAVAZZINI A., MARCHETTI N., GUIOCHON G.: Comparison between the efficiencies of columns packed with fully and partially porous C-18-bonded silica materials, J. Chromatogr. A., *2007*, 1157, 289–303

[6] CAVAZZINI A., GRITTI F., KACZMARSKI K., MARCHETTI N., GUIOCHON G.: Mass-transfer kinetics in a shell packing material for chromatography, Anal. Chem., *2007*, 79, 5972–5979

[7] GRITTI F., LEONARDIS I., SHOCK D., STEVENSON P., SHALLIKER A., GUIOCHON G.: Performance of columns packed with the new shell particles, Kinetex-C18, J. Chromatogr. A., *2010*, 1217, 1589–1603

[8] HORVÁTH K., GRITTI F., FAIRCHILD J.N., GUIOCHON G.: On the optimization of the shell thickness of superficially porous particles, J. Chromatogr. A., *2010*, 1217, 6373–6381

[9] WAGNER B.M., SCHUSTER S.A., BOYES B.E., KIRKLAND J.J.: Superficially porous silica particles with wide pores for biomacromolecular separations, J. Chromatogr. A., *2012*, 1264, 22–30

[10] SCHUSTER S.A., WAGNER B.M., BOYES B.E., KIRKLAND J.J.: Optimized superficially porous particles for protein separations, J. Chromatogr. A., *2013*, 1315, 118–126

[11] HALÁSZ I., NAEFE M.: Influence of column parameters on peak broadening in high-pressure liquid chromatography, Anal. Chem., *1972*, 44, 76–84

[12] ENDELE R., HALÁSZ I., UNGER K.: Influence of the particle size (5-35 μm) of spherical silica on column efficiency in HPLC, J. Chromatogr., *1974*, 99, 377–393

[13] DEWAELE C., VERZELE M.: Influence of the particle size distribution of the packing material in reversed-phase high-performance liquid chromatography, J. Chromatogr., *1983*, 260, 13–21

[14] BILLEN J., GUILLARME D., RUDAZ S., VEUTHEY J.L., RITCHIE H., GRADY B., DESMET G.: Relation between the particle size distribution and the kinetic performance of packed columns. Application to a commercial sub-2 μm particle material, J. Chromatogr. A., *2007*, 1161, 224–233

[15] CABOOTER D., BILLEN J., TERRYN H., LYNEN F., SANDRA P., DESMET G.: Kinetic plot and particle size distribution analysis to discuss the performance limits od sub-2 μm and supra-2 μm particle columns, J. Chromatogr. A., *2008*, 1204, 1–10

[16] GRITTI F., FARKAS T., HENG J., GUIOCHON G.: On the relationship between band broadening and the particle-size distribution of the packing material in liquid chromatography: Theory and practice., J. Chromatogr. A., *2011*, 1218, 8209–8221

[17] SNYDER L., KIRKLAND J., DOLAN J.: Introduction to Modern Liquid Chromatography (John Wiley, Hoboken, NJ) *2010*

[18] GUIOCHON G., FELINGER A., SHIRAZI D.G., KATTI A.M.: Fundamentals of Preparative and Nonlinear Chromatography (Academic Press, Amsterdam) *2006*

[19] JOHNSON N.L., KOTZ S., BALAKRISHNAN N.: Continuous Univariate Distributions, vol. 1 (Wiley, New York), second edn. *1994*

[20] WEISSTEIN E.W.: Change of Variables Theorem, From MathWorld – A Wolfram Web Resource, URL `http://mathworld.wolfram.com/ChangeofVariablesTheorem.html`

[21] GALASSI M., DAVIES J., THEILER J., GOUGH B., JUNGMAN G., ALKEN P., BOOTH M., ROSSI F.: GNU Scientific Library Reference Manual - Third Edition, Network Theory Ltd. *2009*

[22] HORVATH C., LIPSKY S.R. : Peak capacity in chromatography, Anal. Chem., *1967*, 39, 1893–1893

[23] GRUSHKA E.: Chromatographic peak capacity and the factors influencing it, Anal. Chem., *1970*, 42, 1142–1147

HUNGARIAN JOURNAL OF INDUSTRY AND CHEMISTRY

HJIC

Advertise upcoming meetings,

conferences and workshops;

make public announcements;

introduce your research laboratory;

a new product or a service

on the pages of the

Hungarian Journal of Industry and Chemistry

Please contact us if interested!

EDITORIAL OFFICE: UNIVERSITY OF PANNONIA
P.O. BOX 158, VESZPRÉM H-8201 (HUNGARY)
Tel.: +36 (88) 624-746, E-mail: hjic@almos.uni-pannon.hu;
web: hjic.mk.uni-pannon.hu
Felelős szerkesztő: Szilágyi Róbert, PhD
Kiadja: Pannon Egyetem, 8200 Veszprém, Egyetem u. 10.
Levélcím: H-8201 Veszprém, Postafiók 158, Tel.: (88) 624-000

HUNGARIAN JOURNAL
OF INDUSTRY AND CHEMISTRY
VESZPRÉM
Vol. 42(1) pp. 31–37 (2014)

EFFECTS OF WASHING OF RAW MATERIAL ON PROPERTIES OF CARBON NANOTUBE CONTAINING POLY(ETHYLENE-TEREPHTHALATE) COMPOSITES

TÍMEA MOLNÁR,[1] CSILLA VARGA,[1✉] AND LÁSZLÓ BARTHA[1]

[1] Department of MOL Hydrocarbon & Coal Processing, University of Pannonia, Egyetem str.10, Veszprém, H-8200, HUNGARY
✉E-mail: vcsilla@almos.uni-pannon.hu

Our interest has been focused on mechanical recycling of poly(ethylene-terephthalate) (PET) bottle waste, because recycling of plastic waste has crucial importance nowadays. The present article deals with the effects of washing of the secondary raw materials on properties of carbon nanotube (CNT) reinforced composites. In the first step advantageous washing compounds and their concentration were determined. After selecting the proper washing method extrusion moulding characteristics of PET granulates were investigated, and effects of carbon nanotubes as reinforcing additives and also application of coupling agents on the mechanical and rheological properties of composites were studied.

Keywords: carbon nanotubes, coupling agent, poly(ethylene-terephthalate), bottle waste recycling

Introduction

Almost all human activities result in waste generation either directly or indirectly. Satisfying the daily needs for growing amounts of products results in higher consumption of raw materials, higher quantities of processing waste, and also higher amounts of wastes after the end of product life [1–4].

Selectively collected PET bottles derived from municipal solid waste considered as waste plastics of a specific type, but the liquid stored in them contaminates their surfaces. *Fig.1* shows the typical treatment cycle and possible recycling methods for plastic wastes, especially for the PET bottles collected selectively. Washing the surface of the waste materials is an important issue as biofilm can be formed. Therefore, this raw material will be contaminated with some biological content. Removing biofilm can be carried out in water, acidic or alkaline solvents. Effectiveness of the method is measured by using reactions with Folin reagent.

PET has excellent mechanical and chemical properties, therefore, its resistance against chemicals and irradiation is outstanding; however, it can also have serious impact on the environment, because the biodegradation requires a long time, and expensive pre-treatment methods are needed in order to bring them within reach of decomposing enzymes [3–8].

Carbon nanotubes (CNT) are members of the family of fullerenes with cylindrical shapes, where carbon atoms are located at the surface of a cylinder. Typical diameter is between the 1–50 nm regime, length can exceed even the 10 μm scale. Carbon nanotubes have non-polar character. Their surface contains only a few functional groups, which can react with polymers. In order to enhance the interaction between nanotubes and polymer matrices, the nanotube surface needs to be modified by application of coupling agents [7–11].

The given study deals with mechanical recycling of PET bottle wastes by applying secondary raw material for polymer matrix of CNT reinforced composites. After selecting the proper washing method, extrusion moulding characteristics of PET granulates were investigated. Furthermore, the effects of carbon nanotubes as reinforcing additives, and application of coupling agents on the mechanical and rheological properties of composites were studied.

Experimental

Materials

Selectively collected PET bottles waste was used as the polymer matrix in the composites in washed and

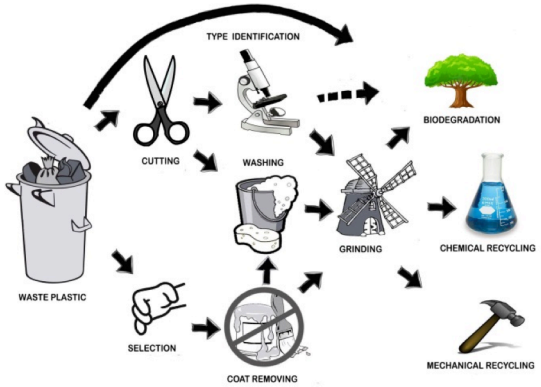

Figure 1: Pre-treatment and recycling of plastic wastes

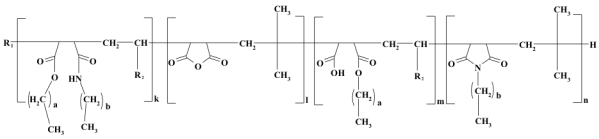

Figure 2: Structure of the ester-amide-imide derivative of the experimental olefin-maleic-anhydride copolymer (R_1: alkyl group with length of the olefinic monomer (C_{16}-C_{18}); R_2: alkyl group with R_1-2 carbon number; a: 3-40, b: 3-32; k: 0,2-2; l: 1-7; m: 1-7 and n: 0,3-2)

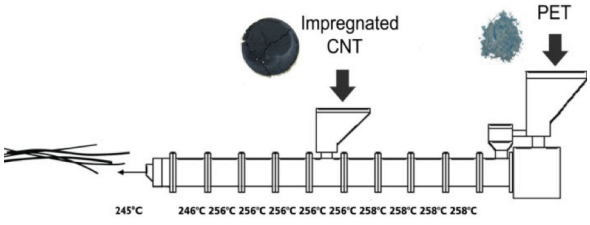

Figure 3: Production of PET composites in a twin-screw extruder

unwashed form. MFI values of the PET granulates were measured, and changed in the interval of 10–14 g (10 min)$^{-1}$ (255 °C, 2.16 kg). Multi-walled carbon nanotubes (MWCNT) were produced at 700 °C by chemical vapour deposition (CVD) process over Fe-Co bimetallic catalyst at the Department of Chemical Engineering, Institute of Chemical and Process Engineering, University of Pannonia. Purity of MWCNT was higher than 90 wt%, diameter was between 10 nm and 20 nm, the average length was above 30 μm and the BET-surface was 200 m^2 g^{-1}. Carbon nanotubes were applied in PET matrix in pristine and surface treated form. For treating surface of the carbon nanotubes experimental olefin-maleic-anhydride copolymer based coupling agents *(Fig.2)* were used with the properties summarized in *Table 1*. The ratios of the functional groups in coupling agents were determined by measuring acid value and saponification number by classical analytical methods and on the second hand the ratios were estimated by a previously developed FT-IR method [12].

Production of Composite Samples

CNT/PET composites were produced by a laboratory twin/screw extruder (LTE 20-44, LabTech Engineering, *Fig.3*). Temperature profiles and screw rotation speed for production were previously determined [13].

Washing of the Waste Material

After the washing process, raw materials from selectively collected PET and PET derived directly from waste deposit were compared. The solutions with 0.05 M concentration were used for both acidic and alkaline washing method. Citric acid and potassium hydroxide were chosen for the acidic and the alkaline wash.

Measurements

To determine the tensile properties of the extruded strings (namely strength, modulus, and extension) an INSTRON 3345 universal tensile testing machine was used. The temperature in the laboratory was 23 °C, while relative humidity was 37% during the mechanical tests that were carried out at 90 mm min^{-1} crosshead-speed. Rheological measurements were carried out in a CEAST Smart RHEO 2000 capillary rheometer at 265 °C. Before measurements, 180 second preheating was applied to all samples.

Structural information about the developed coupling agent was obtained by IR technique using a TENSOR 27 FTIR spectrometer (resolution: 3 cm^{-1}, illumination: SiCGlobar light, detector: RT-DLaTGS type) in the 400–4000 cm^{-1} spectral range.

Scanning Electron Microscopy (SEM) was used to study the morphology of fractured faces of specimens and to follow possible interaction between the reinforcements and matrices on a Phillips XL30 ESEM instrument.

Table 1: Main properties of coupling agents

property	CA-1	CA-2
acid value, mg KOH (g sample)$^{-1}$	12.8	33.1
saponification number, mg KOH (g sample)$^{-1}$	95.3	126.5
molecular weight (M_w)*, g mol^{-1}	3520	3660
polydispersity factor	1.10	1.40
ratio of functional group, %		
anhydride	7.9	12.0
semi-ester	2.7	37.6
ester-amide	44.7	25.2
imide	44.7	25.2

* related to PS standard

Table 2: BET-surface of different carbon nanotubes

samples	surface area
pristine	191.1 m^2 g^{-1}
20% CA-1 coupling agent	125.5 m^2 g^{-1}
15% CA-2 coupling agent	172.3 m^2 g^{-1}
20% CA-2 coupling agent	102.1 m^2 g^{-1}

Results and Discussion

Surface Treating

Effects of surface treatment were studied in two applications. Firstly, the coupling agents on the CNT surface was investigated, thereby properties of pristine CNT were compared to properties of two different coupling agent treated CNTs. BET-surface was measured and surface energy measurements were conducted. Secondly, the effects of concentration of the coupling agent applied on the CNT surface were studied with additive concentration to be 15% and 20%. By the surface treatment the BET surface of pristine CNT reduced at least by 35–40% *(Table 2)*.

On the basis of mesopore volume distribution results *(Fig.4)*, it was determined that coupling agents mainly attached to pores with diameters below 10 nm, because numbers of that pore size decreased the most. Structure

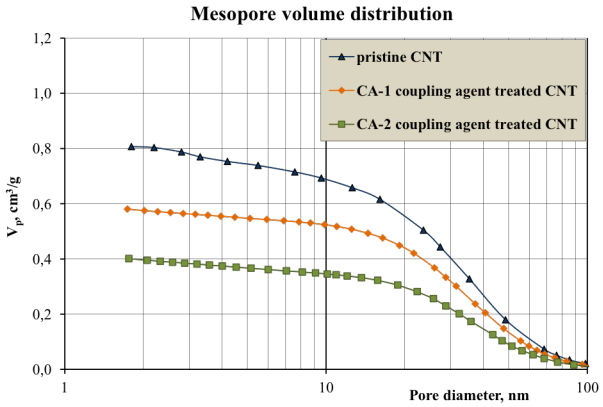

Figure 4: Changes in mesopore volume distribution due to surface treatment (20% coupling agent)

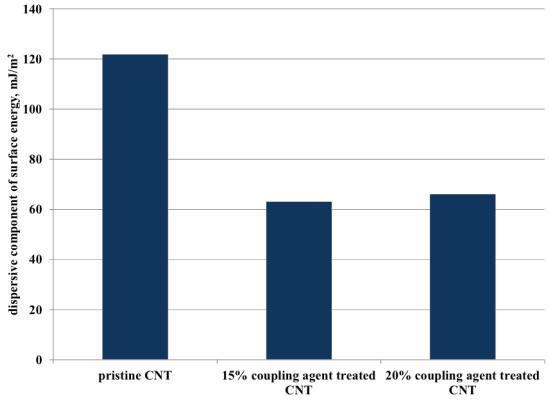

Figure 6: Dispersive surface energy based on Schultz-method (temperature: 70 °C)

of the coupling agent had considerable impact on the distribution since different ratios of decrease were measured in the mesopore volumes, therefore surface interactions with different strength may were evolved between the coupling agent and the CNT.

Concentration of the coupling agent on the CNT surface also influenced the results *(Fig.5)*. Decreasing the concentration from 20% to 15% resulted in an increase in the mesopore volumes to such an extent that almost the values for pristine CNTs were achieved.

Properties of heterogeneous polymer systems are influenced by interfacial interactions and structure; however, no direct method is available to determine strength of interactions. Therefore, models are used generally for their estimation. Inverse gas chromatography measurements can be a useful tool for measuring the surface properties of different fillers and thus, the strength of interactions can be estimated. The dispersive component of surface energy describes London-interactions that can be used for estimation of the non-polar character, while other types of interactions (hydrogen-bond, polar, acid-base, etc.…) are included in the specific component *(Fig.6)*. We found that the dispersive surface energy of the coupling agent treated CNT was half of the pristine one at 70 °C *(Fig.6)*. This is indicative of the surface treated carbon nanotubes likely having lower tendency for agglomeration than pristine CNTs. Constant for the acid-base interactions were calculated based on the GUTMANN equation [14] as summarized in *Table 3*.

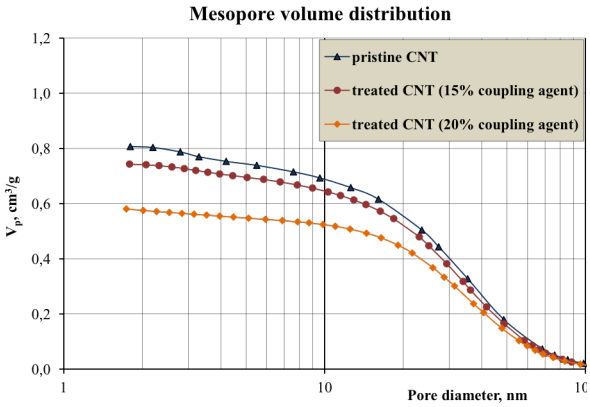

Figure 5: Changes in mesopore volume distribution due to surface treatment with various coupling agent (CA-2) concentrations

Table 3: Acid-base constants calculated by GUTMANN equation [14] at 70 ºC

sample			R^2
pristine CNT	K_a	0.086	0.928
	K_b	0.000	
15% coupling agent treated CNT (CA-1)	K_a	0.086	0.806
	K_b	0.253	
20% coupling agent treated CNT (CA-1)	K_a	0.090	0.849
	K_b	0.213	

On the basis of these results it can be stated that acid character of the pristine CNTs do not change significantly after surface treatment but the basic character improved. On the surface of the treated CNT-s weak basic active centres were predominant over acidic ones.

Effects of Washing

Both acidic and alkaline washing were shown to be effective by which biofilm had been removed from surface of PET granulates with 100% efficiency. Since biofilm cannot stick to the surface of PET due to its crystalline structure biofilm can be removed by application of weak acid or lye.

FT-IR spectra of the granules before and after washing gave the opportunity to study the changes in functional groups of the plastic. It is important to highlight that no significant differences were observed between FT-IR spectra of acidic and alkaline washed samples. Therefore, none of the compounds during washing deteriorated structure of PET *(Fig.7)*.

Effect of Screw Rotational Speed

PET samples were produced at various screw rotational speeds to study their rheological behaviour and also their mechanical properties. Screw rotational speed during processing caused significant differences in viscosities in the low shear rate regime (beyond 500 s^{-1}) *(Fig.8)*.

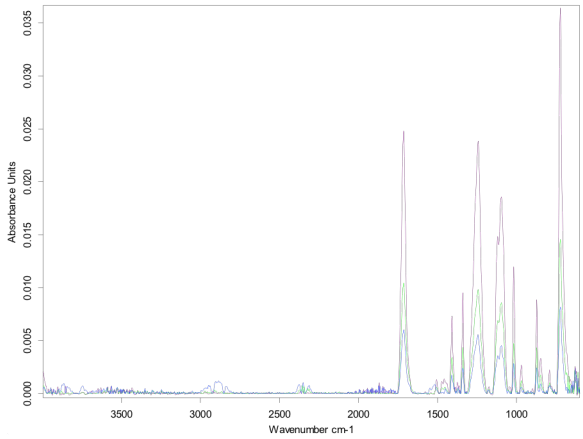

Figure 7: FT-IR spectra of PET sample in the 4000-600 cm^{-1} wavenumber range (purple: potassium-hydroxide; green: citric acid; blue: without washing)

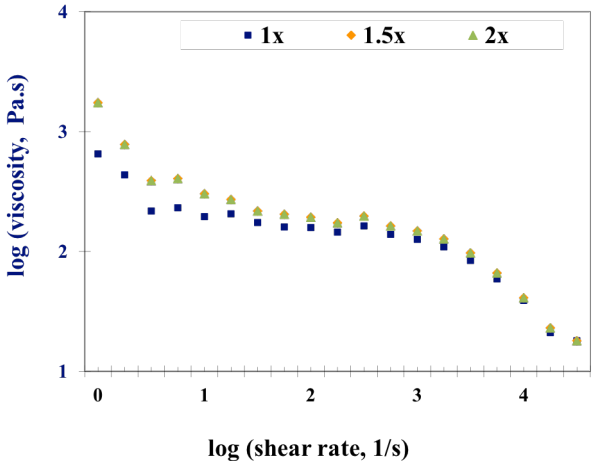

Figure 8: Effect of screw rotational speed on rheological behaviour of PET raw material

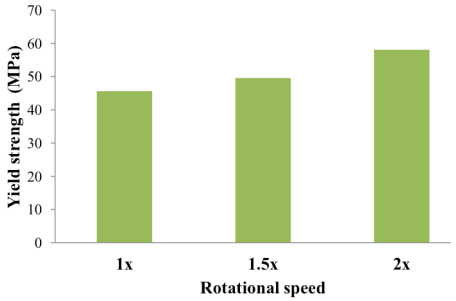

Figure 9: Effect of screw rotational speed on yield strength of PET raw material

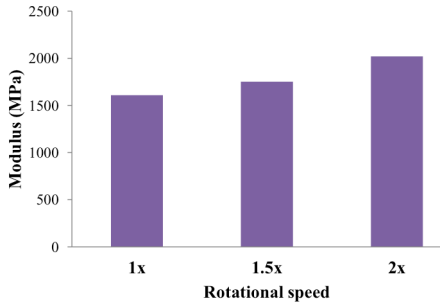

Figure 10: Effect of screw rotational speed on tensile modulus of PET raw material

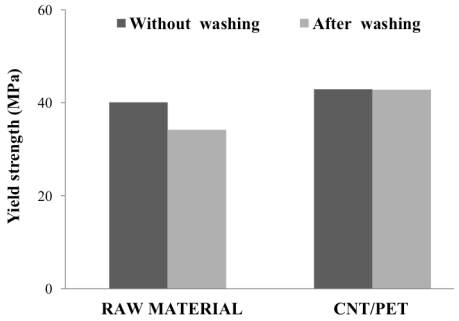

Figure 11: Effects of CNT application on yield strength of PET

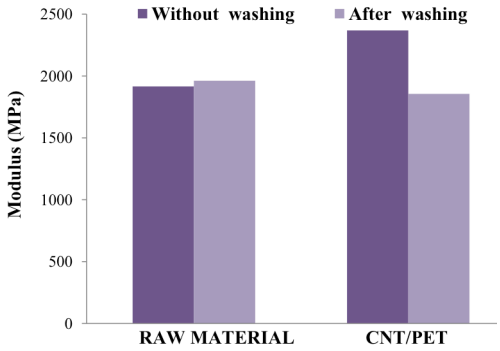

Figure 12: Effects of CNT application modulus of PET

In the medium shear rate region (500-5000 s^{-1}) differences among the viscosities of the samples continuously disappeared. No differences were observed at higher shear rates, above 5000 s^{-1} dedicated to shear rates characteristic for injection moulding. That indicated that all the samples could probably be injection moulded at the same parameters. All the tensile properties (yield strength, modulus) improved by increasing screw rotational speed during processing (*Figs.9* and *10*).

The highest values for the tensile properties were measured for samples produced at the highest screw rotational speed. Sample produced at the lowest rotational speed had values nearly identical to literature data [15]. However, samples processed at the highest rotational speed had 35–40% higher yield strength than the original material used for bottle production. It is important to note that washed PET granulates with the lowest rotational speed could not be produced at the same temperature profile as the plastic melted.

PET Composites Containing Pristine CNT

Washing the raw material caused 15% deterioration in yield strength, but the modulus did not change. Untreated CNT could be introduced into the polymer melts at 2 wt% level both into washed and unwashed PET raw materials by the same side feeder screw rotational speeds. Application of pristine CNT did not influence yield strength of the composites *(Figs.11 and 12)*, so yield strength of CNT/PET samples did not depend on the previous washing of the raw material.

The PET raw materials had *ca.* 2000 MPa tensile modulus either for washed and unwashed plastic, so rigidity of the samples was stated to be the same.

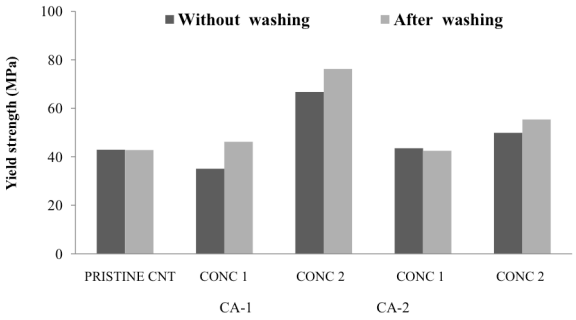

Figure 13: Tensile properties of surface treated CNT containing PET composites

Pristine CNT containing washed PET had 20% lower modulus than unwashed PET based samples had, thereby; the property of the PET raw material was achieved. Adding pristine CNT to washed PET plastic no difference was measured in the modulus compared to the washed PET without any reinforcing.

Effects of Type and Concentration of Coupling Agent

Two different, previously successfully applied coupling agents [13] were used on the surface of CNTs. Concentration of the coupling agents varied from 15% (CONC-1) to 20% (CONC-2) related to the weight of the pristine CNT. With respect of processing, surface treated CNTs were much easier to introduce into the polymer melt. CNT concentration could be elevated up to 2.7–2.9 wt% in the polymer matrix at the same processing parameters using coupling agent treated CNTs instead of pristine type.

Yield strengths of washed PET based composites increased with increasing concentration in the presence of both coupling agents compared to the pristine CNT containing PET sample *(Figs.13 and 14)*. Improvement of 78% for CA-1, and 30% for CA-2 was realized in the presence of coupling agents at the higher concentration (20%). Using unwashed PET, as raw material also resulted in enhancement of yield strength, but to a different extent, such as CA-1 resulting in 55%, while CA-2 causing 16% increase.

Based on the above results, the CA-1 additive was worth applying in higher (20%) concentration due to the achieved more than 50% higher yield strength relative to the pristine CNT containing PET composite. Raw material is worth washing before processing if cost of washing could be balanced by the advantage of the 10 MPa increase in yield strength applying CA-1 coupling agent in 20% concentration. In case of CA-2 additive washing did not influence the properties at the lower (CONC-1) concentration level, but with higher additive concentration (CONC-2) a 14% difference was measured between the composites made from the two raw materials.

Comparing the samples with various additive concentrations an increase was observed in the modulus with increasing concentration for both raw materials and coupling agents. Applying unwashed raw material 34% improvement was realized with CA-1 coupling agent and 32% with CA-2 additive if the concentration

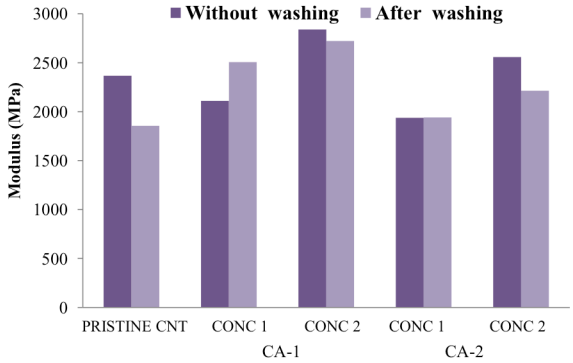

Figure 14: Tensile properties of surface treated CNT containing PET composites

increased from 15% to 20%. A lower degree of improvements were measured for washed PET based samples making the same comparison.

Comparison of pristine and surface treated CNT containing samples showed that coupling agent was advantageous to be applied in higher concentration from the point of view of the modulus either. For unwashed PET based composites application of coupling agents resulted in 10–15% decrease in modulus related to the pristine CNT containing sample. For washed PET based samples making the same comparison changes were calculated to be +45% in case of CA-1, and +20% for CA-2 additive.

The most advantageous observation based on the results is the lack of an effect on the mechanical properties in the investigated interval of raw material quality with respect of washing PET bottle waste, when used as polymer matrix for CNT reinforced composites. This could be realized in easier handling and pre-treating of the raw material before recycling.

SEM graphs

Broken surfaces of samples were studied by Scanning Electron Microscopy. CNTs concentrated at one side of the extruded string in pristine CNT containing samples *(Fig.15A)*. Diameter of the probable carbon nanotube nucleation centres varied *(Figs.15B and C)*. There were agglomerates with diameter of 30–40 μm and also with 5-10 μm number of the latter seemed to be higher. In addition, there were only a few nucleation centres both for washed and unwashed PET based composites.

On the cross section of the extruded strings a crystalline part was rendered likely in larger areas in coupling agent treated CNT containing samples than in pristine CNT/PET samples. In PET containing 15% CA-2 coupling agent a likely crystalline part was found at the middle of the extruded sample *(Fig.16)*. More nucleation centres and more homogeneous structure were observed *(Fig.16)* than in pristine CNT containing sample from the same PET raw material. It is in accordance with the 15% lower CNT content of the pristine CNT/PET composite than the treated CNT containing one. The diameters of the nucleation parts were in the range of 20–30 μm.

Area related to the probable crystalline structure was higher in washed PET based sample on the SEM graphs of the extruded strings *(Fig.17A)*. Nucleation parts were

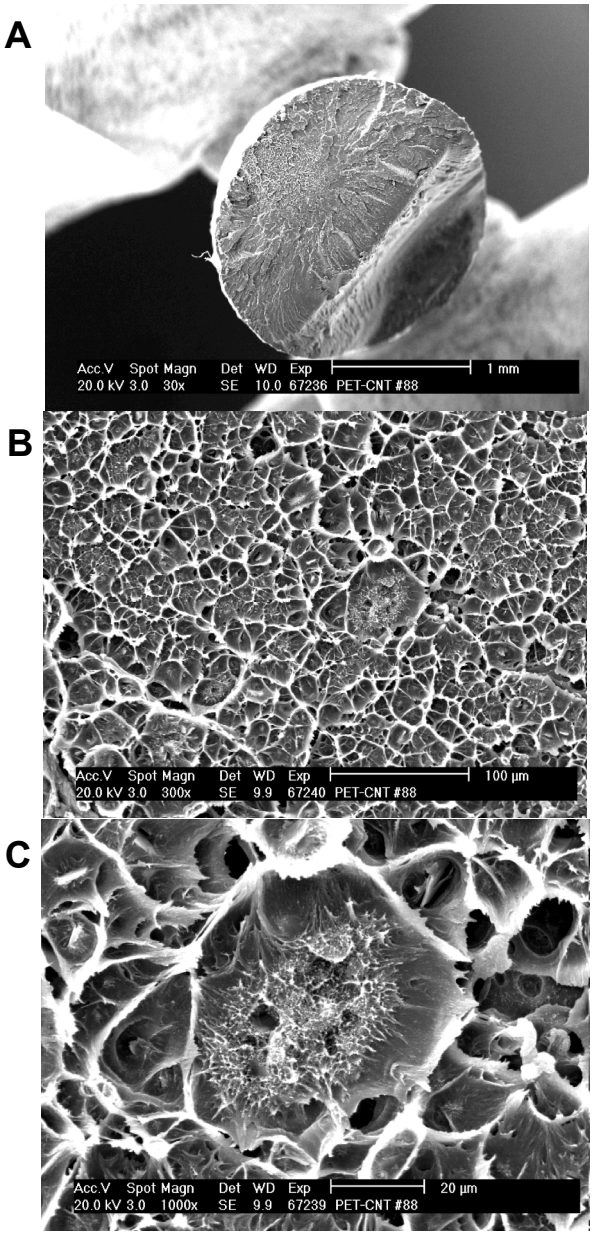

Figure 15: SEM graphs of PET sample containing pristine CNT

located in the middle of the sample and connected to each other diameters were identical to the former sample that was treated *(Fig.17B)*.

Based on the SEM graphs it was concluded that carbon nanotubes were easier to handle and distribute more homogeneously due to surface treating both for washed and unwashed PET raw material, and on the other hand numbers of the nucleation parts and sizes could be influenced.

Conclusions

The present article gave a brief insight into mechanical recycling of PET bottle wastes by applying that secondary raw material for polymer matrix of CNT reinforced composites. After selecting the proper washing method extrusion moulding characteristics of PET granulates were investigated and it was concluded

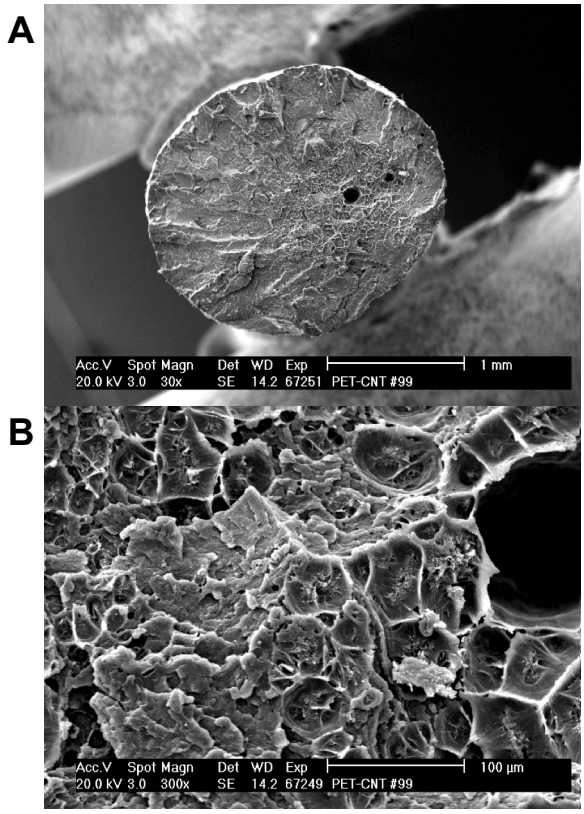

Figure 16: SEM graphs of unwashed PET based sample containing 15% CA-2 coupling agent treated carbon nanotube

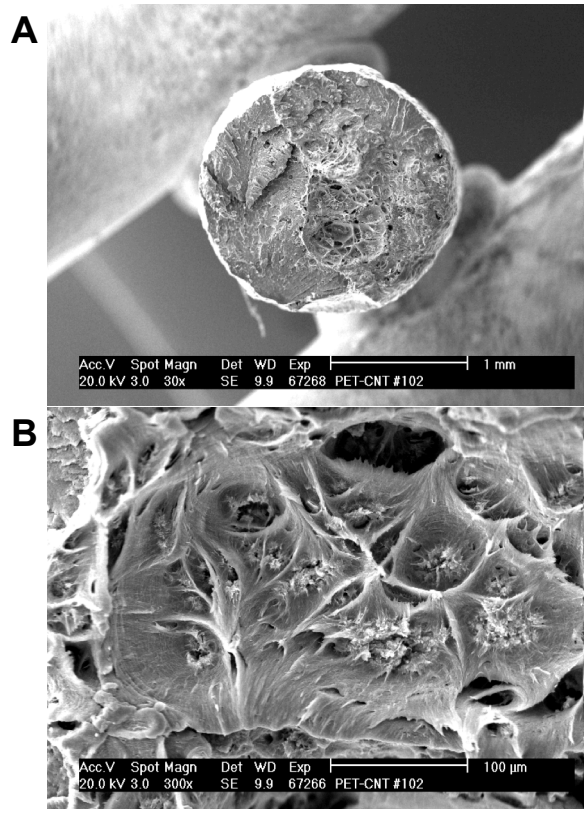

Figure 17: SEM graphs of washed PET based sample containing 20% CA-1 coupling agent treated carbon nanotube

that tensile properties improved by increasing screw rotational speed.

Effects of washing in carbon nanotubes containing PET composites were also investigated where carbon

nanotubes were applied either in pristine or surface treated form. Washing of the waste plastic did not affected yield strength in case of pristine carbon nanotubes containing samples but for coupling agent containing composites mechanical properties significantly changed. If the proper coupling agent was applied in higher concentration, 20% e.g. yield strength improved by higher than 60% while modulus increased at least 20%.

Acknowledgements

This research was supported by the European Union and the State of Hungary, co-financed by the European Social Fund in the framework of TÁMOP-4.2.4.A/2-11/1-2012-0001 'National Excellence Program'. The authors are also grateful for the financial support of this work by the Hungarian State and the European Union under the TÁMOP-4.2.2.A-11/1/KONV/2012-0071 project.

REFERENCES

[1] LA MANTIA F.: Handbook of Plastic Recycling, Shrewsbury, Rapra Technology, *2002*

[2] WÉGNER K.: Towards more efficient waste management, Yearbook of Hungarian Plastic and Rubber Industry, *2013*, 27–32 (in Hungarian)

[3] WU G., LI J., XU Z.: Triboelectrostatic separation for granular plastic waste recycling: A review, Waste Mngnt., *2013*, 33, 585–597

[4] FORTELNY I., MICHALKOVÁ D., KRULIS Z.: An efficient method of material recycling of municipal plastic waste, Polym. Degrad. Stabil., *2004*, 85, 975–979

[5] AKSA W., MEDLES K., REZOUG M., BOUKHOULDA M.F., BILICI M., DASCALESCU L.: Two stage electrostatics separator for the recycling of plastic from waste electrical and electronic equipment, J Electrost., *2013*, 71, 681–688

[6] SÁNCHEZ A.C., COLLINSON S.R.: The selective recycling of mixed plastic waste of polylactic acid and polyethylene terephthalate by control of process conditions, Eu. Polym. J., *2011*, 47, 1970–1976

[7] WANG Y., GAO J., MA Y., AGARWAL U.S.: Study on mechanical properties, thermal stability and crystallization behavior of PET/MMT nanocomposites, Composites Part B, *2006*, 37, 399–407

[8] LOGAKIS E., PISSIS P., POSPIECH D., KORWITZ A., KRAUSE B., REUTER U., PÖTSCHKE P.: Low electrical percolation threshold in poly(ethylene terephthalate)/multi-walled carbon nanotube nanocomposites, Eu. Polym. J., *2010*, 46, 928–936

[9] LI Z., LUO G., WEI F., HUANG Y.: Microstructure of carbon nanotubes/PET conductive composites fibers and their properties, Composites Sci. Techn., *2006*, 66, 1022–1029

[10] FIEDLER B., GOJNY F.H., WICHMANN M.H.G., NOLTE M.C.M., SCHULTE K.: Fundamental aspects of nano-reinforced composites, Composites Sci. Techn., 2006, 66, 3115–3125

[11] BORRELL A., ROCHA V.G., TORRECILLAS R., FERNÁNDEZ A.: Surface coating on carbon nanofibers with alumina precursor by different synthesis routes, Composites Sci. Tehn., *2011*, 71, 18–22

[12] VARGA CS.: Production and investigation of compatibilizing additives for polymer composites, PhD Thesis, University of Pannonia, Veszprém, *2010* (in Hungarian)

[13] MOLNÁR T.: Effects of carbon nanotubes and coupling agents in poly(ethylene-terephthalate) polymer, ITDK report, University of Pannonia, Veszprém, 2011 (in Hungarian)

[14] GUTMANN V.: The donor-acceptor approach to molecular interactions, Plenum Press, New York, *1978*

[15] PÁL K.: Recycling of plastics wastes as secondary raw material, Műanyagipari Szemle, *2006*/2

Acknowledgement

The dedicated issue of the Hung. J. Ind. & Chem. and in part the organization of the 2014 Spring Scientific Students' Meeting at University of Pannonia were made possible from support provided by the National Talent Program of the Educational Research and Development Institute and the Human Resource Support Program of the Ministry of Human Resources within the framework of "Support of TDK Workshops Recognized by the Council of National Scientific Students' Association" (NTP-TDK-13)

National Scientific Students' Association

OFI

Köszönetnyilvánítás

Jelen kiadvány és részben a 2014. évi Tavaszi Tudományos Diáknap a Pannon Egyetemen az Emberi Erőforrások Minisztériuma megbízásából az Oktatáskutató és Fejlesztő Intézet és az Emberi Erőforrás Támogatáskezelő által gondozott Nemzeti Tehetség Program „Az Országos Tudományos Diákköri Tanács által elismert TDK-műhelyek támogatása" (NTP-TDK-13) című pályázatának köszönhetően valósult meg.

HUNGARIAN JOURNAL
OF INDUSTRY AND CHEMISTRY
VESZPRÉM
Vol. 42(1) pp. 39–42 (2014)

INVESTIGATION THE PROPERTIES OF Y-BA-Cu-OXIDE SUPERCONDUCTORS PREPARED BY HYDRAULIC PRESSING AND MOLDING

ANNA MALOVECZKY,✉ MARGIT ENISZ-BÓDOGH, AND TAMÁS KULCSÁR

Institute of Materials Engineering, University of Pannonia, Egyetem str. 10., Veszprém, 8200, HUNGARY
✉E-mail: anna.maloveczky@gmail.com

Levitation applications of superconductors require the fabrication of bulk ceramic superconductors with special shapes. The conventional hydraulic pressing is not suitable for the production of superconductors with complicated forms, so we have applied slip casting to shape bulk superconductors. Superconducting powders with different $YBa_2Cu_3O_y$ (123) and Y_2BaCuO_5 (211) phase content and different (Pt, Pb, Ce) additives were prepared by solid-state reactions. The non-superconducting (211) particles can be considered as flux pinning centres; thus the magnetic properties can be influenced by their amount and particle sizes. The addition of a few weight percent of dopant in the nominal composition can modify the particle size and distribution of the (211) grains. We have investigated and compared the phase compositions, morphologies and magnetic levitation forces of bulk superconductors formed by hydraulic pressing and moulding. The shielding abilities of a moulded superconductor were simulated with the COMSOL Multiphysics 4.4 software.

Keywords: YBCO superconductor, moulding, shielding, modelling

Introduction

The use of superconductivity is promoted by the need for stable high magnetic fields. The high-temperature superconductors are attractive for engineering applications, such as contactless superconducting bearings, trapped field magnets, levitation trains, fusion reactors, and NMR spectrometers. An important application of superconducting magnets is the Magnetic Resonant Imaging (MRI). Superconducting magnetic shielding can be used simultaneously to protect the personnel and other medical equipment from the strong magnetic fields produced by an MRI system.

The relative magnetic permeability of Type I superconductor is theoretically zero, which means when we use it for shielding, it expels the magnetic fluxes from itself. The high-Tc superconductors can also be used for shielding sensitive electronic devices from external electromagnetic fields. Due to the MEISSNER effect [1,2], it is sufficient to surround the volume to be protected by a thin film. For quasi-monocrystalline films of YBaCuO thickness of 1 μm would be sufficient for virtually perfect shielding. A granular ceramic layer would require a larger thickness, but in all cases the thickness and weight of the superconducting shields would be much less than those of magnetic materials providing a comparable effect. For these applications of high-Tc superconductors outstanding magnetic properties and special shapes are required.

The scientific literature suggests two main ways for improving the magnetic properties of superconductors that are structure damaging or doping [3–9]. Both methods work the same way, such as by increasing the amount of pinning centres (such as 211 phase) in the superconducting (123) material and decreasing the size of these centres by addition of different dopants. The damaging method could be done by ion or neutron radiation to destruct the bulk of the material and generate faults.

Preparation of high-Tc superconductors with special, complicated forms is a particular challenge due to their brittle nature. Slip casting, namely pouring low viscosity water-containing slurry into moulds is the oldest ceramic forming method for production of special shapes. For superconductors slip casting of shapes is also possible although the use of water as liquid phase is not optimal due to hydrolysis and other reactions. Another preparation method for ceramic superconductors is tape casting of viscous slurry containing ceramic particles in organic solvent [10].

Materials and Methods

In this work, Y-Ba-Cu-oxid-based superconductive powders were prepared with different 123/211 phase content and different (Pt, Pb, Ce) additives. Shaped bulk superconductors were produced from these powders with hydraulic pressing and moulding. The effects of these parameters were investigated on the phase compositions, morphologies and magnetic levitation forces of the sintered bulk superconductors.

For modelling the superconductor as a shield in different geometries, COMSOL Multiphysics 4.4 software was used that provides a simulating and

Table 1: The peak intensity of the crystalline phases

	Samples		Peak intensity, counts				
	Binder	Solvent	123	211	011		
					$BaCuO_2$	CuO	$BaCO_3$
			d=2.72 Å	d=2.99 Å	d=3.05 Å	d=2.52 Å	d=3.72 Å
1.	polyvinyl formal	dioxane	4460	1122	562	956	-
2.	metylan	dest. water	2952	919	737	725	-
3.	metylan	ethanol	1477	765	679	459	-

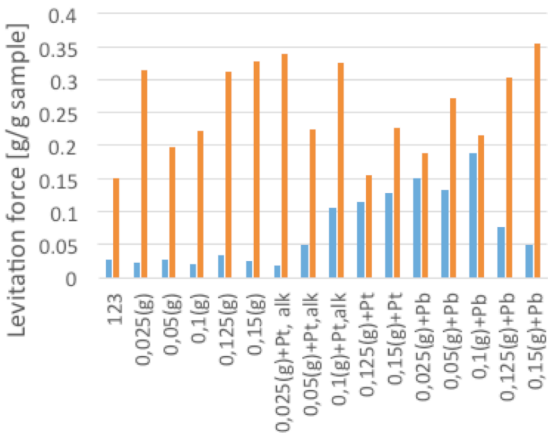

Figure 1: Levitation forces of the heat treated samples

modelling environment using the finite element method. Instead of the original AC-DC module of COMSOL, a module by ROBERTO BAMBILLA was used, which was developed for modelling YBCO superconductors.

Results and Discussions

Samples Made by Hydraulic Pressing

The superconducting samples were prepared by using Y_2O_3, $Ba(OH)_2{\cdot}8H_2O$ and CuO. The latter was obtained by the calcinations of $Cu(OH)_2{\cdot}CuCO_3{\cdot}nH_2O$ with a specific surface area of 18.4 m^2 g^{-1}, $PtCl_4$, PbO and $Ce(NO_3)_3{\cdot}6H_2O$ starting materials. The 123:211 molecular ratio of the nominal compositions was changed in the range of 1.00:0.15. Samples were prepared without additives as well as with 2.0 wt% Ce + 0.5 wt% Pt, and 2.0 wt% Ce + 0.5 wt% Pb dopants.

For sample preparations, barium-hydroxide was ground in agate mortar, but in some cases the pulverization and grinding was made in the presence of alcohol. The mixture of raw materials was homogenized by thoroughly mixing with alcohol in an agate mortar and compacted into disks of 25 mm × 3mm by hydraulic pressing at 70 MPa. Firstly, the samples were pre-reacted at 960 °C for 4 hours to obtain the desired (123+211) phases by solid-state reaction. The heat-treated samples were ground and the powders were pressed into pellets by hydraulic pressing using a pressure of 70 MPa. The relatively dense structure was obtained by liquid state sintering at 1010 °C peak temperature for 6 hours in oxygen atmosphere [11].

The levitation force of the samples after the heat treatments is shown in *Fig.1*. As described in the literature, we also found that the levitation force shows an increasing trend with increasing amount of 211 phases. In the case of Ce+Pt and Ce+Pb dopant containing samples higher levitation forces can be obtained after the first heat treatment at 960 °C. It is notable that the samples prepared from barium hydroxide ground in the presence of alcohol showed improved magnetic properties.

Samples Made by Moulding

Part of the pre-reacted at 960°C ground samples were used for shaping superconductors by moulding. Previously, superconductive slurries were prepared with different organic liquid additives and those were burnt out during the annealing. From these materials only a few were good enough for further studies. Samples providing a proper cohesion and appearing to be homogeneous were selected for future analysis. After heat treatment, X-ray diffraction analysis was used to study the phase composition changes caused by addition of organic materials for deciding if any of the dopants has a negative influence on the superconductor properties.

As shown in *Table 1*, the metylan reduces the amount of the superconducting phase (123) and this leads to the tetragonal, non-superconducting structure. Polyvinyl formal did not have a negative influence on the formation of 123 phase. Thus, the polyvinyl formal binder was chosen with dioxane for further experiments. With respect of ideal concentrations, it was found that 1 wt% of polyvinyl formal/dioxane must be added to the superconducting powders to obtain a slurry with a density of 2.4 g cm^{-3}, which was dense enough, but still can be poured. The second step was to find the appropriate mould form.

Different types of materials were investigated, such as stainless steel, glass, plastic, gypsum, and silicone rubber. The prepared slurries stuck to most of these materials rendering them useless for moulding with the exception of silicone rubber as sample could be removed perfectly. Using this type of moulds we can make superconductors with complex geometry.

The moulded samples were heat treated at the same program as used for hydraulic pressed samples. The moulding technique applies no pressing thus provides a porous structure. However, the pores can lead to poor superconductor properties. To decrease the porosity melt-producing dopants were applied. Ag and Pb with Ce proved to be good in the case of hydraulic pressed samples.

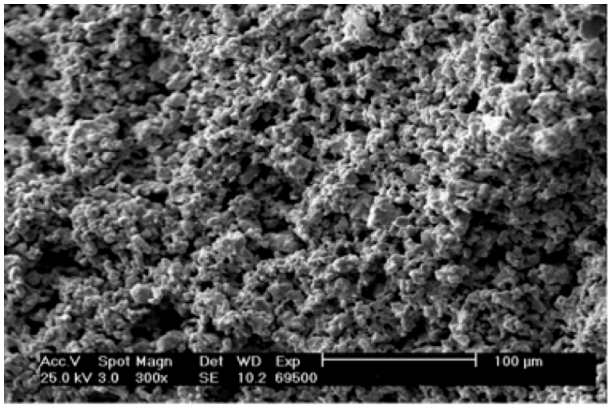

Figure 2: SEM micrograph of the moulded sample ground conventionally

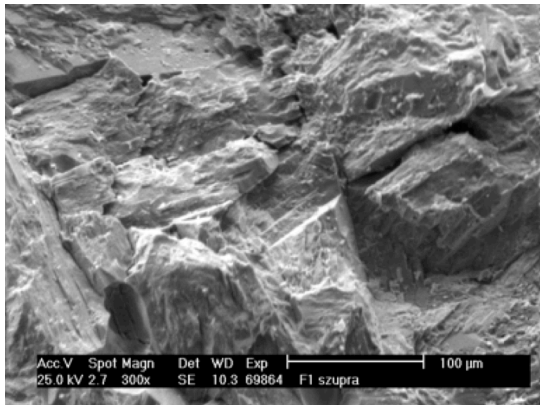

Figure 3: SEM micrograph of the molded sample ground in alcohol

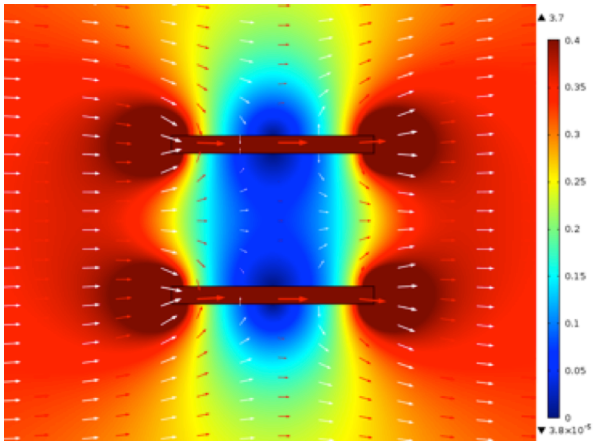

Figure 4: Simulation of iron shield

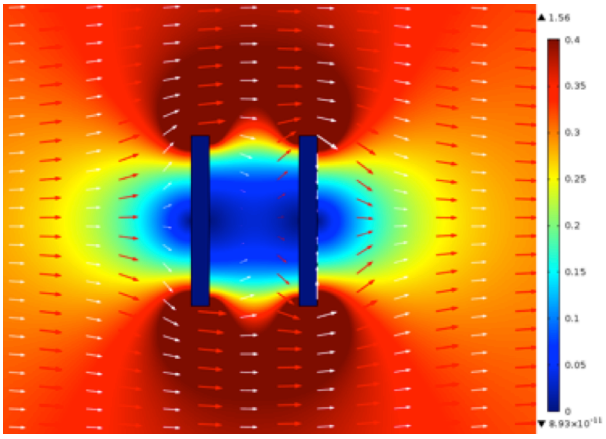

Figure 5: Simulation of superconductor shield

It was found that only in the moulded samples prepared from barium hydroxide ground in alcohol provide enough melt for efficiently fill the pores. The use of dopants alone toward this goal was not sufficient. Furthermore, with this grinding technique, the peritectic temperature of the superconducting phase (123) decreased, which allowed for a more economical heat treatment. It can be proposed that this grinding resulted in particle size reduction of barium hydroxide and the higher specific surface area leading to higher reactivity. In this case bulk superconductor with higher density can be obtained, which has an oriented, large plate-like 123-crystalls containing structure *(Figs.2* and *3)*.

Modelling YBCO as Magnetic Shield

YBCO can shield from magnetic fluxes due to the MEISSNER effect. It works the opposite way than the commonly used ferromagnetic materials, which means that superconductor expels the magnetic fluxes from itself, while iron collects them. Using the COMSOL Multiphysics 4.4 package, the shields of iron and superconductor were compared in *Figs.4* and *5*.

The shielding ability of the superconductor is comparable with iron, and even better. It has the advantage that in alternating magnetic field it does not get heated. The ferromagnetic materials shield poorly in too small and too big fields because they have saturation flux density. Superconductors are being used as shields in various devices [12–16].

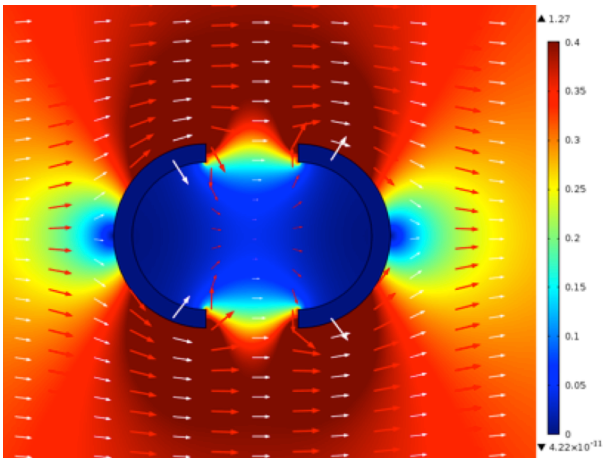

Figure 6: Simulation of shielding for sphell geometry

With a geometry shown in *Fig.6*, very sensitive magnetic devices could be fully shielded and *vice versa* the environment could be protected from a device, which induces strong magnetic field. With the shape in *Fig.7*, for example a skull could be protected in the MRI in case of presence of metal implants in the head.

Theoretically moulding could be used to prepare these shields. It would be cheaper and thin layers could be made, thus more economical wall could be produced by a few thin layers.

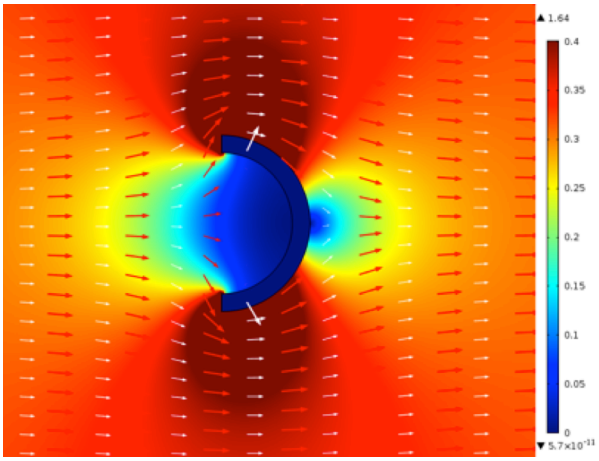

Figure 7: Simulaton of shielding using a semi-sphell geometry

Conclusion

In the case of the hydraulic pressed pellets, the results confirmed those from the literatures. Improved magnetic properties were noticed with the increasing of the 211 phase content. This was further enhanced by the presence dopants. It was found that Pb performs as good as Pt or even a little bit better, which is preferred due to the price of Pt. The grinding of barium-hydroxide in the presence of alcohol provided a denser structure and more melt phase leading to better superconducting properties. Furthermore, it seems that this method decreases the peritectic temperature of the superconducting 123 phase. The homogenization needs to take place after grinding in alcohol to be effective.

The adequate liquid-to-material ratio to make a slurry with 1 wt% polyvinyl formal in dioxane and the ideal moulding form of silicone rubber were determined. This allowed for making complex shaped superconductors. The melt-producing dopants cannot reduce the porosity enough to sufficiently improve the levitation force. Alternative heat treatment programs with slow annealing up to 500 ºC, while all of the organic materials burn out, can avoid the cracks in the structure. Application of vacuum during the moulding can also be useful, since it can eliminate trapped air bubbles from the mass.

Simulations carried out using Comsol Multiphysics 4.4 software indicated YBCO being a good shielding material. Utilization of complex geometries, sensitive devices can be protected, such as skull protection during MRI measurements.

REFERENCES

[1] TAKASH M., TOMIOKA Y., MIYAUCHI T., SATO S., MURAI A., IDO T., WAKITA K., TERADA H., OHKIDO S., MATSUBARA M.: Characterization of a large-scale non-doped $YBa_2Cu_3O_7$-x superconductor prepared by plastic forming without high-pressure molding, J. Amer. Ceram. Soc. *2007*, 90(7), 2032–2037

[2] EVETTS J.: Concise Encyclopaedia of Magnetic and Superconducting Materials, Pergamum Press, Oxford, *1992*, pp. 532–533

[3] MONOT I., LEBLOND C., MARINEL S.M., DESGARDIN G.: Precursor and microstructure control for melt texturing of high-Tc superconductive YBCO ceramics, Development of high-temperature superconducting alternators combining rotating and levitating principles, Russian Academy of Science, Saint-Petersburg, *2002*, pp. 27–45

[4] SHLYK L., NENKOV K., KRABBES G., FUCHS G.: Melt-processed YBCO with Pt or Ce additions: comparison of pinning behaviour, Physica C *2005*, 423, 22–28

[5] RICHES J.D., ALARCO J.A., BARRY J.C.: Effects of PtO_2 and CeO_2 additives on the microstructures of the quenched melts of Y–Ba–Cu–O materials Physica C Superconductivity, *2000*, 336, 43–56

[6] LEBLOND C., MONOT I., PROVOST J., DESGARDIN G.: Optimization of the texture formation and characterization of large size top-seeded-melt-grown YBCO pellets, Physica C, *1999*, 311, 211–222

[7] HARDY V., SIMON C., PROVOST J., GROULT D.: Pinning forces in Bi-2212 single crystals irradiated by 6 GeV Pb ions, Physica C, *1993*, 206, 220–226

[8] WESCHE R.: Magnetic relaxation and flux pinning in $YBa_2Cu_3O_7$ a high-Tc oxide irradiated by 5.3 GeV Pb ions, Physica North-Holland C *1992*, 190, 289–298

[9] HORVAT J., WANG X.L., DOU S.X.: Vortex pinning in heavily Pb-doped Bi2212 crystals Physica C *1999*, 324, 211–219

[10] GRADER G.S., JOHSON D.W.: Forming methods for high Tc superconductors, Thermochimica Acta, *1991*, 174, 239–251

[11] KOMLAI K.: Investigation of the the properties of the incongruent melting reaction of YBa_2Cu_3O-y superconductor phase, M.Sc. Thesis, University of Pannonia, *2013* (in Hungarian)

[12] TAVERNIER S.P.K., VAN DEN BOGAERT F., VAN LANCKER L.: The design of a magnetic shielding for an array of photomultipliers in a strong external field, Nucl. Instrum. Methods, *1979*, 167, 391–398

[13] BITTER T., EISERT F., EL-MUZEINI P., KESSLER M., KINKEL U., MEMT E., LIPPERT W., MEIENBURG W., WERNER R.: A large volume magnetic shielding system for the ILL neutron-antineutron oscillation experiment, Nucl. Instrum. Methods Phys. Res., *1991*, A309, 521–529

[14] TRIPATHI A., VEDAVATHY T.S.: Electromagnetic shielding using superconductors, Pergamon Press Ltd, Oxford,Vol. 2, No. I, *1994*, pp. l–5

[15] SPILLANTINI P.: Active shielding for long duration interplanetary manned missions, Adv. Space Res., *2010*, 45, 900–916

[16] YUSUF S.M., OSGOOD III R.M., JIANG J.S., SOWERS C.H., BADER S.D., FULLERTON E.E., FELCHER G.P.: Magnetic profile in Nb/Si superconducting multilayers, J. Magnet. Magnetic Mat., *1999*, 198–199, 564–566

HUNGARIAN JOURNAL
OF INDUSTRY AND CHEMISTRY
VESZPRÉM
Vol. 42(1) pp. 43–50 (2014)

EFFECTS OF ULTRASONIC DISINTEGRATION, HOT-COMPRESSED LIQUID WATER PRE-TREATMENT, AND STEAM EXPLOSION ON SOLVOLYSIS AND DIGESTIBILITY OF GRAIN SORGHUM STOVER

DÁNIEL CAPÁRI,✉ AND ANDRÁS DALLOS

Department of Physical Chemistry, University of Pannonia, Egyetem str. 10, Veszprém, H-8200, HUNGARY
✉E-mail: capari.daniel@gmail.com

One of the most promising renewable energy crops and biomass feedstock for biogas production in Europe is the C4 plant grain sorghum due to its high photosynthetic efficiency. The release of lignocellulosic material and therefore the acceleration of degradation processes of sorghum stalks and leaves can be achieved using mechanical and thermal pre-treatments, which assist to hydrolyse the cell walls and speed the solvolysis of biopolymers. This study is focused on hot-compressed liquid water, steam explosion and ultrasonic pre-treatments of grain sorghum stover. The effectiveness of pre-treatments was evaluated by means of soluble chemical oxygen demand, biochemical oxygen demand, and by the biogas and methane productivities. The results show that the pre-treatments disintegrated the lignocellulosic structure, increased and accelerated the biogas and methane production, and increased the mesophilic anaerobic digestion potential of grain sorghum stover. Our laboratory tests demonstrated that the steam exploded grain sorghum stover possess the highest biogas productivity.

Keywords: grain sorghum stover; hot-compressed liquid water pre-treatment; steam explosion; ultrasonic disintegration, biogas digestion.

Introduction

The grain sorghum is a possible carbohydrate resource for the simultaneous production of bioethanol and biogas due to its advantages over the traditional agricultural crops. The plants have remarkably good CO_2 absorption ability. Grain sorghum is the fifth most important cereal crop grown in the world. The drought tolerance of sorghum is greater than that of corn. Furthermore, it is able to regenerate after a period of drought. Its productivity is also higher than that of corn, even in dry periods or in lower quality soils. In Hungary, sorghum grows in arid areas as a substitution for fodder corn. Therefore sorghum could be used to cultivate alternative feedstock for bioethanol production [1] and could be a sustainable crop for energy production in Europe. The sorghum grain contains approximately the same amount of starch compared to corn kernels, which makes it attractive as raw material for the production of bioethanol. The agricultural by-product of sorghum-based bioethanol production, the sorghum stover is a valuable bioenergy substrate for biogas digesters, despite the complex lignocellulosic structures of sorghum stalks and leaves and its resistance to decomposition. The utility and the economic feasibility in biogas power plants can be highly increased by different pre-treatment methods, to assist the disruption of the cell wall structure and to speed-up the solubilisation of the biopolymers in the biogas feedstock [2–4]. The purpose of pre-treatments is to remove lignin and hemicellulose, reduce cellulose crystallinity, and increase porosity [5,6] *(Fig.1)*.

Liquid hot-compressed water (LHCW) pre-treatment is a commonly used hydrothermal method. High temperature and high pressure are applied to maintain liquid phase and to avoid vaporization. During the pre-treatment, water is penetrated into the cell structure of the biomass, hydrating cellulose, solubilizing hemicellulose, and slightly removing lignin. LHCW pre-treatment is highly effective for enlarging the accessible and susceptible surface area of cellulose and improving cellulose degradability for microbes and their enzymes [7,8]. After the hydrothermal treatment, the biogas production was increased for pig manure, for municipal sewage sludge and for fruit/vegetable waste

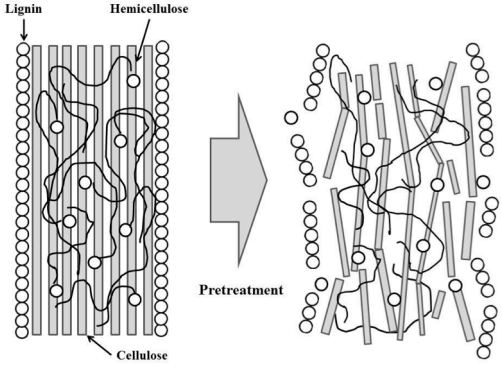

Figure 1: The disintegration of lignocellulosic material by pre-treatments

[9]. The hot water treatment increases the enzymatic hydrolysis and digestion of corn leaf, stalk and fibre [10,11] and the dissolution of solids and xylan of destarched corn fibre [12]. The liquid hot water pre-treatment of sorghum bagasse produced higher solubilisation of hemicellulose and cellulose content enrichment [13]. Combining hydrothermal treatment and enzymatic hydrolysis of sorghum bagasse resulted in improvement of cellulose and total polysaccharides hydrolysis [14].

Steam explosion (SE) is one of the most effective methods for the pre-treatment of lignocellulosic biomass. In this process, the biomass is heated with high-pressure steam for a certain period, than the pressure is reduced to atmospheric pressure as quickly as possible. The biomass is undergone on an explosive decompression by this swift reduction of pressure [6,7]. The high efficiency of the steam explosion treatment is due to the thermo-mechano-chemical destruction applied in the method. Steam-explosion has been used to treat various kinds of lignocellulosic biomass (i.e. softwood, sugarcane bagasse, corn stalk) for enhanced bioethanol and biogas production [15–19]. SIPOS *et al.* [20] demonstrated the efficient effect of pre-treatment by steam on sorghum bagasse characterized by high degree of cellulose hydrolysis. ZHANG *et al.* [21] compared four pre-treatment processes including liquids, steam explosion, lime and dilute acid for enzymatic hydrolysis of sorghum bagasse and pointed out that steam-explosion showed the greatest improvement on enzymatic hydrolysis.

The biogas yields of anaerobic digestion can be also increased by ultrasonic treatments (UT) to support the solubilisation of raw materials. During the ultrasonic treatment, a cyclic sound pressure is used to disintegrate the cell walls by cavitation. The parameters of the sonication are the power, frequency and time of sonication [3,22]. ZHANG *et al.* [23] showed that ultrasonic pre-treatments caused indistinctive effects on bio-hydrogen production. The ultrasonic treatment accelerated the enzymatic hydrolysis of corn stover and sugar cane bagasse cellulose [24] and improved the liquefaction and saccharification of sorghum flour [25]. IMAM *et al.* [26] pointed out the positive effects of ultrasonic plus hot water pre-treatment on the conversion of sweet sorghum to hexose and pentose sugars and on lignin, cellulose and hemicellulose concentrations.

However, no systematic studies on pre-treatments of grain sorghum stover are available in literature. A correct comparison of the various pre-treatments and the selection of the suitable processes for the disintegration of grain sorghum stover as feedstock for enhanced biogas production are the goals and the novelty of this paper. However, the main message of this work is that a perfect testing is only possible, if there are no differences in the microbial communities in different biogas fermenters, in the inocula used, in the substrates cultivated and in the methods applied to assess pre-treatments: chemical analysis, batch tests or continuous AD.

Therefore this work is focused on liquid hot-compressed water, steam explosion and ultrasonic pre-treatments of grain sorghum stover using both fast analytical, biochemical and biomethane potential AD tests to study and comparison the effects of pre-treatments on anaerobic digestion without addition of chemicals. The influence of temperature, contact time of thermal treatments, and the effect of sonication energy on decomposition of lignocellulose on a chemical level were determined using laboratory scale experimental techniques. The effectiveness of thermal and ultrasonic treatments was evaluated by SCOD and BOD_5 concentrations and by the biogas and methane productivities during mesophilic fermentations.

Experimental

Materials

Sorghum stover investigated in this work consists of leaves and stalks of commercial grain sorghum (Milo) hybrid named *Mexican Sweet* (code: HF1) harvested from the B12 field at Kétegyháza, Hungary, and used for pre-treatments and biogas production experiments. This easily grown hybrid with mid-early maturation was developed by J. FECZÁK (Agroszemek Ltd., Szeged, Hungary). Post-harvest residue grain sorghum stover samples were chopped, homogenized, and analysed for dry substance (DS, 93.6%), organic dry substance (94.5%), and ash (5.5%). Deionized water was used in all experiments after cation and anion exchange.

Liquid Hot-Compressed Water Treatments

The LHCW pre-treatments were carried out in a 2 L capacity Parr 4843 type high-pressure reactor at the temperatures of 100, 150 and 175 °C (0.1, 0.5 and 0.9 MPa, respectively) and at various treating time from 10 to 120 minutes. 25 g of grain sorghum stover were used in each experiment and were added to 1000 g of water. The suspension was introduced in the thermal reactor at room temperature and heated to the set temperature. The pulp slurry was mixed by a built-in stirrer at 300 rpm during the entire treating process to avoid temperature gradients. After treatment, the reactor was cooled down to 30 °C by the built-in cooling system of the reactor using cold water-flow and the treated slurry was removed from the vessel.

Steam Explosion Pre-treatments

SE treatments were performed in a steam explosion laboratory unit *(Fig.2)* consisted of a steam generator (2), a digester vessel (6) and a separator cyclone (8). A 2 L capacity PARR 4843 reactor was used for the production of steam with temperatures of 185, 200, and 215 °C and working pressures of 1.1 MPa, 1.6 MPa, and 2.1 MPa, respectively. The SE unit operated in batches and equipped with a digester vessel (6) of 200 cm^3 volume. The digester vessel was filled with 10 g

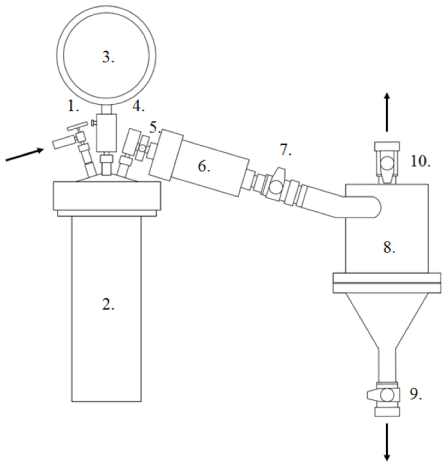

Figure 2: Scheme of the steam explosion apparatus (1. input valve, 2. steam generator, Parr 4843 reactor, 3. pressure gauge, 4. evacuation valve, 5. steam inlet valve, 6. digester vessel, 7. expansion valve, 8. cyclone, 9. sampling valve, 10. steam outlet valve)

feedstock per batch and was heated to the desired temperature, directly with saturated steam led to the vessel, by opening the steam inlet valve (5). No catalysts (additional chemicals) were applied in the process. After the steaming time (1–10 minutes), the expansion valve (7) was opened to rapidly reduce the vessel pressure to the atmospheric one. The steamed sample slurry explosively released into the separator cyclone (8).

Ultrasonic treatments

The ultrasonication was performed in a Vibracell VCX 750 (Sonics & Materials, USA) ultrasonic processor operated at constant sonication frequency of 20 kHz with maximum power input of 750 W. The radiation was carried out by a 25.4 mm diameter titan alloy (Ti-6Al-4V) probe with removable tip and maximum amplitude of 35 μm. Samples of the mixture of grain sorghum stover (1 g) and water (99 g) placed in a temperature-controlled vessel. They were subjected to ultrasonic pre-treatment without additional agitation at different power inputs by adjustment of the amplitude (50, 70 and 100%) and at various sonication durations of from 1 to 10 minutes for each power level. The temperature of the vessel was held constant at 25 °C during the treatment by a high-precision thermo-regulator (Huber Kältemaschinenbau GmbH, Germany).

Aliquot parts of the resulting sorghum stover pulp slurries of samples obtained from pre-treatments were used as substrate in AD test. The rests were filtered to separate the solid fraction from the liquid fraction for analytical measurements (SCOD, BOD_5, pH). A set of untreated, blank samples was also tested for chemical analysis and methane potential by AD as the control points of reference for the treated samples.

Mesophilic Anaerobic Digestions

The anaerobic degradability of untreated, LHCW, SE, and UT pre-treated grain sorghum stover slurries was determined in laboratory scale, using a fermenter system contained 12 Pyrex batch reactors of 1 L capacities. Inoculum for the AD tests was taken from the effluent line of an anaerobic pilot fermenter [27] treating a mixture of swine manure and corn stillage (spent mash remaining after bioethanol distillation) at biogas test facility of DENK Ltd (Kövegyűrpuszta, Hungary). The batch reactors were inoculated by 700 g inocula. Afterwards a batch of 100 g of grain sorghum stover pulp slurry samples was added under nitrogen atmosphere. Furthermore, the digester materials were bubbled with nitrogen gas for 10 minutes to get rid of the air from the liquid phase before each experiment. The batch reactors were kept in a temperature-controlled water bath at 37 °C until they stopped producing biogas. The mesophilic AD tests performed for grain sorghum stover substrates including controls were all done in duplicate. During the 36–40 days mesophilic AD tests the flows of the produced biogas were on-line measured by digital flow meters and the daily and cumulated biogas volumes were stored digitally. The methane content was determined by gas chromatography.

Analytical and Biochemical Measurements

The SCOD, pH, and BOD_5 measurements were carried out on the liquid fractions after 10 min centrifugation at 14,000 rpm and 20 °C with a refrigerated universal high-speed, filtration (0.45 μm) centrifuge (UniCen MR, Herolab, Germany). Colorimetric SCOD concentration was measured by the Standard Methods procedure [28] using a Nanocolor Vario Compact heating block (MACHEREY-NAGEL, Germany) and a MultiDirect photometer (Tintometer/Lovibond, Germany) according to DIN ISO 15705. Biochemical oxygen demand (BOD_5) was determined according to EN 1899-1 and EN 1899-2 by using OxiTop Control 6 OC 100 (WTW, Germany) system. The pH values were measured by a C831 type pH meter (Consort, Belgium) with an RA-0903P sensor (Radelkis, Hungary) after two-point pH calibration (pH = 4.01 ± 0.01 and pH = 7.00 ± 0.01) using DuraCal pH buffers (Hamilton, Switzerland). The surfaces of the grain sorghum stalk were investigated by a PHILIPS XL30ESEM environmental scanning electron microscope (ESEM) with 20 kV accelerating voltage and resolution of 3.5 nm, in secondary electron image mode (SEI), and backscattered electron image mode (BEI).

Results and Discussion

Liquid Hot-Compressed Water Treatments

The influence of LHCW pre-treatments at various temperatures and treating times on SCOD concentration of grain sorghum stover slurry is visualized by 3D mesh segmentation on *Fig.3*.

The results of LHCW pre-treatments show that hot-compressed water has a positive effect in grain sorghum stover disintegration, leading to significant increments in SCOD concentration: +262% at 100 °C, +419% at

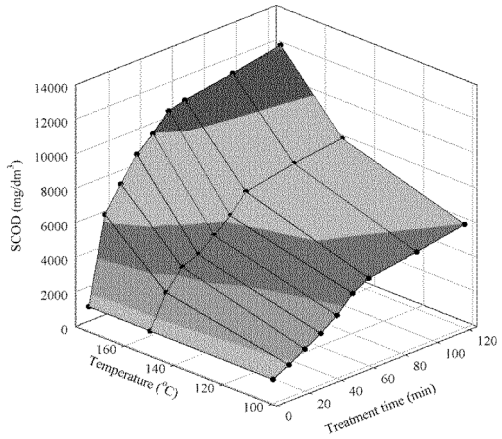

Figure 3: Effects of temperatures and contact times of LHCW pre-treatments on SCOD concentration of grain sorghum stover suspension (●: experimental data points)

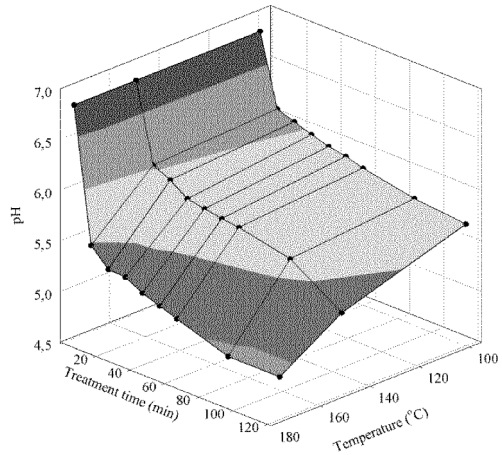

Figure 4: Acidity of grain sorghum stover slurries as the function of LHCW contact time and temperature (●: experimental data point)

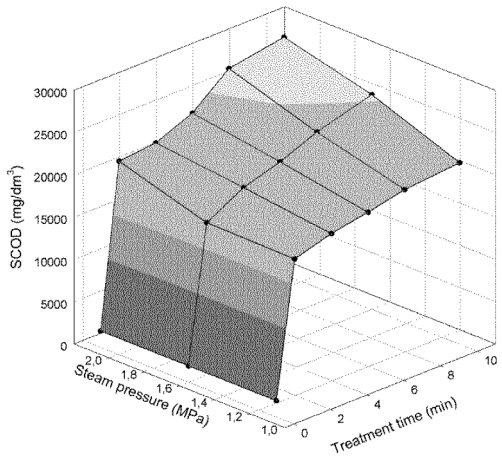

Figure 5: Effects of steam pressures on SCOD concentration levels of grain sorghum stover slurries as the function of the contact time during steam explosion (●: experimental data points)

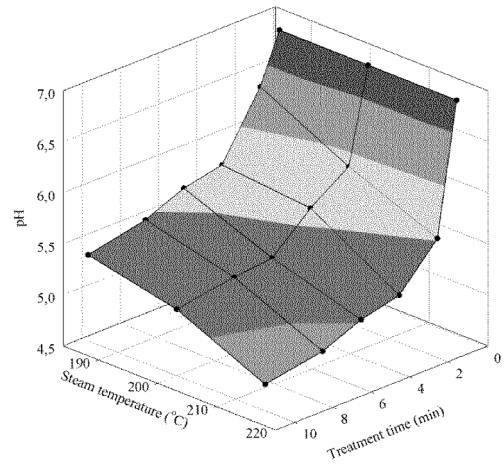

Figure 6: The effect of steam explosion on pH values of treated grain sorghum stover slurry at various steam pressures as the function of the treatment time (●: experimental data points)

150 °C and + 698% at 175 °C with an operating time of 60 min, respectively. The control experiments were performed using untreated grain sorghum stover suspension. Both temperature and time have positive, but not linear effects on SCOD and not to the same degree. The temperature raising has more effect on the solubilisation of grain sorghum stover after 60 minutes than the treating time in agreement with the results of VALO *et al.* [29] who found that treating time had less influence than temperature during thermal treatment of sludge. It is notable that higher solvolysis temperatures resulted in more acidic products as reflected by the low pH level of the grain sorghum stover slurry *(Fig.4)*.

Steam Explosion Pre-Treatments

The pressures and temperatures of SE pre-treatments had significant effect on digestibility of grain sorghum stover. Elevated pressures and temperatures resulted in enhanced solubilisation *(Fig.5)*. The positive pressure effect may be explained by the increased disintegration caused by higher-pressure drop at the end of treatment. Compounds that are more soluble were released from the grain sorghum stover during the steam explosion and made the resulting slurry available to subsequent bacterial degradation.

The pressure effect is quasi-linear and the effect of contact time can be modelled by an exponential-to-maximum function. Compared to the untreated grain sorghum stover, the SCOD concentrations of the slurries increased by a factor of 8.9, 9.6, 10 at 185, 200, and 215 °C, respectively, with an operating time of 3 min, respectively. Additional, the pH value decreased with pre-treatment pressure (steam temperature) and with the contact time *(Fig.6)*. The formation of acidic degradation products during disintegration of grain sorghum stover slurry by steam explosion agree well with the observation of GUO *et al.* [30] at corn stalk steam explosion.

Ultrasonic Treatments

The efficiency of ultrasonic irradiation of grain sorghum stover was quantified by SCOD concentration of the slurry as a function of contact time and power input in terms of ultrasonic amplitude level (%) and specific sonication energy. Results of ultrasonic treatments are shown in *Fig.7*, where the values of the SCOD

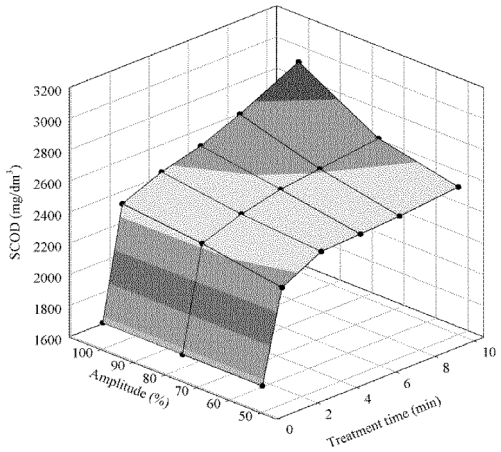

Figure 7: The effect of sonication energy on SCOD concentration level of grain sorghum stover slurry as the function of sonication time and relative ultrasound amplitude (●: experimental data points)

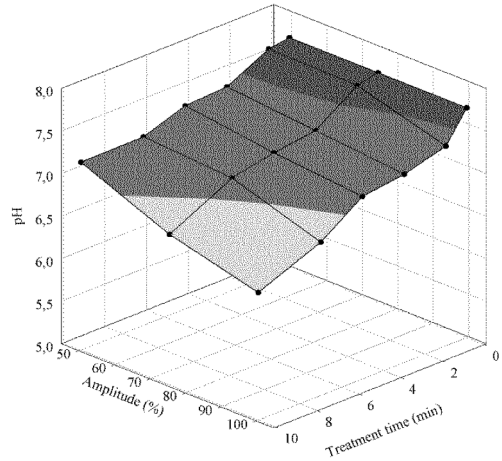

Figure 9: The effect of sonication power on the pH values of grain sorghum stover slurries as the function of the sonication time (●: experimental data points)

concentrations are presented for each value of the ultrasonic amplitude level (%), and sonication time. The SCOD of the pulps increased with the ultrasonic power demonstrating the effectiveness of the cavitation energy to disrupt the cell walls of the plant parts. The SCOD concentration excess reached +105%, +109%, and +133% at 50%, 70%, and 100% amplitude level, respectively, with a contact time of 3 min.

The ultrasonic power and the pre-treatment time affect the SCOD to a different degree. The raising of SCOD values by treating time is stabilized after 3 minutes. These can be described by an exponential-to-maximum function. The effect of energy-input on SCOD is quasi-linear (R^2 = 0.942) as demonstrated by the data shown in *Fig.8*, where SCOD values are plotted against the specific sonication energy. The SCOD concentrations were increased by the sonication energy; however, no power-saturation phenomenon was observed. The sonication energy over the minimal energy of 1kJ g^{-1} DS is the most effective for breaking up cells [31].

The pH values of the sonicated grain sorghum stover slurries decreased monotonously with pre-treatment time and sonication power on a small scale *(Fig.9)*

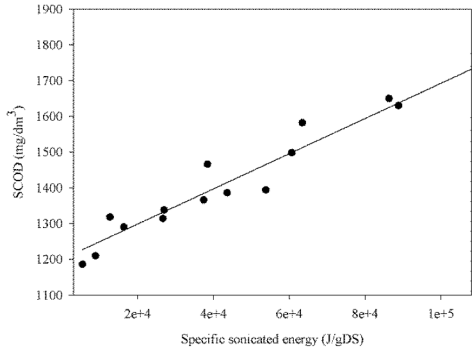

Figure 8: SCOD change in grain sorghum stover slurry as a function of specific sonication energy (●: experimental data points)

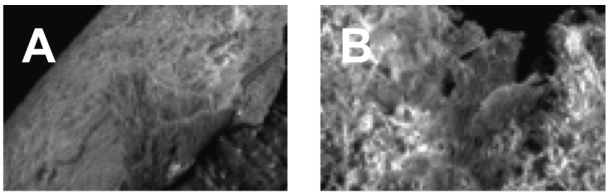

Figure 10: ESEM pictures of the surface on untreated (A) and by ultrasonic treated (B) grain sorghum stalks at 100× magnification

suggesting that local temperature effects caused by cavitation bubbles were not enough to accelerate the hydrolytic processes resulted in acidic degradation product.

Environmental Scanning Electron Microscopy

The ESEM pictures of the surfaces on untreated and by ultrasonic treated grain sorghum stalks are shown in *Fig.10* at 100× magnification. The surface of the treated sorghum stalk was altered *(Fig.10B)* from the appearance of defective plant tissues. *Fig.10B* shows a heterogeneous appearance compared to the homogeneous surface of the untreated stalk *(Fig.10A)*.

The comparison of the pre-treatment results of the chemical analysis, the SCOD concentration, and pH changes of grain sorghum stover slurries suggested that the most effective disintegration method is the steam explosion to disrupt the lignocellulosic structure of grain sorghum stover and partial hydrolysis of it molecular components. However, results of these fast methods can only indicate how much structures of lignocellulosic materials broke down on a chemical level. Nevertheless, greater decomposition of the lignocellulose structures does not necessarily prove enhanced biogas production, because inhibitors for methanogenesis reactions can also be produced through hydrolytic processes during steam explosion. Furthermore, one has to take into account the high energy needs of treatments at elevated temperatures. According to the results of fast chemical analyses (SCOD and pH), the optimal conditions for the LHCW, steam explosion and ultrasonic treatment of grain sorghum stover were established as 150 °C / 30 min, 200 °C / 3 min and 100% ultrasound amplitude / 3 min (at 25 °C), respectively. However, to study the real effect of optimal conditions of the investigated pre-

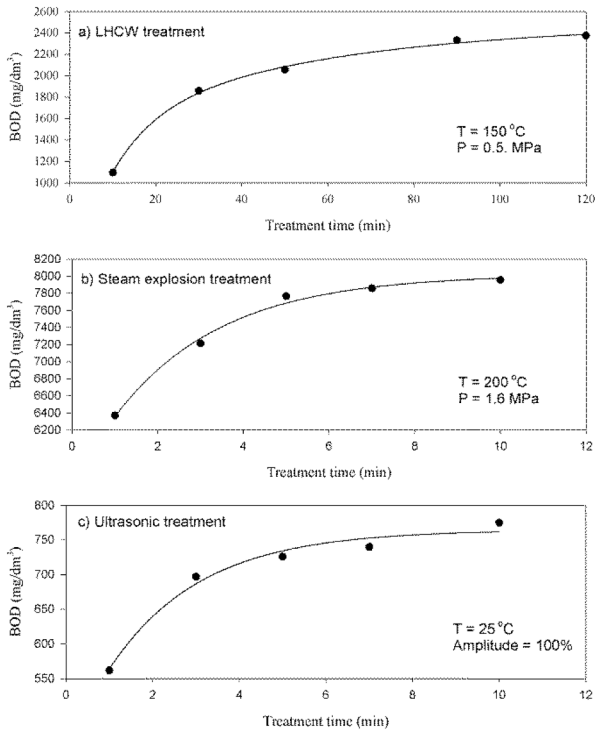

Figure 11: Comparison of the BOD_5 test of filtrates of grain sorghum stover slurries after various pre-treatment methods

treatments additional biochemical tests like BOD and biomethane potential determinations are necessary.

Biochemical Oxygen Demand

A comparison of the biochemical oxygen demands of filtrates of grain sorghum stover slurries after pre-treatments at the optimal conditions is given in *Fig11*. The results of the BOD_5 tests support the observations from chemical analysis. Actually, all three methods investigated are appropriate for pre-treatment of grain sorghum stover, because the BOD_5 values systematically increased in filtrates of grain sorghum stover slurries with the treatment time under the conditions investigated. However, the highest BOD_5 values were obtained in filtrates after steam explosion, therefore the steam explosion seems to be the most effective disintegration method to disrupt the lignocellulosic structure of grain sorghum stover and to partially hydrolyse its molecular species, resulting in the formation of bacterially digestible substrate.

Biogas Production by Mesophilic Anaerobic Digestions

Biogas and biomethane production tests were carried out using grain sorghum stover slurries pre-treated under stated optimal conditions (LHCW: 150 °C / 30 min, steam explosion: 200 °C / 3 min, and ultrasonic treatment: 100% ultrasound amplitude / 3 min at 25 °C). Daily as well as the final biogas and methane production (normalized volumes at 0 °C and 101.15 kPa) were determined. The results are shown as a function of the digestion time in *Figs.12* and *13*. The specific gas productions were calculated by dividing the

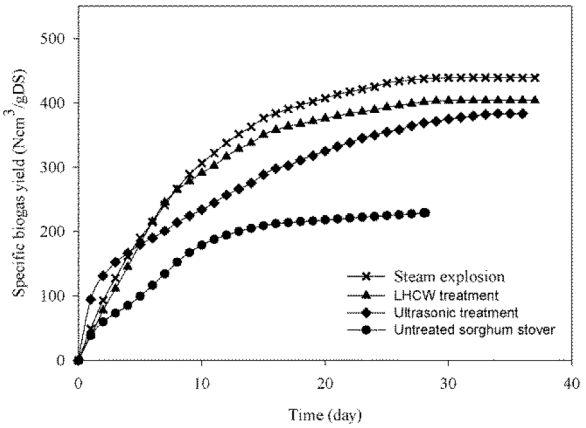

Figure 12: Specific cumulative biogas yield (Ncm^3/g DS) of grain sorghum stover substrates after pre-treatments

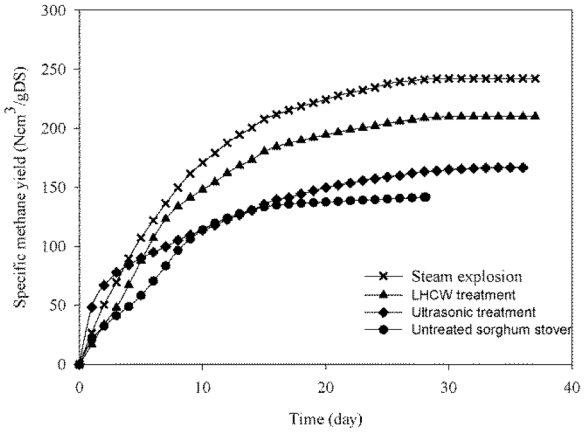

Figure 13: Specific cumulative methane yield ($Ncm^3\ g^{-1}$ DS) of grain sorghum stover substrates after pre-treatments

cumulated gas amount with the total DS of the substrates. As reference, the untreated material was used in the same amount. In agreement with the results of chemical analytical and biochemical tests after pre-treatments, the specific total biogas and methane yields obtained for treated grain sorghum stover substrates were significant higher than that of the untreated control.

As seen in *Fig.12*, biogas productions began immediately, without a lag period after starting the degradation of grain sorghum stover. The fastest biogas production at the beginning was detected at the ultrasonicated substrate. However, the highest biogas production was observed during the fermentation of steam-exploded substrate. The biogas production proceeded in constant and high daily biogas production for treated substrates until the 30^{th} day of hydraulic retention time. This observation is notable, because the application of pre-treatments can decrease the usual cycle time for biogas fermentation and increase the production of biogas with higher methane content. The comparison of the biomethane yields is given in *Fig.13.* Methane production, as the major result of anaerobic digestion of pre-treated grain sorghum stover, was markedly increased by the three pre-treatments. The highest biomethane production rate was observed at the substrates after ultrasonic and steam explosion pre-treatments. The biomethane production rate of LHCW

treated substrate was lower, probably due to the low pH of the pre-treated grain sorghum stover slurry.

Our laboratory tests have shown that the steam exploded substrate possess has the highest biogas production potential (439 Ncm^3 g^{-1} DS) during hydraulic retention times of 36 days with 55% methane content. The steam explosion pre-treatment increased the biomethane yield by +72% to 242 Ncm^3 g^{-1} DS. The LHCW pre-treated substrate has the second highest biogas production potential (403 Ncm^3 g^{-1} DS) during hydraulic retention times of 36 days with 52% methane content, the LHCW pre-treatment increased the biomethane yield by 49% to 210 Ncm^3 g^{-1} DS. This yield increment is higher than that was obtained by QIAO *et al.* [9] for various biomass wastes after hydrothermal treatment. The substrate after ultrasonic pre-treatment has a biogas production potential of 383 Ncm^3 g^{-1} DS during hydraulic retention times of 36 days with 44% methane content, the ultrasonic pre-treatment increased the biomethane yield by 18% to 167 Ncm^3 g^{-1} DS. The low biogas and methane yields of ultrasonic treated grain sorghum stover can be explained by the superficial effect of ultrasonic cavitation.

Conclusions

The results of chemical, biochemical analyses and biogas/biomethane potential test obtained by mesophilic anaerobic digestion were presented. It was found that LHCW treatment and steam explosion are the most effective biomass pre-treatment for increasing the solubilisation of the organic matters of grain sorghum stover. Laboratory testing of anaerobic digestibility of pre-treated slurries have shown that the grain sorghum stover has high biogas potential. It can serve as biogas feedstock and could reduce the energy consumption of sorghum-based bioethanol production in the future. The LHCW and steam explosion biomass pre-treatment techniques can reduce the cycle time and improve the biogas production via disintegration of the complex and compact plant structures of grain sorghum stover.

ACKNOWLEDGEMENTS

This research was supported by TÁMOP 4.2.4. A/2-11-1-2012-0001 „National Excellence Program – Elaborating and operating an inland student and researcher personal support system". The project was subsidized by the European Union and co-financed by the European Social Fund. Authors also gratefully acknowledge the support of the Hungarian State and European Union under the TÁMOP-4.2.2.A-11/1/KONV-2012-0071 project.

REFERENCES

[1] SALDIVAR S.R.O.S., CARRILLO E.P., ALVAREZ M.M.: Method for obtaining bioethanol from sorghum grain (Sorghum Bicolor L.Moench) comprising steps involving decortication and hydrolysis with proteases. Patent application number: US 20110014671 A1, *2011*

[2] MCMILLAN J.D.: Pre-treatment of Lignocellulosic Biomass, in: Enzymatic Conversion of Biomass for Fuels Production (Eds: M.E.HIMMEL, J.O.BAKER, R.P.OVEREND), ACS Symposium Series, *1994*, 566, 292–324

[3] CESARO A., NADDEO V., AMODIO V., BELGIORN V.: Enhanced biogas production from anaerobic codigestion of solid waste by sonolysis, Ultrasonics Sonochemistry, *2012*, 19(3), 596–600,

[4] HARUN M.Y., RADIAH A.Z.D., ZAINAL ABIDIN Z., YUNUS R.: Effect of physical pre-treatment on dilute acid hydrolysis of water hyacinth *(Eichhornia crassipes)*, Biores. Technol., *2011*, 102(8), 5193–5199

[5] SUN Y., CHENG J.: Hydrolysis of lignocellulosic materials for ethanol production: a review, Biores. Technol*., 2002*, 83(1), 1–11

[6] HAGHIGHI MOOD S., HOSSEIN GOLFESHAN A., TABATABAEI M., SALEHI JOUZANI G., NAJAFI G.H., GHOLAMI M., ARDJMAND M.: Lignocellulosic biomass to bioethanol, a comprehensive review with a focus on pre-treatment. Renew. Sustain. Energy Rev., *2013*, 27, 77–93

[7] ZHENG Y., ZHAO J., XU F., LI Y.B.: Pre-treatment of lignocellulosic biomass for enhanced biogas production, Prof. Energy Comb. Sci., *2014*, 42, 35–53

[8] VAN WALSUM G.P., ALIEN S.G., SPENCER M.J., LASER M.S., ANTAL JR. M.J., LYND L.R.: Conversion of lignocellulosics pretreated with liquid hot water to ethanol. Appl. Biochem. BioTechnol. A*, 1996*, 57–58, 157–170

[9] QIAO W., YAN X., YE J., SUN Y., WANG W., ZHANG Z.: Evaluation of biogas production from different biomass wastes with/without hydrothermal pre-treatment. Renewable Energy*, 2011*, 36 (12), 3313–3318

[10] SU D., SUN J., LIU P., LÜ Y.: Effects of Different Pre-treatment Modes on the Enzymatic Digestibility of Corn Leaf and Corn Stalk, Chinese J. Chem. Engng., *2006*, 14(6), 796–801

[11] DIEN B.S., LI X.L., ITEN L.B., JORDAN D.B., NICHOLS N.N., O'BRYAN P.J., COTTA M.A: Enzymatic saccharification of hot-water pretreated corn fiber for production of monosaccharides, Enzyme Microbial Technol., *2006*, 39(5), 1137–1144

[12] WEIL J., SARIKAYA A., RAU S., GOETZ J., LADISCH C., BREWER M., HENDRICKSON R., LADISCH M.: Pre-treatment of corn fiber by pressure cooking in water, Appl. Biochem. Biotech., *1998*, 73(1), 1–17

[13] ROHOWSKY B., HÄULER T., GLADIS A., REMMELE E., SCHIEDER D., FAULSTICH M.: Feasibility of simultaneous saccharification and juice co-fermentation on hydrothermal pretreated sweet sorghum bagasse for ethanol production, Appl. Energy, *2013*, 102, 211–219,

[14] DOGARIS I., KARAPATI S., MAMMA D., KALOGERIS E., KEKOS D.: Hydrothermal processing and enzymatic hydrolysis of sorghum bagasse for fermentable carbohydrates production, Biores. Technol., *2009*, 100(24), 6543–6549

[15] SÖDERSTRÖM J., PILCHER L., GALBE M., ZACCHI G.: Two-step steam pre-treatment of softwood by dilute H_2SO_4 impregnation for ethanol production, Biomass Bioene., *2003*, 24(6), 475–486

[16] KAAR W.E., GUTIERREZ C.V., KINOSHITA C.M.: Steam explosion of sugarcane bagasse as a pre-treatment for conversion to ethanol, Biomass Bioene., *1998*, 14(3), 277–287

[17] XU G.Z., FAN S.Y., ZHANG B.L., LIU J.B.: Anaerobic Fermentation Characteristics of Corn Straw Pretreated by Steam Explosion, Adv. Mat. Res., *2012*, 512–515, 334–337

[18] WANG X.T., CAI H.Z., LIU L.S.: Experimental Study on Anaerobic Fermentation of Steam Explosion Pretreated Corn Stalk, Adv. Mat. Res., *2011*, 183–185, 1975–1978

[19] VARGA E., RÉCZEY K., ZACCHI G.: Optimization of steam pre-treatment of corn stover to enhance enzymatic digestibility, Appl. Biochem. Biotechnol., *2004*, 113–116, 509–23

[20] SIPOS B., RÉCZEY J., SOMORAI ZS., KÁDÁR ZS., DIENES D., RÉCZEY K.: Sweet Sorghum as Feedstock for Ethanol Production: Enzymatic Hydrolysis of Steam-Pretreated Bagasse, Appl. Biochem. Biotechnol., 2009, 153(1–3), 151–162

[21] ZHANG J., MA X., YU J., ZHANG X., TAN T.: The effects of four different pre-treatments on enzymatic hydrolysis of sweet sorghum bagasse, Biores. Technol., *2011*, 102(6) 4585–4589

[22] APUL O.G., SANIN F.D.: Ultrasonic pre-treatment and subsequent anaerobic digestion under different operational conditions, Biores. Technol., *2010*, 101(23) 8984–8992

[23] ZHANG K., REN N., GUO C., WANG A., CAO G.: Effects of various pre-treatment methods on mixed microflora to enhance biohydrogen production from corn stover hydrolysate, J. Env. Sci., *2011*, 23(12), 1929–1936

[24] YACHMENEV V., CONDON B., KLASSON T., LAMBERT A.: Acceleration of the enzymatic hydrolysis of corn stover and sugar cane bagasse celluloses by low intensity uniform ultrasound, J. Biobased Mat. Bioene., *2009*, 3(1), 25–31

[25] SHEWALE S.D., PANDIT A.B.: Enzymatic production of glucose from different qualities of grain sorghum and application of ultrasound to enhance the yield, Carbohydr. Res., *2009*, 344(1), 52–60

[26] IMAM T., CAPAREDA S.: Ultrasonic and high-temperature pre-treatment, enzymatic hydrolysis and fermentation of lignocellulosic sweet sorghum to bio-ethanol, Int. J. Ambient Ene., *2012*, 33(3), 152–160

[27] FÖRHÉCZ J., REGŐS J., GÖBLÖS SZ., DALLOS A.: Planning, construction and testing of a biogas pilot plant with mesophilic biodigester, Prof. 37th International Conference of Slovak Society of Chemical Engineering, Tatranské Matliare, Slovakia, Ed.: MARKOS, J., *2010*, pp. 325

[28] APHA, Standard Methods for the Examination of Water and Wastewater, 20th ed.American Public Health Association, Washington, DC, USA, *1999*,

[29] VALO A., CARRÈRE H., DELGENÈS J.P.: Thermal, chemical and thermo-chemical pre-treatment of waste activated sludge for anaerobic digestion, J. Chem. Technol. Biotechnol., *2004*, 79, 1197–1203

[30] GUO P., MOCHIDZUKI K., CHENG W., ZHOU M., GAO H., ZHENG D., WANG X., CUI Z.: Effects of different pre-treatment strategies on corn stalk acidogenic fermentation using a microbial consortium, Biores. Technol., *2011*, 102(16), 7526–7531

[31] BOURGRIER C., CARRÈRE H., DELGENÈS J.P.: Solubilisation of waste-activated sludge by ultrasonic treatment, Chem. Eng. J., *2005*, 106, 163–169

HUNGARIAN JOURNAL
OF INDUSTRY AND CHEMISTRY
VESZPRÉM
Vol. 42(1) pp. 51–56 (2014)

DEVELOPMENT OF A REACTION STRUCTURE IDENTIFICATION ALGORITHM

JÁNOS KONTOS,[1]✉ LÁSZLÓ RICHÁRD TÓTH,[2] AND TAMÁS VARGA[2]

[1] Department of Physical Chemistry, University of Pannonia, Egyetem St. 10, Veszprém, H-8200, HUNGARY
[2] Department of Process Engineering, University of Pannonia, Egyetem St. 10, Veszprém, H-8200, HUNGARY
✉E-mail: kontosjan@gmail.com

The most important step in the design procedure of a chemical reactor is the understanding the chemical reaction network (CRN), which will take place in that reactor. The structure of a CRN as representation of the reaction mechanism contains all the elementary reaction steps that are required to convert the reagents into products. The aim of the reaction mechanism analysis is the identification of the route how the system goes from its initial to the end state. In order to do this, a lot of knowledge is required about chemistry supplemented with some analytical measurements. In this work, we focus on the development of an algorithm, which requires a few data inputs to reveal all the reaction steps that are important in the reactor design point of view. It is trivial that the structure of a dynamic system cannot be determined without the identification of the model parameters that belong to that structure. Hence, the algorithm reported here can be used to obtain the parameters of the reaction rate equations for each identified chemical reaction. First, the structure is identified followed by its parameters. In this study the processed data are obtained by a CRN generator, which is applied to generate random CRNs based on some specified parameters to reach maximal reaction order. Concentration profiles, which characterize each CRN at a specific reaction rate constants combination, are obtained as a result of simulations based on the randomly generated CRNs. The developed algorithm for reaction mechanism identification is based on a modified type of linear least-squares method (LLSM) in which the searching variables must be higher than zero, since the reaction rate constants cannot have negative values. The developed algorithm is tested in different cases to check the applicability of LLSM in reaction structure identification procedure and the obtained results show that with some further improvements the proposed algorithm can be applied solving more complex identification tasks.

Keywords: chemical reaction network, structure identification, non-negative least-squares method, CRN generator

Introduction

One of the most important tasks during the design procedure of any chemical technology is the engineering design of the conversion subsystem and to ensure the optimal and safe operation. Hence, before starting the design of a technology phenomena with impact on the dynamic behaviour of the subsystem must be identified. The most crucial part of the conversion subsystem is the chemical reactor in which we try to control the processes that was identified on the basis of laboratory experiments. In this work we proposed a method to support the identification of the individual reaction steps and their rates in a chemical reaction network (CRN).

Numerous literature examples can be found that describe different methodologies to generate the structure of CRNs, as representations for reaction mechanisms [1, 2]. The reaction mechanism of a reaction system represents all the elementary reaction steps, which are required to convert the reagents into products. Hence, the aim of reaction mechanism identification is the determination of the intermediate steps, which take the starting materials to the final products. Trivially, it is challenging to follow and model the movements of all the molecules in a system in full detail. However, we can describe a reaction system on the basis of the cumulative effects of great number of molecules in specific states. Such specific states are the formation of stable intermediates.

The intermediates are chemical species produced in the elementary reaction steps. Often, it is possible to detect them by experimental methods. The produced amount of these intermediates is sometimes very low and they react very fast to produce another intermediate or final product. Hence, the identification of the latter components and the measurement of their concentrations can be challenging. Most of the reactions take place through multiple intermediate steps. These scenarios are called multi-step reactions. In a single reaction step, the sign of stoichiometric coefficients represent that a given molecule is a reagent (-) or product (+), and the absolute value of these coefficients give how many moles are consumed/formed.

The transient states of a reaction system and the intermediates can be investigated with two kinds of methods on the basis of whether *a priori* knowledge of reaction kinetics is available or not [3]. The foundation of the reaction mechanism analysis is the precise identification of all intermediates and their

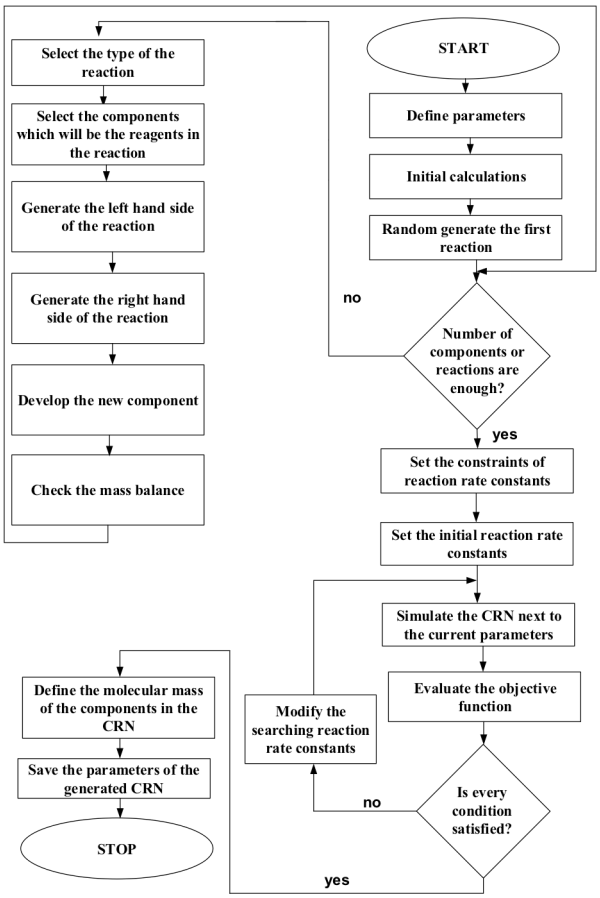

Figure 1: The scheme of the proposed CRN generator

concentration. With the lack of this information the stoichiometry of the reaction cannot be revealed reliably. The nature and the amount of the products can contain as much information as a well-qualified chemist requires identifying the reaction mechanism of an unknown reaction system. The proposed algorithm can support this process in case we have lack of experience in the identification of the structure of a CRN and parameters of kinetic expressions, which describe the rate of the reaction steps considered in the CRN.

The essence of the parameter identification process is the solution of a constrained minimization problem in which the objective function can be the sum of squared error between the measured and the calculated component concentration profiles. The searching variables are the unknown parameters in the kinetic expressions (i.e. pre-exponential factor, activation energy, reaction order).

The role of the structure identification is the definition of correlated variables and their mathematical formalization. In our case, the identification means the selection of reaction steps that can take place in the reactor. The identification tasks can be solved by the application of linear least-squares method (LLSM) [4]. The main challenges using this method are the definition of the correct initial conditions for the applied searching algorithm and the speed up of the identification procedure.

One of the most important simultaneous methods is the incremental approach, which applies a hierarchical modelling methodology to decompose the complex identification problem into simpler sub-problems [5]. The method applies target factor analysis to identify the suitable structure of the unknown CRN. This method has been successfully applied in reaction mechanism identification process in a multi-phase system based on concentration and calorimetric measurements [6].

Correlation metric method was developed to analyse the strength of the connections between the components in the system, which is based on the qualitative analysis of the measured data [7]. Qualitative trend analysis was also applied in reaction mechanism identification algorithms to divide the entire experimental time into shorter periods in which the correlations are analysed between the concentrations of components [8].

In this work, our aim is to develop a simple, but reliable method for structure identification of CRNs, which need as few data as possible. In our case the input of the algorithm is only the list of components and concentration profiles, which are the result of the simulation based on randomly generated CRNs. These CRNs were generated based on user specified parameters, such as maximal reaction order. On the basis of the randomly generated CRNs, the concentration profiles for each CRN at a specific reaction rate constants combination are determined. The algorithm developed for reaction mechanism identification is based on a modified LLSM method, in which the searching variables must be higher than zero, since the reaction rate constants cannot have negative values.

Development of Simulation Methods

Since our aim is to develop a generally applicable algorithm to support the identification process of CRNs with unknown structure, we developed a CRN generator, which can be applied to randomly generate CRNs based on some structural parameters, such as the maximum number of components or reactions in CRN.

There are many examples in literature for developing a CRN generator that analyses the affinity of molecules taking part in reactions [9], applies mixed integer programming to build up reaction networks [10], or using group contribution method to generate the structure of the CRN and the kinetic parameters of the reaction steps in that network [11].

In this work we developed a simple CRN generator that randomly generates a CRN from randomly generated components. In this generator, we define probabilities in situations for building different kinds of CRNs. For example, if we would like to have more decomposition reactions in the CRN then the probability of this type of reaction is increased. The scheme of the developed CRN generator can be seen in *Fig.1*.

The first step of the algorithm of the CRN generator is the definition of the parameters of the desired CRN, such as the probabilities of the different types of reactions. In this step the maximal number of building block types in a component and the maximal number of specific building blocks in a component are defined.

The next step is the development of the first reaction step in which we define a new component next to the components that are already in the component list. The stoichiometric coefficients of the reaction are randomly generated based on the user-defined parameters. The composition and the chemical formula of the added component are determined based on the material balance of the reaction. With the first reaction step, it is checked whether the numbers of components and reactions in the generated CRN are enough.

If the user defined value of these parameters are higher than the current values the CRN generator starts to build a new reaction with selecting the reaction type, the components. Based on the CRN parameters it randomly generates stoichiometric factors for that new reaction and checks the material balance. Components that are involved in more reactions have a smaller chance to be chosen for the next new reaction building iteration.

If there are enough components or reactions in the generated CRN, the algorithm steps to the next phase in which it randomly generates the reaction kinetic constants for reactions in the CRN. In this phase, the algorithm randomly generate kinetic parameters, while maintaining the same order of magnitude of the reaction rates, to make it harder to find out the structure of the generated CRN. Particle swarm optimization method has been applied to solve this constrained optimization problem, where the objective function is defined as the difference of the integral of reaction rates over the time [12].

General Reactor Model

The kinetic experiments are usually performed in a tempered flask that can be modelled as an isothermal batch reactor. All the reagents are added to the unit with or without catalyst and samples are taken from the reaction mixture in specific times. As mentioned earlier the simplest case is considered as we have only concentration measurements from a batch reactor. However, the developed algorithm can be improved and the processability of data can be widened with the application of mathematical models of other reactor types.

Hence, at this point of the development of the proposed algorithm, we consider that the unit in which the kinetic experiments are performed is a well-mixed, isothermal batch reactor. The model of a batch reactor should be developed first to contain component mass balance equations. Applying the well-mixed assumption the component mass balances can be simplified and we obtain the equations:

$$\frac{dc_i}{dt} = R_i \qquad i = \{A;B;C;...\}, \tag{1}$$

where I identifies the components in the system in which we have N_c components; c_i is the concentration of the i^{th} component [mol m^{-3}]; R_i is the component source of the i^{th} component [mol m^{-3} s^{-1}], which can be calculated as:

$$R_i = \sum_{j=1}^{N_R} \upsilon_{ji} \cdot r_j , \tag{2}$$

where j identifies the reaction in the system; N_R gives the number of reactions considered; ν_{ji} is the stoichiometric coefficient of the i^{th} component in the j^{th} reaction; r_j is the reaction rate of the j^{th} reaction [mol m^{-3} s^{-1}], which is calculated with following expression:

$$r_j = k_j \prod_{i=\{A;B;C;...\}} c_i^{n_{ji}} , \tag{3}$$

where n_{ji} denotes the order of i^{th} component in j^{th} reaction [1], k_j is the reaction rate constant of the j^{th} reaction [the unit is dependent on the order of the reaction, [mol^{1-n} m^{3n-1} s^{-1}], where n is the summarized reaction order in j^{th} reaction:

$$n = \sum_{i=\{A;B;C;...\}} n_{ji} \quad . \tag{4}$$

This summarized reaction order is equal to the absolute value of the stoichiometric coefficient of the i^{th} component in the j^{th} reaction, if the given component is a reagent in a given reaction, otherwise it is 0. The developed general reactor model has been implemented in MATLAB.

Proposed Algorithm for Structure Identification of CRN

Our primary aim is to develop an algorithm, which can be efficiently applied in reaction mechanism identification tasks on the basis of concentration profiles. In this phase, we considered that the concentration profiles are known for all the components in the system. It is a simplification with respect of practical problems; however, in this work we aim to evaluate if a simple method of LLSM is suitable for a complex task.

LLSM is based on the minimization of a special model error, which is based on comparing the measured to the calculated time series. In our case, the time series are the numerical derivatives of the concentration profiles. Based on the measured concentration profiles the change in concentration during two sampling steps can be calculated as a numerical derivative with respect to length of that time step. If we have N_k samples, the difference in k^{th} sample can be defined as follows:

$$\frac{\Delta \hat{c}_i}{\Delta t}(k) = \hat{c}_i(k) - \hat{c}_i(k-1) \quad , \tag{5}$$

where k is the current sample; $\Delta \hat{c}_i$ is the difference of the measured concentration of i^{th} component in between k and $k-1$ sampling steps; Δt is the time difference between k and $k-1$ sampling steps.

If we calculate this difference for all the components and in every sampling steps we get a matrix which has $k-1$ rows and as many columns as many components we assume in the system. Based on the calculated concentration profiles another matrix can be built with the calculated variables. In our case the sum of the

squared differences between these two matrices is defined as the model error, which should be minimized during the identification process:

$$E = \sum_{\mathrm{i}=\{\mathrm{A;B;C;...}\}} \sum_{\mathrm{k}=1}^{N_\mathrm{k}} \left(\frac{\Delta \hat{c}_\mathrm{i}}{\Delta t}(k) - \frac{\Delta c_\mathrm{i}}{\Delta t}(k) \right)^2, \tag{6}$$

where E is the calculated model error, which is basically the difference of the measured and calculated component sources defined with *Eq.(2)*; Δc_i is the calculated changes in concentrations of i^{th} component from *Eq.(1)*, but the steps is equal with the sample times of measurement.

To make it easier to follow the process we define *Eq.(6)* using vectors instead of sums:

$$E = \left(\overline{\Delta \hat{c}} - \overline{\Delta c} \right)^T \left(\overline{\Delta \hat{c}} - \overline{\Delta c} \right), \tag{7}$$

where the length of vectors are $N_\mathrm{c}(N_\mathrm{k}\text{-}1)$ (i.e. the change in concentrations of components should be calculated in every sample time except in the initial phase) and defined with the following structures:

$$\overline{\Delta \hat{c}} = \begin{bmatrix} \Delta \hat{c}_\mathrm{A}(1) \\ \Delta \hat{c}_\mathrm{B}(1) \\ \vdots \\ \Delta \hat{c}_\mathrm{A}(2) \\ \Delta \hat{c}_\mathrm{B}(2) \\ \vdots \\ \Delta \hat{c}_\mathrm{A}(k) \\ \Delta \hat{c}_\mathrm{B}(k) \\ \vdots \end{bmatrix}, \quad \overline{\Delta c} = \begin{bmatrix} \Delta c_\mathrm{A}(1) \\ \Delta c_\mathrm{B}(1) \\ \vdots \\ \Delta c_\mathrm{A}(2) \\ \Delta c_\mathrm{B}(2) \\ \vdots \\ \Delta c_\mathrm{A}(k) \\ \Delta c_\mathrm{B}(k) \\ \vdots \end{bmatrix}. \tag{8}$$

The task in LLSM is the minimization of the model error defined in *Eq.(7)* by manipulating the model parameters, such as the reaction rate constants of all the possible reaction steps, which are the building blocks of the unknown CRNs. Hence, to use LLSM in reaction mechanism identification process first we need to collect all the possible reaction steps, which can take place in the system based on the defined component list. To get the necessary reaction steps, we generate all the possible combination of reactions, which satisfy the material balances. A given reaction step has to be further processed, since some reaction steps can be produced from each other with linear combinations. Thus, only the independent reactions should be kept in the reaction set. The resulted reaction set is represented in a matrix (i.e. in stoichiometric matrix):

$$\overline{\overline{\upsilon}}_{RS} = \begin{array}{c} \\ 1 \\ 2 \\ \vdots \end{array} \begin{array}{c} \begin{array}{ccc} A & B & \cdots \end{array} \\ \begin{bmatrix} \upsilon_{1A} & \upsilon_{1B} & \cdots \\ \upsilon_{2A} & \upsilon_{2B} & \cdots \\ \vdots & \vdots & \ddots \end{bmatrix} \end{array}, \tag{9}$$

which has the same number of rows and columns as the number independent reactions and components are considered in the system, respectively.

After the possible reaction steps have been automatically collected, all the reaction steps of the set are considered as the part of the unknown CRNs. Based on the reaction set the mathematical model of the system is automatically generated based on *Eqs.(1)-(3)*. The unknown parameters in this model are the reaction rate constants for all reactions in the reaction set.

The calculated concentration differences in *Eq.(7)* can be obtained using *Eq.(10)* on the basis of the general reactor model *(Eqs.(1-3))*:

$$\overline{\Delta c} = \overline{\overline{\upsilon}}\,\bar{k}\,\overline{\overline{c}}, \tag{10}$$

where $\overline{\overline{c}}$ denotes a special matrix in which a diagonal matrix is repeated from sample time to sample time and in the diagonal matrices we calculate the concentration product term in *Eq.(3)* in every sample time. The following general matrix shows the structure of the resulting diagonal matrix in this step if we have N_R reactions in the reaction set:

$$\overline{\overline{c}} = \begin{bmatrix} \prod_{i=\{A;B;C;...\}} \left(c_\mathrm{i}(0)\right)^{\mathrm{n}_{1\mathrm{i}}} & 0 & \cdots \\ 0 & \prod_{i=\{A;B;C;...\}} \left(c_\mathrm{i}(0)\right)^{\mathrm{n}_{2\mathrm{i}}} & \cdots \\ \vdots & \vdots & \ddots \\ \prod_{i=\{A;B;C;...\}} \left(c_i(1)\right)^{n_{1i}} & 0 & \cdots \\ 0 & \prod_{i=\{A;B;C;...\}} \left(c_\mathrm{i}(1)\right)^{\mathrm{n}_{2\mathrm{i}}} & \cdots \\ \vdots & \vdots & \ddots \\ \prod_{i=\{A;B;C;...\}} \left(c_\mathrm{i}(k-1)\right)^{\mathrm{n}_{1\mathrm{i}}} & 0 & \cdots \\ 0 & \prod_{i=\{A;B;C;...\}} \left(c_\mathrm{i}(k-1)\right)^{\mathrm{n}_{2\mathrm{i}}} & \cdots \\ \vdots & \vdots & \ddots \end{bmatrix} \tag{11}$$

$\overline{\overline{\upsilon}}$ denotes a special matrix in which the stoichiometric matrix representing the reaction set *(Eq.(9))* is repeated as many times as the sample times minus one:

$$\overline{\overline{\upsilon}} = \begin{bmatrix} \overline{\overline{\upsilon}}_{\mathrm{RS}} \\ \overline{\overline{\upsilon}}_{\mathrm{RS}} \\ \vdots \end{bmatrix} \tag{12}$$

$\bar{k}$ indicates reaction rate constant vector for all the reactions in the reaction set.

By applying LLSM, the structure of the unknown CRN can be identified since the reaction rate constants that can be the part of the unknown CRN will have different values than zero at the end of the identification process and all the other reactions in reaction set get zero value. Based on *Eqs.(7)* and *(10)* we can solve the minimization problem and the following expression is the result for the calculation of reaction rate constants for all reactions in the generated reaction set:

Table 1: A randomly generated CRN with CRN generator

	A	B	C	D	E	k [-]
R01	-1	-1	1	1	0	1.5590
R02	2	0	0	1	-1	1.0184

$$\bar{k} = \left[\left(\left(\bar{\upsilon}\right)' \times \bar{c}\right)' \times \left(\left(\bar{\upsilon}\right)' \times \bar{c}\right)\right]^{-1} \times \left(\left(\bar{\upsilon}\right)' \times \bar{c}\right)' \times \overline{\Delta \hat{c}} \qquad (13)$$

Reactions with zero reaction rate constants indicate that they cannot be part of the unknown CRN. This means that at the end of the identification process we get the reaction rate constants as well, next to the structure of the CRN.

Results and Discussion

Since we do not have measurements from a real system in this work the developed CRN generator has been applied to randomly generate some CRNs. *Table 1* shows two reaction steps in the unknown CRN. We have defined five components (**A**-**E**) in the system. **A** and **B** components are reagents in the first reaction step (**R01**), in which **C** and **D** components are produced. However, in the second reaction (**R02**) only **E** is consumed while 2 moles of **A** and 1 mole of **D** are produced. The last column of *Table 1* shows the exact values of reaction rate constants. The unit of reaction rate constants can be determined for the j^{th} reaction based on the sum of the reaction orders of each component in that reaction:

$$\left(\frac{\text{mol}}{\text{m}^3}\right)\left(1 - \sum_{i=\{A;B;C;...\}} n_{\text{ji}}\right) \cdot \frac{1}{s} \qquad (14)$$

Table 2 shows the five components (**A**-**E**) that are built from nine (**a**-**j**) building elements. These building elements can be imagined as atoms or groups. The numbers in the matrix represents the stoichiometric coefficients of composition. The last row shows a fictitious molecular mass of the components in the system.

Based on the molecular mass and the number of building elements in the components all the independent reaction steps were generated as shown in *Table 3*. The 22 possible reaction steps can be found for the five components from *Table 2*. The unknown reaction mechanism should be built from these reaction steps. In *Table 1* we saw that we need only two of these steps and as it can be seen in the last column of *Table 3* with the proposed algorithm we can find these two reactions of **RS01** and **RS16**. However, the algorithm identifies a third possible reaction step, **RS13**, which can be the part of the unknown CRN. As can be seen in the last column of *Table 3*, the reaction rate constant corresponding to this reaction step is very low. This means **RS13** should not be considered as the part of the unknown CRN.

Table 2: The generated compound matrix

	A	B	C	D	E
a	9	0	1	8	26
b	10	0	8	2	22
c	7	1	1	7	21
d	2	10	7	5	9
e	4	12	13	3	11
f	12	0	1	11	35
g	8	0	6	2	18
h	11	5	7	9	31
j	6	1	3	4	16
M [mass mol^{-1}]	359	195	252	302	1020

Table 3: The resulted reaction step matrix with the identified reaction rate constant

RS ID	A	B	C	D	E	k [-]
RS01	-1	-1	1	1	0	1.626
RS02	-3	-1	1	0	1	0
RS03	-2	0	0	-1	1	0
RS04	-2	6	3	-4	0	0
RS05	-3	5	4	-3	0	0
RS06	-4	4	5	-2	0	0
RS07	-5	3	6	-1	0	0
RS08	0	4	5	0	-2	0
RS09	-3	3	6	0	-1	0
RS10	5	-3	-6	1	0	0
RS11	3	-3	-6	0	1	0
RS12	4	-4	-5	2	0	0
RS13	0	-4	-5	0	2	0.004
RS14	3	-5	-4	3	0	0
RS15	2	-6	-3	4	0	0
RS16	0	-6	-3	3	1	0
RS17	2	0	0	1	-1	1.051
RS18	0	-2	2	3	-1	0
RS19	1	1	-1	-1	0	0
RS20	0	2	-2	-3	1	0
RS21	3	1	-1	0	-1	0
RS22	0	6	3	-3	-1	0

After the above simple task, we tested our method in nine other cases. We defined a quantitative measure to check the correctness of the identified kinetic parameters as the mean average difference between the known and the identified reaction rate constants:

$$MAE = \frac{1}{N_{\text{dr}}} \sum_{l=1}^{N_{\text{dr}}} \left| \hat{k}_l - k_l \right| \qquad (15)$$

where N_{dr} is the number of reactions in unknown CRN; l identifies the current reaction rate constant; $\hat{k}$ is the reaction rate constant value what we are looking for, such as the last column in *Table 1* for **CRN01**.

Table 4 presents the number of reaction steps in the unknown CRN ($N_{\mathbf{dr}}$), the number of components (N_{c}) in the system, the number of the possible reaction steps (N_{r}) as a representation of the size of the reaction set, if the algorithm can find the perfect reaction steps or not, and MAE values when available from *Eq.(15)*.

Table 4: Testing the developed algorithm in case of 10 CRNs

CRN ID	N_{dr}	N_c	N_r	match	*MAE* [-]
CRN01	2	5	22	y	0.0498
CRN02	3	5	40	n (1/3)	-
CRN03	3	5	11	y	0.0983
CRN04	2	5	17	y	0.0268
CRN05	4	5	26	y	0.1197
CRN06	2	5	13	y	0.0146
CRN07	3	5	10	y	0.0216
CRN08	4	5	119	n (0/4)	-
CRN09	3	5	85	n (0/3)	-
CRN10	4	5	19	y	0.0748

Based on the results in *Table 4* it can be seen that the proposed algorithm has some limitations in this phase. However, if the size of the reaction set is relatively small it gives very good agreement with the desired parameters. This means that we should improve this method to make possible the analysis of more complex problems with it. If the algorithm cannot find the perfect match for the unknown CRN a ratio is given which shows how many of the reaction steps are correctly identified from the unknown mechanism.

Conclusions

The structure of a CRN represents all the elementary reaction steps that are required to convert the reagents into products. Hence, the aim of reaction mechanism identification is to discover the intermediate steps, which connect starting materials with the final product. The proposed algorithm can support this process even in the case, when we lack knowledge about the reaction mechanism and/or kinetic parameters.

The applied structure identification method is based on linear least-square method. The measured and calculated concentration profiles are compared and the difference between these profiles is minimized during the identification process. The proposed algorithm for reaction mechanism identification was implemented in MATLAB.

The results of initial testing showed promising results for this simple method being applicable for a complex task; however, the proposed algorithm should be improved toward processing reaction sets. The given implementation of the algorithm for batch reactor models can be easily extended to other reactor models, which enables to employ our method to realistic problems from chemical industry.

Acknowledgements

This research was supported by the European Union and the State of Hungary, co-financed by the European Social Fund in the framework of TÁMOP 4.2.4.A/2-11-1-2012-0001 ‘National Excellence Program’.

REFERENCES

[1] DELVIN S.: Organic Reaction Mechanism, Sarup & Sons, New Delhi, *2002*

[2] GROSSMAN R.B.: The Art of Writing Reasonable Organic Reaction Mechanisms, Springer, New York, *2003*

[3] FRIESS S.L., LEWIS E.S.: Investigation of Rates and Mechanisms of Reactions, John Wiley & Sons, New York, *1963*

[4] WALTER E.: Identification of Parametric Models from Experimental Data, Springer-Verlag, Berlin *1997*

[5] BENDEL M.L., BONVIN D., MARQUARDT W.: Incremental identification of kinetic models for homogeneous reaction systems, Chem. Eng. Sci., *2006*, 61, 5404–5420

[6] SRINIVASAN S., BILLETER J., BONVIN D.: Extent-based incremental identification of reaction systems using concentration and calorimetric measurements, Chem. Eng. J., *2012*, 207–208, 785–793

[7] SAMOILOV M., ARKIN A., ROSS J.: On the deduction of chemical reaction pathways from measurements of time series of concentrations, Chaos, 2001, 11, 108–114

[8] VARGA T.: Qualitative Analysis Based Reaction Mechanism Identification, Chem. Eng. Trans., *2013*, 35, 769–774

[9] RATKIEWICZ A., TRUONG T.N.: Application of Chemical Graph Theory for Automated Mechanism Generation, J. Chem. Inf. Comput. Sci., *2003*, 43, 36–44

[10] FIRST E.L., GOUNARIS C.E., FLOUDA C.A.S: Stereochemically Consistent Reaction Mapping and Identification of Multiple Reaction Mechanisms through Integer Linear Optimization, J. Chem. Inf. Model, *2012*, 52, 84–92

[11] WEST R.H., ALLEN J.W., GREEN W.H.: Automatic Reaction Mechanism Generation with Group Additive Kinetics, ChemInform., *2012*, 43, 36–258

[12] KENNEDY J., EBERHART R.: Particle swarm optimization in Neural Networks, Proc. IEEE International Conference on Neural Networks, Perth, Australia, *1995*, 4, 1942–1948

Acknowledgement

The dedicated issue of the Hung. J. Ind. & Chem. and in part the organization of the 2014 Spring Scientific Students' Meeting at University of Pannonia were made possible from support provided by the National Talent Program of the Educational Research and Development Institute and the Human Resource Support Program of the Ministry of Human Resources within the framework of "Support of TDK Workshops Recognized by the Council of National Scientific Students' Association" (NTP-TDK-13)

National Scientific Students' Association

OFI

Köszönetnyilvánítás

Jelen kiadvány és részben a 2014. évi Tavaszi Tudományos Diáknap a Pannon Egyetemen az Emberi Erőforrások Minisztériuma megbízásából az Oktatáskutató és Fejlesztő Intézet és az Emberi Erőforrás Támogatáskezelő által gondozott Nemzeti Tehetség Program „Az Országos Tudományos Diákköri Tanács által elismert TDK-műhelyek támogatása" (NTP-TDK-13) című pályázatának köszönhetően valósult meg.